PB92-169382

Study to Determine the Feasibility of Using a Ground-Penetrating Radar for More Effective Remediation of Subsurface Contamination

Foster Wheeler Enviresponse, Inc., Edison, NJ

Prepared for:

Environmental Protection Agency, Cincinnati, OH

May 92

U.S. Department of Commerce
National Technical Information Service
[redacted]

PB92-169382

EPA/600/R-92/089
May 1992

A STUDY TO DETERMINE THE FEASIBILITY OF USING A GROUND-PENETRATING RADAR FOR MORE EFFECTIVE REMEDIATION OF SUBSURFACE CONTAMINATION

by

Dennis G. Douglas, Alan A. Burns, Charles L. Rino, Joseph W. Maresca, Jr.
Vista Research, Inc.
Mountain View, California 94042

Contract No. 68-03-3409

Project Officer
James Yezzi
Superfund Technology Demonstration Division
Risk Reduction Engineering Laboratory
Edison, New Jersey 08837

RISK REDUCTION ENGINEERING LABORATORY
OFFICE OF RESEARCH AND DEVELOPMENT
U.S. ENVIRONMENTAL PROTECTION AGENCY
CINCINNATI, OHIO 45268

♲ *Printed on Recycled Paper*

REPRODUCED BY
U.S. DEPARTMENT OF COMMERCE
NATIONAL TECHNICAL INFORMATION SERVICE
SPRINGFIELD, VA 22161

DISCLAIMER

This material has been funded wholly or in part by the United States Environmental Protection Agency under Contract 68-C9-0033 to Foster Wheeler Enviresponse, Inc. It has been subject to the Agency's peer and administrative review, and it has been approved for publication as an EPA document. Mention of trade names or commercial products does not constitute endorsement or recommendation for use.

FOREWORD

Today's rapidly developing and changing technologies and industrial products frequently carry with them the increased generation of materials that, if improperly dealt with, can threaten both public health and the environment. The U.S. Environmental Protection Agency is charged by Congress with protecting the nation's land, air, and water resources. Under a mandate of national environmental laws, the agency strives to formulate and implement actions leading to a compatible balance between human activities and the ability of natural systems to support and nurture life. These laws direct the EPA to perform research to define our environmental problems, measure the impacts, and search for solutions.

The Risk Reduction Engineering Laboratory is responsible for planning, implementing, and managing research, development, and demonstration programs to provide an authoritative, defensible engineering basis in support of the policies, programs, and regulations of the EPA with respect to drinking water, wastewater, pesticides, toxic substances, solid and hazardous wastes, and Superfund-related activities. This publication is one of the products of that research and provides a vital communication link between the researcher and the user community.

This publication describes a research project that investigated the application of advanced radar systems to detecting contaminants present in soil and groundwater. Ground-penetrating radar, in combination with sophisticated data-processing techniques, was found to be a viable means not only of detecting the contaminant substance and defining its extent but also of distinguishing this substance from natural subsurface features.

Risk Reduction Engineering Laboratory
E. Timothy Oppelt, Director

ABSTRACT

Remediation of toxic spills is often costly and entails cumbersome procedures. The traditional method is to drill core samples in the area where the contaminant is thought to be present and then analyze these in a laboratory. The denser the sampling grid, the more effective it is; unfortunately, it is also more expensive to implement and more damaging to the environment. A nonintrusive method of detecting subsurface contamination, therefore, would be highly desirable. Toward this end, the use of ground-penetrating radar (GPR) to locate and map subsurface contamination was investigated. If GPR proves effective, it can be combined with conventional methods to ensure better placement of drilling sites and to reduce the number of samples necessary. The objective of this work was to assess the capability of GPR to identify natural subsurface features, detect man-made objects buried in the soil, and both detect and define the extent of contaminated soil or groundwater.

Several conclusions emerged from this study. The technology for the envisioned GPR already exists. In terms of hardware, it was found that a radar system with a very high figure of merit is required if the system is to operate effectively in all three generic subsurface environments modeled in this study. (These three environments contain the subsurface features that are representative of seven out of ten "common cases," as defined by EPA, found at remediation sites.) In terms of signal processing, it was found that for typical GPR systems synthetic-aperture-radar (SAR) processing is required; this conclusion was based on three reasons: (1) better horizontal resolution is achieved with SAR processing; (2) SAR processing allows the system to operate at lower frequencies and thus achieve deeper penetration; and (3) SAR processing reduces ambient noise, which improves the detection and identification capabilities of GPR.

It is recommended that simple proof-of-principle experiments be undertaken to validate the models developed in this study. To the extent that the experiments prove successful, GPR may become a significant tool in rapidly identifying and cost-effectively remediating subsurface contamination.

This report was submitted in fulfillment of Contract No. 68-C9-0033 by Vista Research, Inc., under the sponsorship of the U. S. Environmental protection Agency. This report covers a period from December 12, 1990, to May 20, 1991; work was completed as of May 13, 1991.

TABLE OF CONTENTS

Disclaimer ii

Foreword iii

Abstract iv

List of Figures vii

List of Tables ix

Acknowledgments x

1 Introduction 1

    1.1.1 Current Remediation Practices and Problems 1

    1.1.2 Application of Ground-Penetrating Radar to Remediation 1

    1.1.3 Report Organization 3

  1.2 Objectives and Approach 5

    1.2.1 Objectives 5

    1.2.2 Technical Approach 5

2 Conclusions 7

3 Recommendations 10

4 Radars and Radar Signal Processing 12

  4.1 Radar Fundamentals 12

  4.2 Ground-Penetrating Radars 17

  4.3 Short-Pulse and Synthetic-Pulse Radars 23

  4.4 Real- and Synthetic-Aperture Signal Processing 24

5 Radar Figure of Merit 27

  5.1 Introduction 27

  5.2 Figure-of-Merit Derivation 27

    5.2.1 Short-Pulse Radars 27

    5.2.2 Synthetic-Pulse GPRs 29

  5.3 Figures of Merit for Typical Radars 30

  5.4 Processing-Gain Contribution to Figure of Merit 32

  5.5 Environmental Contributions to Figure of Merit 34

  5.6 Section Summary 35

6 Soil Characteristics, Soil Model, and Soil Geometries 36

  6.1 Classification and Distribution of Soil Types 36

  6.2 Characteristics of Soils and Contaminants 38

6.3 Modeled Soil and Contamination Geometries 40
6.4 Dielectric Properties of Soils and Soil Mixtures 43
6.5 Section Summary 44
7 Detection Strategies 45
7.1 Introduction 45
7.2 Summary of Strategies 46
7.3 Model IB Strategy: Reflection from a Contaminant/Water Interface in Soil 47
7.4 Model IA Strategy: Reflection from a Thin Layer of Contaminant Sandwiched between Layers of "Dry" and Wet Soil 49
7.5 Model II Strategy: Volume Scattering from Soils 56
7.6 Model II Strategy: Deducing Changes in the Local Average Refractive Index ... 65
7.7 Section Summary 66
8 Radar System Design 68
9 Numerical Analytic Model 72
9.1 Introduction 72
9.2 The INS Model 73
9.3 Signal Processing 76
9.4 Representative Examples 77
References 94

Appendices

A. Real Signals, Analytic Signals, and Complex Envelopes A-1
B. Calculations of Dielectric Constant, Conductivity, and Attenuation Coefficient for Various Soils and a Petroleum Contaminant B-1
C. Modified Booker-Gordon Scattering Formula C-1
D. Correlation Function for Soil Variability Model D-1

LIST OF FIGURES

4.1 Block diagram of a generic radar. 13

4.2 Examples of radar displays. 15

4.3 Typical GPR pulse waveform. 18

4.4 Block diagram of a short-pulse GPR. 19

4.5 Example of a typical conventional GPR output display. 21

4.6 GPR pulse intensity and hard-limited output. 22

4.7 Short-pulse and synthetic-pulse radar waveforms: (a) a short-pulse radar transmits a short burst of nearly sinusoidal signals; (b) a Fourier transform gives a "spectrum" of the waveform; (c) a synthetic pulse transmits the spectrum in a series of sinusoidal signals over the range of frequencies; (d) a Fourier transform gives the effective waveform. 24

4.8 Block diagram of a synthetic pulse radar system. 25

6.1 Triangular Classification Chart for soil. 37

6.2 Distribution of soil deposits. 38

6.3 Models of subsurface conditions. In Model IA (a), the contaminant floats on the water table; in Model IB (b) there is a gradual transition from wet to dry, but the immiscibility of the contaminant with water causes a boundary to form at some point; in Model II (c) the contaminant forms a plume that travels downward. 42

7.1 Profiles of dielectric constant vs. depth: (a) distinct water table, and (b) indistinct water table. 50

7.2 Incident vs. reflected signal. 52

7.3 Real part, imaginary part, and magnitude of the reflection coefficient vs. layer thickness of a contaminant-saturated layer sandwiched between dry and water-saturated soils (30% porosity and 0.03 S/m water conductivity. 53

7.4 $|\Re r(t)|/|r(t)|$ and $|\Im r(t)|/|r(t)|$ vs. layer thickness for a contaminant-saturated layer sandwiched between dry and water-saturated soils (30% porosity and 0.03 S/m water conductivity). 54

7.5 $|\Re r(t)|/|r(0)|$, $|\Im r(t)|/|r(0)|$, and $|r(t)|/|r(0)|$ vs. layer thickness for a contaminant-saturated layer sandwiched between dry and water-saturated soils (30% porosity and 0.03 S/m water conductivity). 55

7.6 Magnitude of the real part of ***r*** and the ratio of the imaginary to real parts vs. frequency (30% porosity, 5-cm thickness, and 0.03 S/m water conductivity). 56

9.1 Unprocessed simulated returns for Q=140-dB GPR. Point targets are located at 10-m and 30-m depths. 80

9.2 Processed returns for Q=140-dB GPR in perspective with 60-dB logarithmic display. 81
9.3 Unprocessed simulated returns for Q=160-dB GPR. Point targets are located at 10-m and 30-m depths. 82
9.4 Processed returns for Q=180-dB GPR. Upper target is visible. 83
9.5 Unprocessed returns for Q=180-dB GPR. Point targets are located at 10-m and 30-m depths. 84
9.6 Processed returns for Q=180-dB GPR. Both targets are visible. 85
9.7 Unprocessed returns for Q=190-dB GPR. 86
9.8 Processed returns for Q=190-dB GPR. 87
9.9 Unprocessed returns for Q=220-dB GPR. 88
9.10 Processed returns for Q=220-dB GPR. Processing sidelobes are visible for target at 10 m. 89
9.11 Unprocessed returns for Q=220-dB GPR with two closely spaced targets at 10-m and 15-m depths. 90
9.12 Processed returns for Q=220-dB GPR with closely spaced targets. 91
9.13 Unprocessed returns for Q=220-dB GPR illuminating a wedge of randomly located scatterers. 92
9.14 Processed returns from Q=220-dB GPR illuminating wedge. 93

LIST OF TABLES

5.1 Specifications for a "Typical" Commercially Available GPR 31

6.1 Electromagnetic Characteristics for Common Geologic Materials 39

6.2 Dielectric Constants of Typical Contaminant Materials 40

7.1 Detection Strategy Summary 46

7.2 Plane-Interface Complex Reflection Coefficient at 100 MHz 49

7.3 ε_{ave}, $< (\varepsilon_r - 1)^2 >$, and $< \xi^2 >$ vs. Porosity and Mixture Type 60

7.4 ε_2 and $< \xi^2 >$ for a Mixture of Rocks and 30% Porosity Soil 60

7.5 Minimum Q vs. $\overline{d}$ 62

7.6 ε_{ave} and $\varepsilon_{ave}^{1/2} < \xi^2 >$ for $\overline{d} = 2.5$ cm, $\overline{s} = 10$ cm Stones in Various Soils 63

7.7 Backscatter Quantities for Solid Particles Imbedded in Dry, Low-Loss, 30%-Porosity Soil at 10-m Depth ($T_{obs} = 3000$ s) 64

8.1 Values of Q_{min} Necessary to Detect Various Targets in Various Environments with SNR of 10 dB 70

9.1 Model Parameters 75

ACKNOWLEDGMENTS

This research report was prepared by Vista Research, Inc., for the U.S. Environmental Protection Agency's (EPA's) Risk Reduction Engineering Laboratory (RREL) on Contract No. 68-C9-0033. James J. Yezzi of the Releases Control Branch was the Technical Program Monitor on the Work Assignment for EPA/RREL. Technical review was provided by Mr. Yezzi and by Anthony N. Tafuri, Section Chief, Releases Control Branch. The authors would also like to acknowledge Foster Wheeler Enviresponse, Inc., for their support during the project. This document was edited by Monique Seibel and prepared for publication by Pamela Webster.

Section 1

INTRODUCTION

1.1 Background

1.1.1 Current Remediation Practices and Problems

Remediation of a petroleum or chemical release from an underground storage tank (or a hazardous waste storage site) requires that the horizontal and vertical extent of the contaminated soil and groundwater region be located and quantified. This is traditionally accomplished by preparing a plan to define drill sites, taking core samples at the planned sites, and then analyzing the cores at a laboratory. A map based upon the contamination found in the samples is then prepared, and is used to guide the cleanup operation. Since drilling and analysis operations can be costly, it is desirable to minimize the number of samples while still preparing an adequate map of the contaminated area.

Reducing the number of corings taken per unit area, while reducing cost, generally leads to undersampling of the site. Concentrating a given number of corings in a limited area, while increasing the sample density, presumes knowledge about the location and spatial extent of contaminated areas. Further, since there is usually little geological information available about the contaminated sites, even a fine sampling does not ensure that the contaminated areas will be found. This is because fracture regions and fissures can channel liquid contaminants away from the spill (or release) site. Thus, any point-sampling scheme is potentially flawed.

A substantial reduction in the number of core samples could be achieved if better tools were available with which to prepare a drilling plan. These tools would create a "map" of the subsurface features, with nearly continuous spatial coverage. Advanced ground-penetrating radar (GPR) is one such tool that may offer the performance necessary to create these maps. Such a system could be used in conjunction with conventional core-and-analyze techniques to substantially improve remediation efficiency.

1.1.2 Application of Ground-Penetrating Radar to Remediation

The Risk Reduction Engineering Laboratory (RREL) of the Environmental Protection Agency (EPA) has investigated the feasibility of using remote sensing techniques for a variety of subsurface detection problems. For example, acoustic emission techniques have been used to detect the failure of earthen structures such as dams, embankments, and so on [1]. The RREL has also examined the feasibility of using acoustic sounding techniques, but problems were encountered in efficiently coupling the transmitted pulse to the ground. Recently, the RREL investigated the use of 17 different remote sensing techniques for the detection of buried containers [2]; this effort entailed an extensive literature search and a field evaluation of four of the remote sensing systems. One of these systems was a short-pulse GPR; this system had advantages over the other three methods examined (a metal detector, an electromagnetic induction system, and a magnetometer) because it could detect both metallic and nonmetallic buried containers.

RREL also evaluated the potential of continuous-wave (CW) and short-pulse GPR techniques for mapping subsurface features [3]. Only limited success was achieved with the CW system; however, as noted by Koerner and Lord in this work, further improvements to the electronics and signal processing would be required before any definitive conclusions could be made about the capability of the CW measurement approach.[1] Better success was achieved with the more conventional short-pulse GPR, but again the authors pointed out similar shortcomings in the system used in the evaluation.

GPRs have been proposed repeatedly for applications involving sensing or mapping the location (or likely location) of underground contaminants. Some experimental evidence of the successful use of GPR for this purpose has been presented. However, this evidence is largely anecdotal and lacks quantitative support. Thus, those positive results appear as special cases that cannot be extrapolated to general situations. This deficiency arises from the lack of a quantitative model for the effect of contaminants on those properties of soils that affect GPR performance and, hence, GPR performance specifications. The work described below will show that the lack of success in these prior programs can be largely ascribed to use (or considerations) of radars whose performance levels are insufficient for the task and to a need for much more intensive data processing.

While the literature indicates that radar measurement systems may have the potential to improve remediation efforts, such potential has yet to be realized. Three key elements are lacking in the radar studies: (1) a quantitative model of the effect of contaminants on the radar-relevant properties of soils, (2) understanding and "matching" the radar characteristics to the environment and the target(s) to be detected so as to get the best possible signals, and (3) developing the signal-processing methods to take best advantage of the signals returned from the subsurface scatterers.

---

[1] In principle, the CW system was capable of excellent performance; its main deficiency was that an inadequate number of discrete CW frequencies were available for use. It will be seen later that a multiple-tone CW system with a large number of frequencies constitutes a "synthetic-pulse" radar, which offers a potential performance greatly exceeding that of a conventional, short-pulse GPR.

This report describes the results of a program whose purpose was to examine potential radar designs and signal-processing concepts in terms of estimated radar performance in various soil conditions and stratigraphy, with various moisture levels, and with various objects and contaminants. The design elements included radar parameters (e.g., center frequency, bandwidth, power, receiver sensitivity, dwell time, and so on) and signal processing concepts (real aperture and synthetic aperture) that would allow researchers to "match" the soil and detection targets (objects and contamination materials). Matching the radar design to the environment is important since the performance of a ground-penetrating radar is related to the environment in which it must operate. Generally, the lower the frequency and the higher the power, the better the penetration of the electromagnetic wave into the soil. However, lower frequencies will result in poorer spatial resolution. Thus, an optimum balance is sought; this work seeks to determine that "optimum" design.[2]

1.1.3 Report Organization

Section 1 of this report gives some background information on ground-penetrating radar and describes the objectives of the work assignment reported here; it also outlines the technical approach taken to accomplish the objectives.

Section 2 provides the conclusions resulting from the technical work, and highlights the key technical findings of each of the task elements.

Section 3 recommends that a "proof-of-principle" experiment be conducted to confirm and validate the findings of this work assignment; Section 3 also summarizes the rationale for this recommendation based upon the findings reported in this work.

Section 4 of the report introduces the technical effort with a brief discussion of ground-penetrating radars and how they compare to ordinary "air-path" radars. This section describes the key differences between a "real-pulse" radar and a "synthetic-pulse" radar---the two types of radars considered in this work. The section also includes a brief discussion of real-aperture and synthetic-aperture (coherent) signal processing---the two signal processing methods discussed in this work.

Section 5 of the report introduces and develops the concept of a "figure of merit," Q, that expresses the performance of the GPR radar system (radar plus signal processing plus environment) in terms of a single number. After this concept has been developed, Qs for existing real-pulse and synthetic-pulse radars are calculated based upon information provided by the manufacturers; the effect of processing gain is discussed; and the environmental contributions in Q are defined in terms of the radar cross section of the scatterers in the environment. This section shows that the potential performance of synthetic-pulse radars is 40 dB to 60 dB greater than that of real-pulse radars.

---

[2] In the context of the work described here, "optimum" refers to the best balance of radar designs from among those considered, in the context of a given set of environmental parameters (soils and targets).

Section 6 describes the soil modeling work performed in support of the radar design objective. This section summarizes the classification of soil types and the broad distribution of these soils throughout the United States, and then discusses the electromagnetic characteristics of various soils and some likely contaminant materials. Following this, two basic soil/contamination geometries are introduced. These two geometries, which can be used to represent a wide variety of possible subsurface conditions, are used as the basis for the detection strategies, presented in Section 7.

In Section 7, Q and the soil models are brought together. Here, a Q_{min} is determined as the minimum value of *radar* Q necessary to detect various types of contamination in various geometries, for various signal processing schemes. The section addresses the issues of particle size and moisture content and how they relate to the detection problem, as well as the contamination geometry. Section 7 will show that to detect a contaminant layer at a depth of 10 m in moderately dry, moderately fine-particle soils, a Q of about 160 to 180 is needed---a Q that can be achieved with a real-pulse radar and coherent processing. To detect a contaminant plume at 10 m in this same soil, however, a radar with a Q of 200 to 220 is required; this Q can be achieved with a synthetic pulse radar and coherent processing.

Section 8 describes the design of the radar, drawing on the results of the previous sections. The radar design, defined in terms of Q, is heavily dependent upon the environment in which it must operate and the targets it must detect in that environment. A table is presented that summarizes the required Q for a variety of soil environments, targets and target depths.

Section 9 provides a description of and the results obtained from a numerical model that was developed to estimate GPR radar propagation and scattering in any desired scenario, and to provide displayed examples of radar output for various spatial sampling schemes. The data in this section complement that of Section 7 and graphically illustrate the need for high-Q radars and coherent processing techniques for tasks that entail the detection of low-cross-section targets in difficult environments.

Some of the key reference material used during the performance of this work assignment is listed at the back. In addition, there are four appendices that describe particular aspects of the work in Sections 6 and 7.

1.2 Objectives and Approach

1.2.1 Objectives

The objective of the work reported here is to determine the circumstances under which a GPR can be used for more effective remediation of a release of petroleum or other chemical substances into the soil and groundwater. In particular, the goal is to determine whether a radar with appropriate signal processing can achieve significantly better performance against remediation targets (soils and contaminants) than prior results have shown and whether such a radar warrants a number of proof-of-principle and demonstration-measurement programs. In this context, "more effective remediation" means a reduction of, or better placement of, monitoring wells required for initiating, tracking, and verifying remediation. To realize a substantial improvement over conventional monitoring techniques, it is necessary to show that a radar system can be used to: (a) rapidly develop accurate maps of the main features of the subsurface topography with sufficient resolution to improve the placement of monitoring wells and reduce their number, and (b) develop maps of subsurface objects and contaminated regions.

This objective entails radar design and trade-off studies to "match" the radar configuration and signal processing to the resolution, sensitivity, and depth penetration necessary for the radar to "see" the subsurface features and detect contaminated regions.

1.2.2 Technical Approach

Prior work ([4], [5],and [6], for example) has shown that the propagation of electromagnetic energy through soils is determined by the frequency of the propagating wave and the electrical properties of the propagation medium, in particular the *dielectric permittivity*. (The dielectric permittivity is used to calculate the complex dielectric constant, complex reflection coefficient, loss tangent, and attenuation coefficient). Thus, before the performance of various ground-penetrating-radar and processing designs can be assessed, the properties of the medium in which the radar waves will propagate must be determined. Accordingly, the approach selected for this work initially concentrated on finding a suitable soil model---one that could express the electrical properties of soils over the range of frequencies of interest.

After a suitable soil model was located and implemented, two additional radar-performance models were developed that used the soil model as a source for input parameters. One model developed was analytical; this model examined radar performance using the *radar equation* as the starting point. A second, numerical, model was also developed. This model calculated and visualized the radar processes as seen in (x, depth) "slices" through the soil. In addition to creating visual examples of the radar processes for both real-aperture and synthetic-aperture radars, the numerical model allows the consequences of various spatial sampling schemes to be explored. These two models calculate and (in the case of the numerical model, visualize) radar performance in terms of engineering units---watts, radar cross section, time, meters, and so on---units that are both meaningful and essential to a quantitative understanding of how various configurations might be expected to perform in different conditions.

An assessment of radar performance in situations representative of actual sources, contaminants, and hydrogeology requires that these conditions be somehow presented to the radar modeling codes. To this end, three soil-contamination geometries were developed in this work. These three geometries can be configured to comprehend seven of the ten hydrogeological/contaminant scenarios posed by the EPA as "...common combinations of sources, contaminants, [and] hydrogeology" [7].[3] These three geometries were used to represent various generic conditions. Assessment of the performance of the radars and signal-processing methods was accomplished by comparing the outputs of the analytical and numerical models for various types of radars and their characteristics and for real- and synthetic-aperture signal-processing methods, and for various combinations of soil, moisture content, and contaminant configuration.

While an assessment can be made based upon relative performance, a complete assessment of a selected design must include one or more detection strategies, that is, estimates of how the radar data are used to detect the selected targets (objects and/or contaminants), and estimates of how well the system would work in various environmental conditions. To this end, this work also included the development and evaluation of the detection strategies necessary for successful utilization of the best design resulting from the analytical and numerical models.

---

[3] Leaks over two connected aquifers, over crystalline fractured rock, and over karst terrain are not presently incorporated into Vista Research's model.

Section 2
CONCLUSIONS

The objective of this study was to determine under what circumstances and with what configuration a ground-penetrating radar can be used for more effective remediation of release of petroleum or other chemical substances into the soil and groundwater. In the pursuit of this objective, several radar-system alternatives were considered---each of which was based upon existing, and therefore, achievable, technology. The system realization has both hardware and software (i.e., signal processing) alternatives.

The consideration of alternative designs for the radar system required the development of a "figure of merit," which was derived from fundamental and well-founded radar design principles and which encompassed hardware and software considerations. This work considered the relative performance of several existing radar designs: a typical short-pulse radar, a short-pulse radar with higher transmitter power, and a synthetic-pulse radar. The results of this work showed that, although the short-pulse and synthetic-pulse radars were mathematically equivalent, the synthetic-pulse radar offered 40 to 60 dB better performance than the short-pulse radar because the former could transmit far greater power per spectral line than the latter. Furthermore, the results of this stage showed that, while the improved performance offered by the synthetic-pulse system was not often needed for the usual "hard-target" GPR applications, such improvements are essential for the detection of small changes in dielectric constant such as would be expected in a situation where a small region (or thin layer) of contamination was encountered.

Two signal-processing methods were also included in this stage of the work: real-aperture and synthetic-aperture (SAR) processing. The results of this work showed that synthetic-aperture (coherent) processing offered a significant advantage for remediation applications over the usual incoherent processing because such processing, while computation-intensive, afforded a higher effective of signal-to-noise ratio and reduced clutter from adjacent reflections. To detect modest levels of most common contaminants, at depths of 10 to 15 m, and in moderately conducting soils, it was estimated that a combined radar-processing figure of merit of 200 to 220 dB is necessary. Considering the current radar technology, it was determined that this level of figure of merit could only be achieved by combining a synthetic-pulse radar with synthetic-aperture processing. It was also determined that one can obtain an additional processing gain of 35 dB by using a 3000-s observation time to collect data from a three-dimensional volume and then SAR-processing these data; the figure of merit could thus be effectively increased by 35 dB, which would mean better performance of the GPR in detecting the desired target.

As part of the radar design assessment task, a numerical model was developed that could illustrate the nature of radar returns from various modeled soils and geometries, and show the processing gains of different signal-processing methods. To support this effort, a model was developed that described the electrical characteristics of soils and of various potential contaminant materials at radar frequencies from about 20 MHz to about 200 MHz. This work determined that, for the radar frequencies considered, the dielectric constant and attenuation coefficient associated with these soils (with the exception of wet clays and ionic (salt-laden) silts and sands) were not fundamental obstacles to the propagation of radar energy through the medium. Further, this work showed that, for the range of radar frequencies most suitable to radar energy penetration to a working-goal-depth of about 10 m (in nominal soil conditions), consistent with the bandwidth necessary for adequate resolution, the dielectric constants and attenuation coefficients were nearly constant over the spectral range.

The second stage of the work entailed the development of useful geological and contamination geometries that could describe various contamination layers and plumes. These geometries were needed so that the performance of the radar designs could be tested against the modeled electrical characteristics of the bulk materials. This work led to the development of three essential geometries that represented seven of the ten "common cases" of remediation configurations described by the EPA.

One important outgrowth of this work was that it became clear that a "typical" remediation site suitable for a baseline test could not easily be defined, because the soil properties, moisture content, and contamination environment differed dramatically at each of the sites described in the literature. An almost limitless combination of factors could be ascribed; this made the radar design assessment difficult because not every combination could be addressed. To deal with this lack of a "typical site," a generic soil condition (comprised of a sand-clay mixture) was selected. The assessment work entailed adding various moisture and contaminant contributions to this soil mix, appropriate to the geometry considered. This "soil" is roughly equivalent to the "synthetic soil matrix" (SSM) developed by the EPA as representative of Superfund sites [8,9].

The numerical model allowed the effects of various spatial sampling schemes to be examined. This model showed that, with the incoherent signal processing usually applied to GPR data, the wide beamwidths associated with GPRs created a confusing display of the subsurface environment; these results were consistent with the images usually created by commercial GPRs. The numerical model also showed that when synthetic-aperture processing was used, the background noise in the radar images was reduced and discrete scatterers in the radar field of view were tightly localized.

A significant portion of the design assessment task addressed various detection strategies. That is, given a radar and a geometry, this work sought to identify key strategies that could be used to deduce the presence (or lack) of contamination in the subsurface returns from the processed data. This was a central effort in the work (after the basic feasibility of using synthetic-pulse radar and SAR processing for remediation support had been established). This work resulted in two novel findings. First, it appears that for contaminants with low dielectric constants (which includes most non-ionic materials), there can be large contrasts in volumetric scattering (up to 7 dB) between contaminated and uncontaminated regions. Such contrast ratios are well within the detection range for a system with a high figure of merit, such as the synthetic-pulse radar with SAR processing designed in this work assignment. Second, it was determined that a thin layer of contaminant "floating" on the water table will produce a measurable signal if the layer is more than a few centimeters thick; the appearance of such a signal at some point in a survey would indicate the presence of contaminant there. However, the nature of this signal is such that it might be difficult to distinguish it from a local change in the depth of the water table, so its overall utility is questionable, even though it is surprisingly strong. On the other hand, thicker layers will produce a strong and distinctive signal. Strong signals will also be produced if abrupt transitions are induced at the boundaries between a lighter, immiscible contaminant and a water table with gradually increasing saturation. It is shown that volumes of pure fine and very fine soil particles (such as found in silts and clays) can greatly degrade the performance of a GPR. These soils are usually found with some fraction of larger imbedded particles such as sand grains. The analytical model has determined that the presence of these larger particles facilitates the detection of contaminated regions.

Section 3

RECOMMENDATIONS

This work assignment has shown that, for the environments and contamination geometries modeled here, a radar with a high figure of merit combined with coherent signal processing can detect contamination under a wide range of conditions. Such a radar can be achieved with existing technology.

The scope of the work accomplished here, however, represented an idealized soil environment and did not comprehend a largely inhomogeneous propagation medium. In an extreme case, this type of soil environment can lead to poor estimates of the radar propagation velocity, which limits the ability of the coherent processing to properly "register" the scatterers. It can also lead to an increase in the radar clutter field, which decreases the otherwise achievable signal-to-noise ratio. On the other hand, the detection of contaminants is facilitated by the presence of small irregularities in an otherwise "pure" soil as a result of the increased volume scattering that occurs.

While the results of the work assignment showed two-dimensional coherent processing (surface distance, depth) was necessary to detect, deep, low-contrast targets, important performance gains could be achieved using three-dimensional techniques (surface area, depth). This type of data collection (and processing) will be necessary in order to enhance weak targets in a cluttered environment, and it is essential to provide a vehicle for "intelligent," understandable displays.

Thus, while the results of this work indicate that ground-penetrating radar is likely to be useful in improving remediation work under many circumstances, they are based on modeled data and cannot be considered conclusive. While modeling of environments is possible in principle, such work would not (because of the clutter) realistically or economically model any particular environment. Therefore, unless an experiment is performed to test and validate the models and the findings resulting from this work, the use of GPR for remediation purposes will remain an unanswered question.

It is recommended that an experimental program be conducted, using a synthetic-pulse radar combined with synthetic-aperture signal processing. It is recommended that the initial experiments be "proof-of-principle" measurements. The objective of these initial experiments would be to calibrate a GPR in terms of figure of merit and other needed parameters, and to collect a limited set of subsurface data at a quantified site so that the findings of this work could be validated and the use of high-figure-of-merit radars in real environments might be better understood. It is further recommended that in the initial experiments data be collected and coherently processed three-dimensionally.

To the extent the proof-of-principle is successful and confirms the potential for using radar in remediation work, an expanded measurement and demonstration program could be undertaken.

Section 4

RADARS AND RADAR SIGNAL PROCESSING

The object of the work reported here is to determine if a ground-penetrating radar can be used to detect subsurface contamination. Thus, radar concepts and radar signal-processing techniques are inseparably intertwined with the electromagnetic properties of soil and contaminants. While it is not the purpose of this report to provide an exposition in the area of radars and signal-processing methods, some tutorial information about radars and radar signal processing may be desirable as a background for the more detailed descriptions provided later. Therefore, this section of the report provides a brief overview of some essential radar and signal processing concepts.

4.1 Radar Fundamentals

RADAR is an acronym for RAdio Detection And Ranging. A radar operates by radiating electromagnetic energy and detecting the echo returned from objects that reflect the incident energy. The amount of energy reflected from electrically nonconducting, or weakly conducting, objects (e.g., rocks, plastic pipes, etc.) is related to the differences between the *dielectric constant* of the object and the dielectric constant of the surrounding medium. A metallic, conducting object (such as a drum or pipe) is usually a better reflector than a nonconducting one. The radiated energy of a radar (the transmit *waveform*) is usually a short *pulse* or series of pulses, but some specialized radars use other types of waveforms.

The character of the detected echo can provide information about the reflecting object(s) [10]. For example, the distance to the reflecting object(s) can be determined by measuring the time delay between transmission and echo reception and multiplying by the speed of propagation of the electromagnetic energy. Or, the amplitude of an echo signal can be used to gain information about the scattering properties of the target object, or object's size, if the radar system is calibrated and if it has sufficient range resolution. In a *coherent* radar system, the phase of the detected echo can provide information such as the speed of the target (actually, the vector component of velocity directed towards the radar), or its scattering properties. A high degree of coherence means that the relative timing and frequency of the radar signals are well controlled or measured (to a small fraction of the period of the radar center frequency); coherence is an essential requirement for synthetic-aperture radar and synthetic-pulse radar signal processing.

A block diagram of the basic parts of a generic radar system appears in Figure 4.1. In this radar, the oscillator is used as the basic frequency reference, and the waveform generator acts to gate the oscillator signal on and off to form pulses. The clock is used to control the timing of the signals; that is, the width of the pulse, the pulse repetition frequency (prf) (i.e., the temporal spacing between successive pulses), and so on. The power amplifier boosts the low-level voltages from the oscillator/waveforming circuits to high levels for transmission. The T/R switch serves to isolate the transmitter section of the radar from the receiver, since a powerful signal injected into a sensitive receiver could damage or introduce non-linear saturation effects in the sensitive front end of the receiver.[4] In most cases, the radar antenna is built with significant directionality (or high gain or narrow beamwidth), so that the radar has the ability to resolve targets in angle, or has angular resolution. A notable exception to this is the case of a *synthetic aperture radar*, where the antenna is often physically small to achieve a wide beamwidth, and directionality is obtained through movement of the antenna. Signal processing is used to focus the number of wide beams into a single tightly focused beam, as described in a later section.

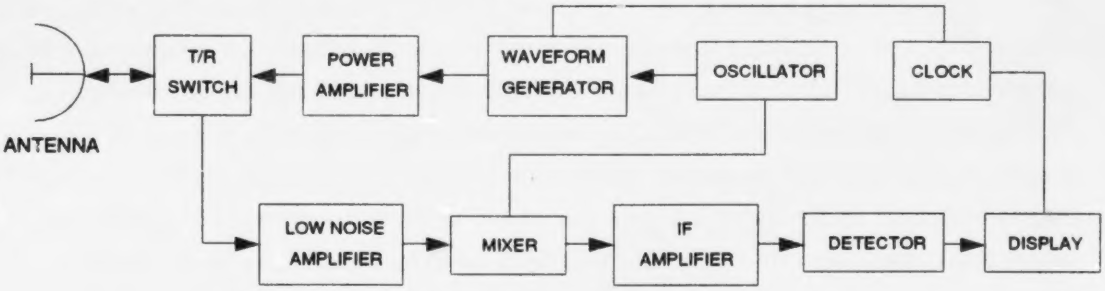

Figure 4.1. Block diagram of a generic radar.

The receiver section of a simple radar is usually comprised of a low-noise amplifier, followed by a mixer, followed by amplification and display. The echo signal returned to the radar is greatly reduced in amplitude compared to the strength of the transmitted signal. This is due to three main factors. First, beam spreading the causes the power density of the transmitted pulse to decrease as it propagates away from the radar. Second, the target intercepts and then scatters back only a fraction of the energy incident on it. Finally, the receiving antenna intercepts only part of that scattered energy. In addition to these factors, the propagating medium itself can absorb some of the energy propagating in both directions (in air this *path attenuation loss* is generally small, but for a ground-penetrating radar the attenuation can be very high). Furthermore, the antenna itself is not 100% efficient in radiating (and receiving), since some energy is absorbed in the antenna itself and some is reflected away. Thus, to pick up the returned echo, the radar's receiver must be very sensitive. Furthermore, the receiver must be *low-noise* so that the echo signals are not dominated by the internal "electronic" noise in the receiver.

---

[4] Directional couplers, or separate but closely spaced transmitting and receiving antennas, are sometimes used instead of a T/R switch.

As the echoes are returned to the antenna, they are amplified and mixed with signals from (or derived from) the reference oscillator to create an intermediate frequency; then they are detected to recover the time series of the echo(es). In a more complex radar, the mixer and detector might be replaced by a coherent detector that senses the phase relationship between the transmitted and received signals, thus providing the *complex* or *quadrature* components of the echo(es). The coherent signals can provide information about the radial velocity of the echo(es) by means of the temporal Doppler frequency shift, and other useful information, as described below.

There are many different types of displays for radar information. The simplest is the *A-scan*, illustrated in Figure 4.2a, where the time series of the returning echoes are individually shown on a cathode ray tube (CRT), for example. By saving the echoes and displaying a series of them displaced vertically or laterally, a *B-scan* (or *waterfall)* display can be created, such as is illustrated in Figure 4.2b.[5] If the radar antenna rotates, the A-scan data can be saved and displayed on radial lines corresponding to the pointing angle of the radar antenna. If the amplitude of the echo is represented by the intensity of the corresponding displayed point, a *PPI* display is created, as illustrated in Figure 4.2c; this is the most common display format for search-and-track radars. (It is noted that data from ground-penetrating radar are usually displayed in an intensity-modulated version of the B-scan format).

Radar echoes are usually measured in time, from the time of transmit to the time the echo is received. The distance between the radar and the echoing object is determined from the range equation

$$R = c_p\left(\frac{\Delta t}{2}\right), \tag{4.1}$$

---

[5] In traditional GPR work, this display is often referred to as a "wiggle" plot.

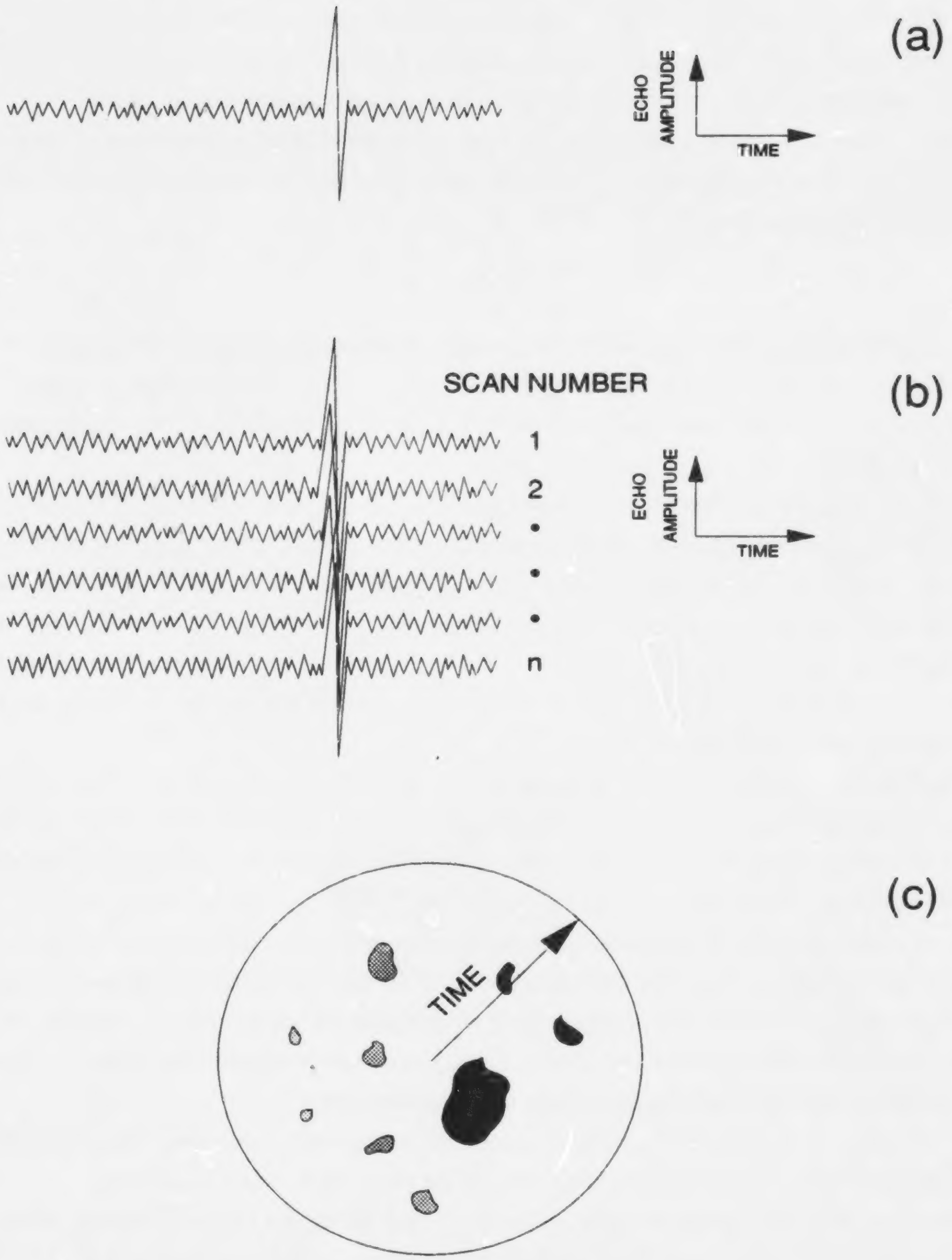
(a)
ECHO AMPLITUDE
TIME
SCAN NUMBER
1
2
•
•
•
n
(b)
ECHO AMPLITUDE
TIME
(c)
TIME

Figure 4.2. Examples of radar displays.

where R is the distance to the echo, Δt is the time difference between the transmitted and received signals, and c_p is the speed of propagation of the radar energy in the medium. The range resolution of a radar system is determined by the spectral bandwidth, B, of the system---wide-band systems imply short-duration pulses and thus better resolution or ability to separate two closely spaced echoes. That is, the range resolution is related to the pulse width, $\Delta\tau\,(\approx 1/B)$, according to

$$\Delta R = c_p\left(\frac{\Delta\tau}{2}\right). \tag{4.2}$$

For example, a radar with an effective pulse duration of 10 ns requires a bandwidth of 100 MHz. In air, its resolution is 1.5 m (4.5 ft). In soil, it will be about half that, or about 0.75 m (2 ft). Note that a recording bandwidth of about 100 MHz would be required to capture the radar signals.

The radar principle has been applied to systems operating at a wide range of frequencies, from high-frequency (HF) radars that operate at a few megahertz to laser radars that operate at optical frequencies. While radar was originally developed as a military tool to detect and track aircraft and ships, it has established itself as an important instrument in civilian areas such as environmental monitoring (weather radar) and law enforcement (speed radars). Radar is also establishing itself in civil engineering, where it is being used for nondestructive testing, fault location, and other applications.

There are literally dozens of variations on the basic radar theme described above. Most of these variations serve to optimize radar performance for a particular mission or objective. Each of these variations may include coherent and incoherent radars, encompass numerous transmit waveforms (e.g., simple pulse, chirped pulse, CW, and others) and antenna configurations (e.g., steerable antennas, phased arrays, synthetic arrays, and so on), and each may utilize a variety of signal-processing techniques appropriate to the mission. Some are designed for the detection of motion or temporal change; others are designed for the precise measurement of range and angle. Still others are designed to quickly search or examine broad volumes of space. Some designs are best suited for airborne or space applications.

When one considers the essential requirements for a ground-penetrating radar, most of the specialized radar types can be eliminated, leaving the basic pulse radar. In ground-penetrating radar, the basic pulse radar is commonly referred to as a *short-pulse* radar, implying that the radar has a wide bandwidth. Another type of ground-penetrating radar is the *synthetic-pulse* radar. While these two radars are mathematically equivalent, the differences in the way the equivalent temporal transmit waveforms are formed lead to significant implementation and performance differences. Conventional, short-pulse GPRs and synthetic-pulse GPRs are discussed and contrasted in Section 4.3.

4.2 Ground-Penetrating Radars

Radars have traditionally been used to search for (and track) air-, sea-, space-, or land-based targets from ground-based, airborne, and space-based platforms. In these applications, the propagation medium is air (or vacuum) and the propagation velocity is essentially constant at 3 x 10^8 m/s (air density fluctuations can affect radar signals to some degree). However, since electromagnetic waves can penetrate rock and soil to varying degrees, the system can become a ground-penetrating radar. There are, however, significant differences between GPRs and free-space radars in terms of both propagation and echoing characteristics. For a GPR the propagation medium has a strong influence on the radar signals; it is usually highly variable from one location to another and generally inhomogeneous at every location. In particular, soils contain varying degrees of water and ionic materials that strongly affect the propagation and attenuation of the electromagnetic wave. Generally, the speed of propagation of the radar signals will be much slower for GPRs than for free-space radars; if the propagation medium is inhomogeneous, the propagation speed will vary with position. These media are also sometimes dispersive, so the propagation speed varies with the radar frequency (even across the bandwidth of the radar).

GPRs generally differ from conventional radars in several significant ways. First, they need to operate at short range and with high resolution, both of which imply a wide bandwidth (or a short pulse length). Second, the attenuation of electromagnetic waves in the ground generally increases substantially as the center frequency of the radar is raised, thus making low-frequency operation more desirable. GPRs thus tend to have remarkably high ratios of bandwidth to center frequency, or a high *fractional bandwidth* (fractional bandwidths of GPRs often exceed unity, and the concept of a "center frequency" can itself become fuzzy). Figure 4.3 illustrates some features of a typical GPR pulse, which here is one and one-half "carrier" cycles long. Special techniques have been developed over the last two decades to generate the required wideband signals; these technologies have led to the successful commercial use of GPRs. Figure 4.4 shows a block diagram of a typical short-pulse GPR.

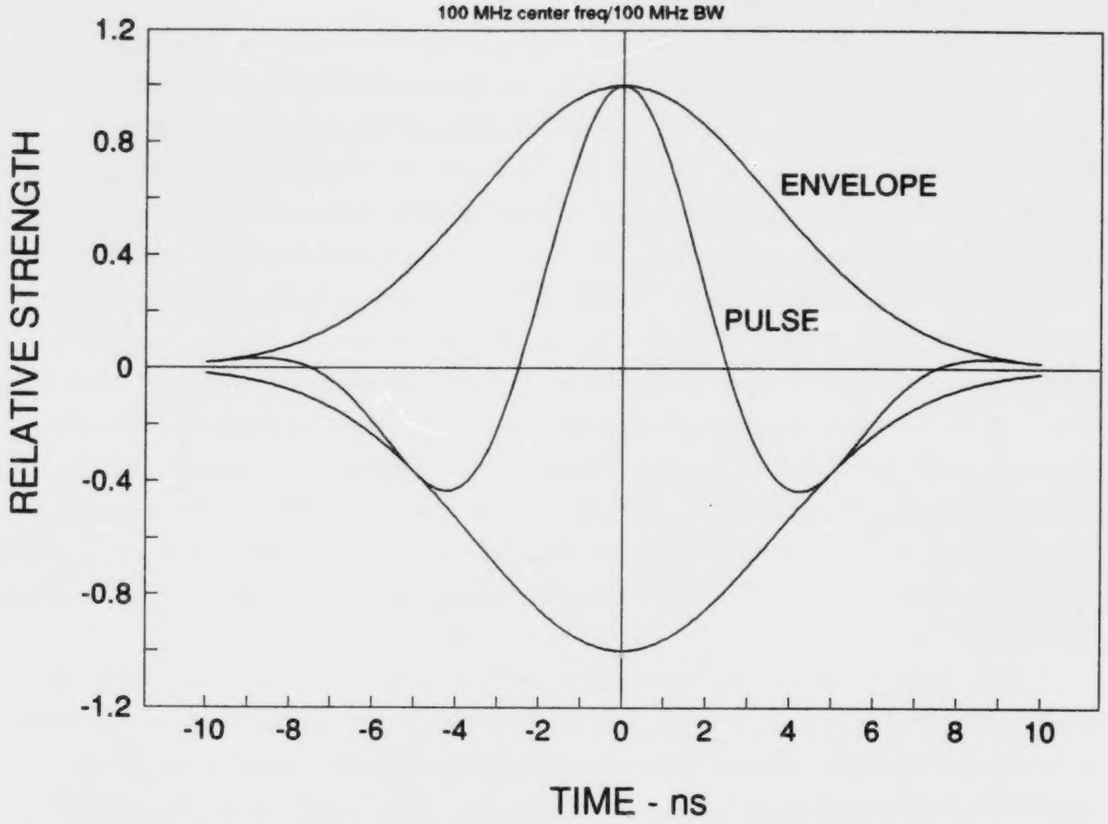

Figure 4.3. Typical GPR pulse waveform.

Perhaps the most distinguishing feature (and limiting factor) of a GPR is the antenna. Clearly, GPR antennas must themselves have wideband capabilities. They need to be in intimate contact with the ground to avoid reverberations due to signals reflecting back and forth between the surface and the antenna.[6] For the same reason, the transmission line coupling the transmitter to its antenna must be as short as possible to minimize reverberations due to impedance mismatches at either end. Waveguide transmission lines are also to be avoided because they are dispersive and have limited bandwidths. Multi-element and large antennas are generally ruled out because (1) there will be unacceptable differential delays between the arrival times of the radar pulses at the individual elements, (2) they require the use of long transmission lines, and (3) it would be difficult to move such an antenna around. Consequently, GPRs characteristically

---

[6] This is a problem for airborne GPR systems, which are used when rapid surveys under difficult or immediately dangerous conditions are required. Besides being costly, airborne GPRs incur a sizable system penalty due to poor transmission through the air/ground interface (which can be avoided in non-airborne GPRs by designing the antennas to operate efficiently when in contact with the ground). Reverberation has been a problem for helicopter-borne systems under low-altitude flight conditions. (Airborne GPRs are not, in the present analysis, under consideration for remediation purposes.)

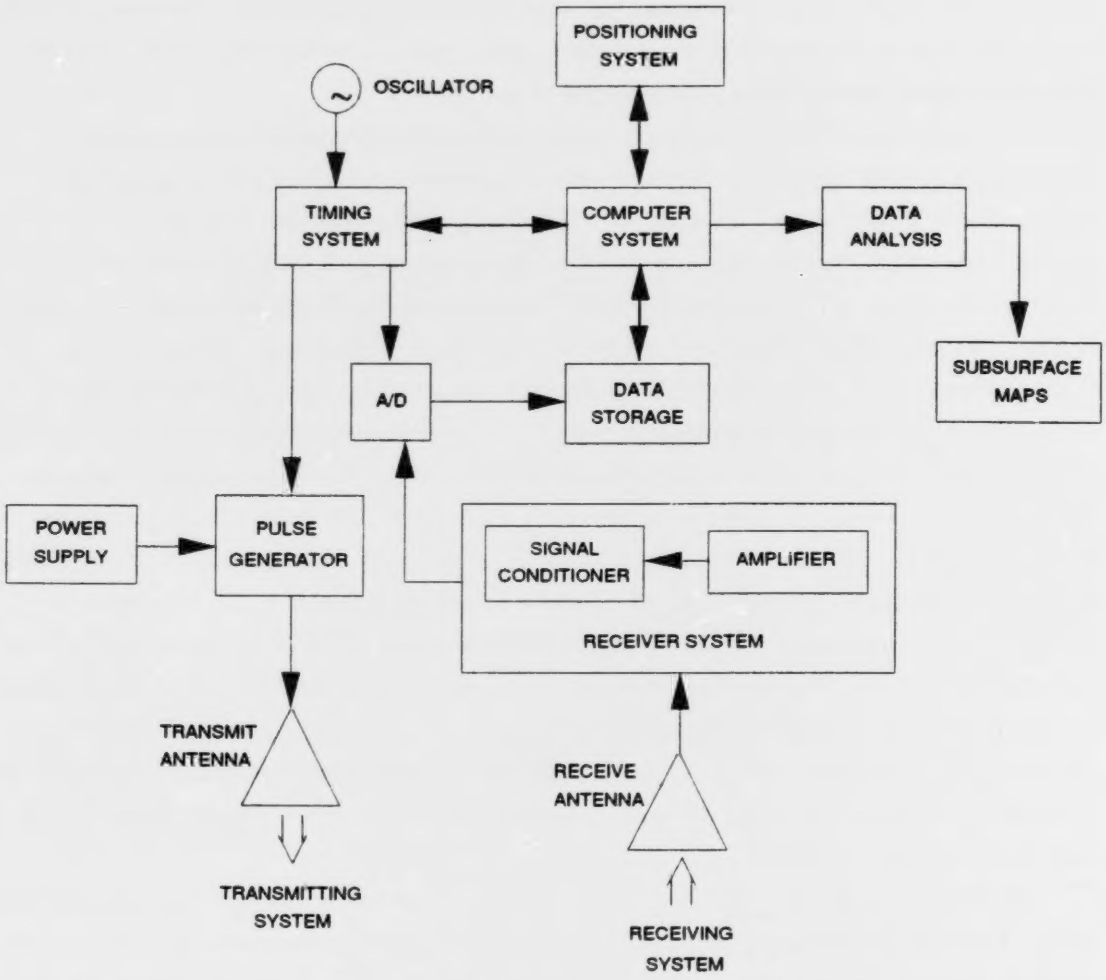
POSITIONING SYSTEM
OSCILLATOR
TIMING SYSTEM
COMPUTER SYSTEM
DATA ANALYSIS
SUBSURFACE MAPS
A/D
DATA STORAGE
POWER SUPPLY
PULSE GENERATOR
SIGNAL CONDITIONER
AMPLIFIER
RECEIVER SYSTEM
TRANSMIT ANTENNA
RECEIVE ANTENNA
TRANSMITTING SYSTEM
RECEIVING SYSTEM

Figure 4.4. Block diagram of a short-pulse GPR.

have small antennas and hence little directionality. In addition, the customary GPR antenna must couple the radar power into (and out of) the soil as efficiently as possible while minimizing radiation into the surrounding air to avoid contaminating the radar signal with unwanted echoes from above-ground objects and structures.

Considerable effort has been expended to develop optimum GPR antennas. Because it is small and affords a wide bandwidth, the most common type is a "bow-tie" dipole antenna (similar to those used for UHF TV reception--which is also a wideband application) that has been placed in a metal cavity loaded with lossy material. These lossy materials act to impede radiation into the air and to improve the coupling into the ground. To avoid using a transmission line, the transmitter is usually integrated into the antenna. Typically, the transmitter itself is merely a narrow-pulse generator. In this configuration, the transmitting antenna itself becomes the device that most strongly determines the radar-pulse duration and shape. The strength of the transmitted pulse is determined by the amount of power that can be switched rapidly. Typical short-pulse radars are limited to pulse energies of microjoules.

To avoid using a T/R switch, which would excessively compromise the transmitter performance in GPR applications, separate receiving antennas are employed. Conventional short-pulse GPRs also usually dispense with the mixing and intermediate-frequency amplification stages. Rather, the *entire* received signal (carrier plus modulation) is directly displayed, recorded, or sampled and digitized. Consequently, GPRs are intrinsically coherent radars; this feature lends GPRs to processing that requires coherence (e.g., SAR processing). Older GPRs (and, still, most commercially available ones) employ sampling oscilloscope technology to stretch the time duration of the echo-vs.-time delay (or range) to the point where it can be handled by a practical recording system. In this technique, a single sample is taken per radar pulse, and subsequent samples are taken at progressively later times with respect to the start of the transmitted pulse to build up a complete radar sweep. A large number of transmitted pulses are necessary to complete a single sweep. Time-dilation factors of 1000 are not uncommon; this, for example, would reduce the recording bandwidth requirement from 100 MHz to 100 kHz. The downside is that the radar energy is used inefficiently (which reduces its "figure of merit"). Recently, fast transient digitizers have become available; these digitizers can capture an entire radar sweep per pulse. Although such digitizers would greatly improve the effective performance of a GPR, this work was unable to identify any commercially available GPR that currently uses them.

As might be expected, GPR displays are also somewhat unconventional in traditional radar terms. The typical GPR output consists of a hard-limited, intensity-modulated plot of the echo strength vs. range. A typical output is illustrated in Figure 4.5 [11]. Very little signal processing is normally done, which accounts for the seemingly complex, busy, and difficult-to-comprehend nature of these plots. Expert interpretation is often required before one can understand this type of display.[7]

---

[7] It is likely that this situation grew out of the high cost and unavailability in field environments of the computing power needed to adequately process the data, not from a lack of understanding. Most GPR applications involve locating discrete objects in real time, which normally does not require sophisticated processing. Rather, a trained operator manipulates the radar to achieve the desired result. For the present remediation application, however, sophisticated processing is essential.

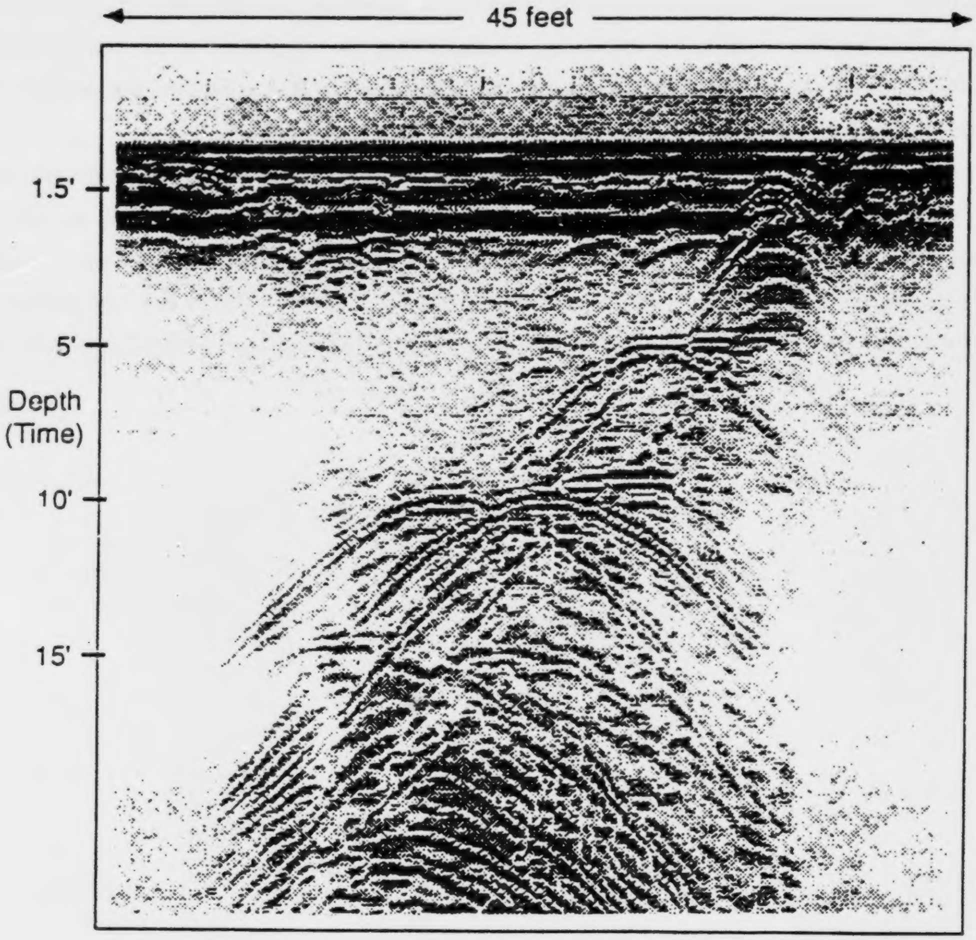

Figure 4.5. Example of a typical conventional GPR output display.

Much of the apparent complexity of GPR displays comes from the low directionality of the usual GPR antennas. Echoes from underground objects are received over a sizeable span of radar locations, which gives rise to the hyperbolic arcs regularly seen in GPR output displays. That is, radar energy reflected from a specific underground point is not well localized in the display. Another artifact typically seen comes from the fact that the data presented are essentially raw. This results in the banded appearance of echoes in typical GPR displays. As described above in connection with Figure 4.3, a typical radar signal consists of a pulse-like envelope on a carrier waveform. The amplitude and phase of the envelope carries the information. For standard GPR radars, there are sufficient cycles of carrier present to make a clear and unambiguous estimation of the envelope. For short-pulse (wideband) signals, on the other hand, the envelope cannot be easily obtained electronically, and instead, substantial computation is necessary to mathematically recover the envelope, as discussed in Appendix A. GPR manufacturers have taken the expedient of presenting the magnitude of the real signal. While this approach is certainly easy to implement, and more or less preserves the outline of the envelope, it also retains the internal structure of the GPR signal. Thus, a one-and-one-half-cycle-long GPR signal, for example, has approximately three peaks and would appear in a display as three wide, dark bands with narrower light bands in between, as illustrated in Figure 4.6. A complex, "squiggly" plot is produced when many targets are present. Multiple reflections, such as between a buried object and the surface, further confuse the raw picture. Besides merely confusing the eye, these artifacts are clutter that hide the desired information.

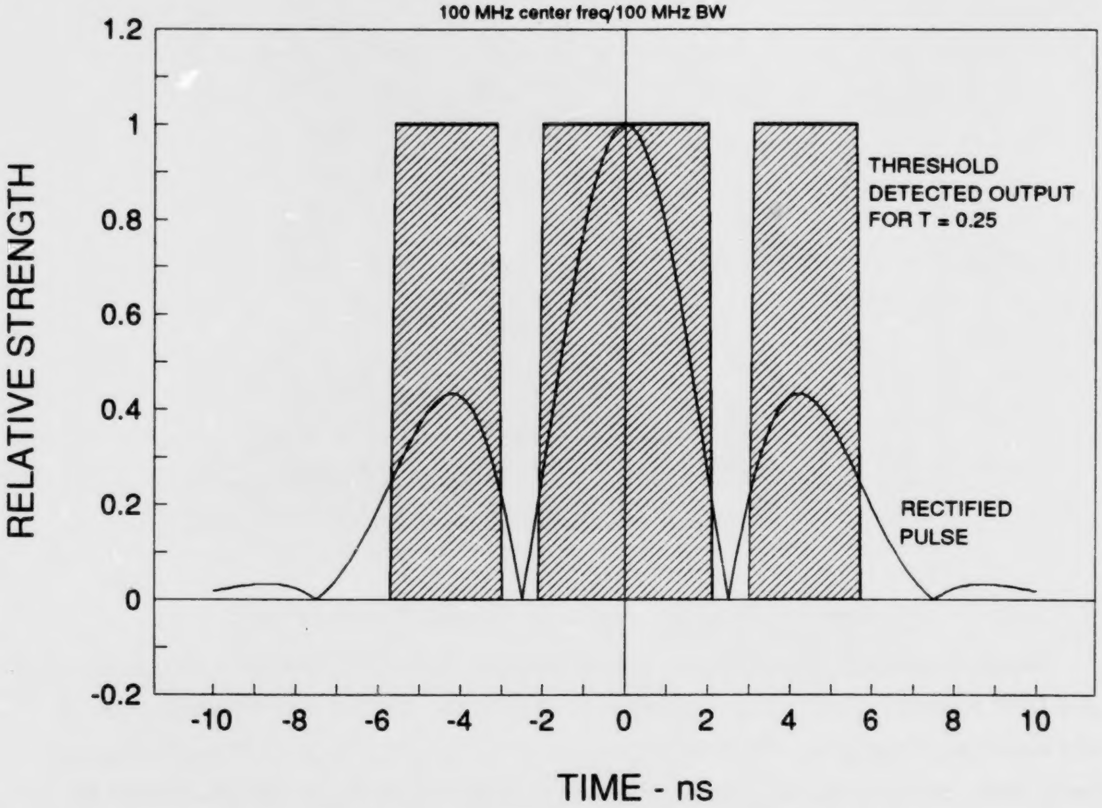

Figure 4.6. GPR pulse intensity and hard-limited output.

It was noted at the beginning of this section that the strength of an echo is related to the difference in dielectric constant between the target and the medium. For ground-penetrating radars, the differences in dielectric constant between contaminants and soils with varying features may be small. Therefore, unlike the traditional free-space radars and their targets, a GPR used to improve remediation effectiveness may not directly sense a contaminant "target" and separate these returns from the weak echoes caused by the surrounding soil. Rather, inhomogeneous soils (varying particulates, rocks, other objects, and so on) can return strong *clutter fields* that compete with the desired target, whose echoes may be weak. (Buried objects such as pipes, barrels, tanks, and so on, however, may produce strong returns with respect to the clutter.) Thus, while there are few conceptual differences between GPRs and free-space radars, the data returned by these systems may be much different and may entail different signal processing in order to extract the desired information.

4.3 Short-Pulse and Synthetic-Pulse Radars

A repetitive pulse signal such as that produced by a conventional GPR has a waveform and spectral magnitude similar to that shown in Figures 4.7a and 4.7b. The spectrum consists of a series of narrow lines separated by the prf. Its overall extent is roughly the reciprocal of the individual pulse duration, and the width of the individual spectral lines is roughly the reciprocal of the duration of the pulse train.

Since the temporal and spectral representations are a Fourier transform pair, they are entirely equivalent. Either one is a complete description of the signal. Consequently, it is possible to start by generating a spectrum of discrete electromagnetic tones, or lines, and add them together to synthesize a pulse train. Figures 4.7c and 4.7d show the direction of the process. The line spacing determines the effective prf, the overall span of the tones (or their total number) establishes the pulse width, and each line has a (narrow) bandwidth determined by its duration.[8] This scheme, of course, requires that the timing, or phase, of each line be carefully controlled.

While the short-pulse and synthetic-pulse radars are mathematically equivalent, the advantage of the latter results from the recognition that the lines do not have to be transmitted at the same time to produce, mathematically, the same result. Thus, each line can be transmitted sequentially at relatively high power without saturating the electronics. Synthesis is done after echo reception, by a computer, which is relatively indifferent to dynamic range. Of course, careful timing is necessary to synthesize the pulse train, and care must be taken to appropriately sample the received signals. Weak echoes are temporally superimposed upon a large signal due to leakage of the transmitted tone into the receiver and to echoes from the surface and from near-surface features. Clever schemes have been implemented to deal with this issue. Such schemes, combined with the long time it takes to sequentially transmit all the tones, reduce the figure of merit of synthetic-pulse GPR systems; nevertheless, the advantage gained by the synthesis process outweighs the disadvantage. It will be seen that synthetic-pulse GPRs not only do better than conventional short-pulse radars, they enable exploitation of a potentially powerful contaminant detection strategy not previously contemplated. A block diagram of a typical synthetic-pulse radar is illustrated in Figure 4.8.

---

[8] Details of these relationships are presented in Section 5.

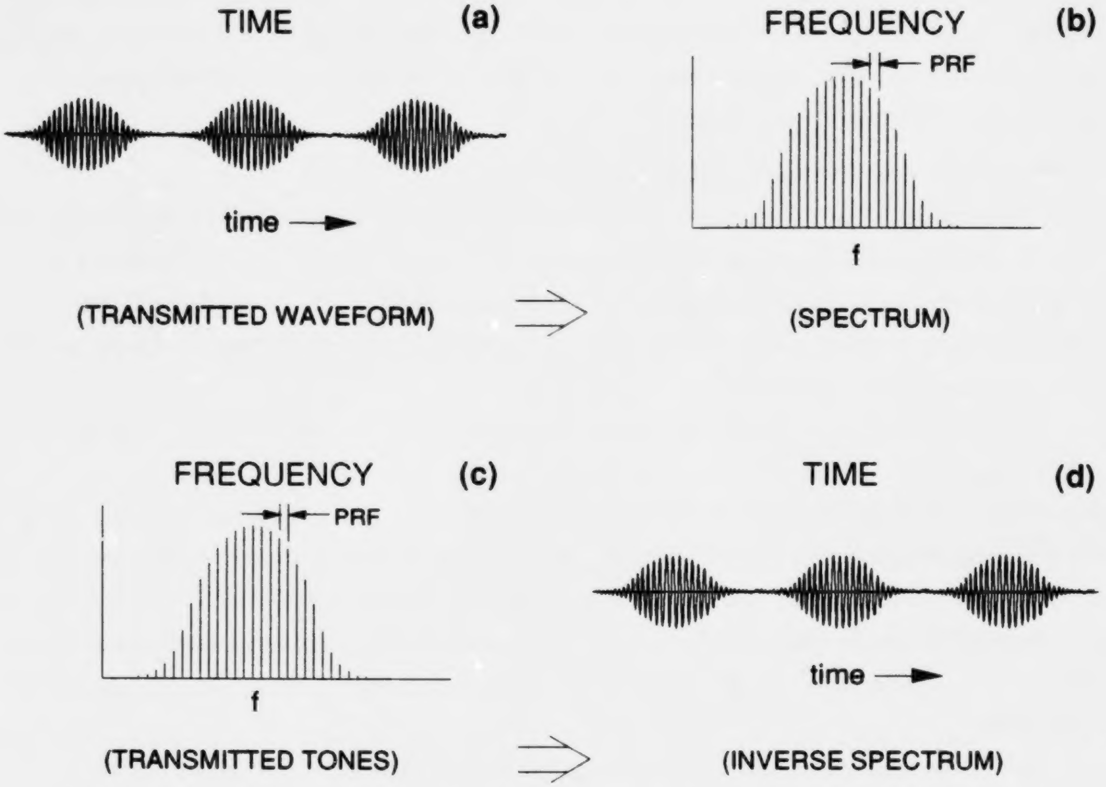

Figure 4.7. Short-pulse and synthetic-pulse radar waveforms: (a) a short-pulse radar transmits a short burst of nearly sinusoidal signals; (b) a Fourier transform gives a "spectrum" of the waveform; (c) a synthetic pulse transmits the spectrum in a series of sinusoidal signals over the range of frequencies; (d) a Fourier transform gives the effective waveform.

4.4 Real- and Synthetic-Aperture Signal Processing

The distinction between real- and synthetic-aperture radars is quite analogous to that between short- and synthetic-pulse waveforms. A narrow-beam, real-aperture antenna is many rf wavelengths wide, and, if the phasing across the aperture is done properly, instantaneously forms the beam much the same way the components of a wide spectrum add coherently to form a narrow pulse. There is an equivalent Fourier-transform relationship between the spatial signal across the aperture and the beam, and, analogously, the angular beamwidth is roughly the reciprocal of the effective aperture width measured in rf wavelengths.

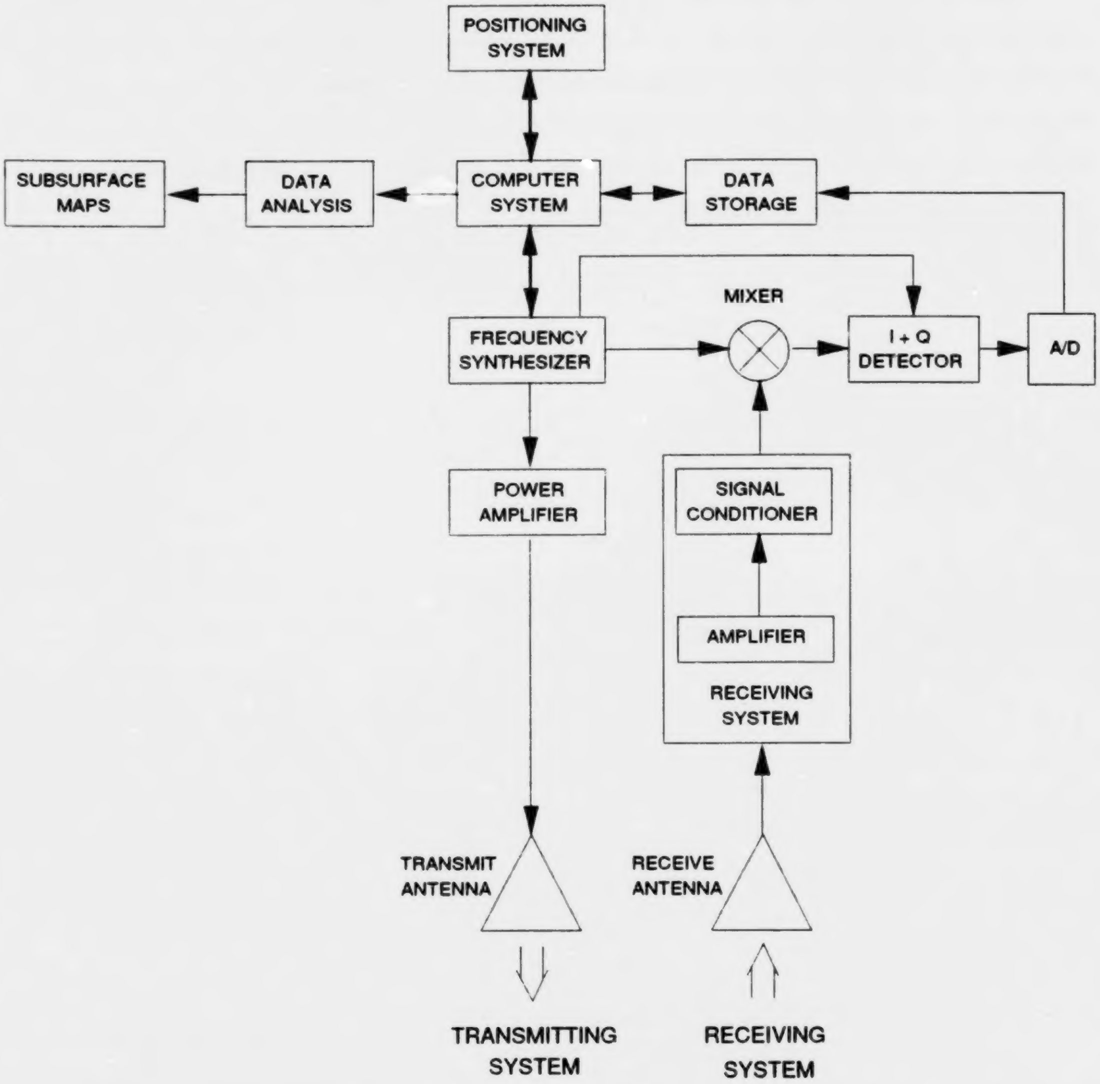
POSITIONING SYSTEM
SUBSURFACE MAPS
DATA ANALYSIS
COMPUTER SYSTEM
DATA STORAGE
MIXER
FREQUENCY SYNTHESIZER
I + Q DETECTOR
A/D
POWER AMPLIFIER
SIGNAL CONDITIONER
AMPLIFIER
RECEIVING SYSTEM
TRANSMIT ANTENNA
RECEIVE ANTENNA
TRANSMITTING SYSTEM
RECEIVING SYSTEM

Figure 4.8. Block diagram of a synthetic-pulse radar system.

Just as it is possible to synthesize a narrow pulse by sampling in the spectral domain, it is possible to synthesize a narrow beam by sampling in the spatial domain, by moving a small antenna across the span of the aperture desired for synthesis. Again, careful phasing and sampling are necessary. Various means of synthesizing apertures (i.e., SAR processing), including computer processing, have been developed. SAR systems are usually employed from airborne platforms, although the principles can be applied to GPR applications. Skolnik [10] and Brown and Porcello [12] provide excellent, in-depth descriptions of SAR systems.

GPR applications add another degree of complexity to the SAR picture because of the wide spectral extent of the signals. As will be discussed in Section 5, however, SAR processing can dramatically improve the performance of a radar. It is necessary to SAR-process each frequency in the spectrum when the fractional bandwidth is large.[9] This process is described in Section 9. In this GPR remediation application, it is necessary to use SAR processing to localize the echoes and thus clean up the output display.

---

[9] An alternative and completely equivalent approach, called "time-migration," can be applied. Here, the processing is done by shifting and summing signals sampled in the time domain at each small-antenna position. Actually, since it turns out to be more efficient to accomplish the mathematical operations in the frequency domain (due to the FFT algorithm), migration is actually usually accomplished by first spectrally transforming the data from the time to the frequency domain. "Migration" is a term borrowed by GPR workers from its seismic-exploration analogue.

Section 5

RADAR FIGURE OF MERIT

5.1 Introduction

Different GPR configurations and specifications often make it difficult to make comparative evaluations between units. Some means of comparing the sensitivities or performance of different radars and types of radars is needed. Here, a "figure of merit" is developed to quantify radar performance.

5.2 Figure-of-Merit Derivation

5.2.1 Short-Pulse Radars

The starting point is the radar equation, which gives the received power, P_r, in terms of various radar and external (environmental) parameters:

$$P_R = \frac{P_T G_T G_R \lambda^2 \sigma_{rcs} e^{-2\alpha R}}{(4\pi)^3 R^4}, \tag{5.1}$$

where

P_R is the transmitted radar power,

G_T is the transmitter antenna gain,

G_R is the receiver antenna gain ($=G_T = G_R = G$, when the same antenna (or identical antennas) are used for transmitting and receiving),

λ is the rf wavelength,

σ_{rcs} is the target radar cross section (rcs),

α is the attenuation coefficient, and

R is the effective target range in the medium (soil).

This expression is strictly true only for a narrowband radar; in general one needs to account for the frequency variations of all the parameters. For these purposes, however, the expression suffices.

The power received by the radar competes with additive noise, P_N, which is given by

$$P_N = F_S k T_0 B_N .$$

These new parameters are:

F_S, the system noise factor,

k, the Boltzmann constant (1.38×10^{-23} J/°K)

T_0, the reference temperature (290°K), and

B_N, the system noise bandwidth.

GPRs usually coherently add or average a large number of pulses to improve the signal-to-noise ratio (SNR). If m pulses are added, the SNR is

$$m\frac{P_R}{P_N}.$$

Thus the SNR becomes

$$m\frac{P_R}{P_N} = \left(\frac{f_{prf}P_T G^2}{F_S k T_0 B_N}\right)(T_{obs})\left(\frac{\lambda^2 \sigma_{rcs} e^{-2\alpha R}}{(4\pi)^3 R^4}\right). \tag{5.2}$$

The first factor on the right embodies the radar-specific parameters, and is defined as the figure of merit:

$$Q = \frac{f_{prf}P_T G^2}{F_S k T_0 B_N}. \tag{5.3}$$

Q is thus the average power output of the radar transmitter divided by the noise spectral density of the receiver. The larger Q is, the smaller the subsurface feature change detectable by the GPR. Note that Q has units of Watts/(Watts/Hz), or seconds.

At this point it is necessary to make a distinction between GPRs that use sampling-oscilloscope technology and those that use transient digitizers. For the former, a single sample is taken per transmitted pulse, and the range at which the sample is made is gradually increased until an entire range "sweep" is made. In this case the effective prf is

$$f_{prf} = \frac{\text{true prf}}{\text{number of samples per sweep}}.$$

More advanced (and expensive) pulsed GPRs record all the relevant range cells from each pulse (or sweep) at once, which can substantially increase f_{prf} and Q.

For a pulsed radar, optimum SNR is obtained under matched-filter conditions, where the pulse length is related to the noise bandwidth according to

$$\Delta\tau \approx \frac{1}{B_N}.$$

Noting that the resultant factor $\tau P_T G^2$ in the expression for Q is just the total radiated energy in a pulse, E_T, we have

$$Q = \frac{f_{prf}E_T}{F_S k T_0} = 2.5 \times 10^{20} \times \frac{f_{prf}E_T}{F_S}. \qquad (5.4)$$

This says that Q is proportional to the product of the sweep rate (the effective pulse repetition rate) and the energy per transmitted pulse.

If the pulse-length/bandwidth matched condition is not met, a bandwidth correction factor, C_B(where $C_B \geq 1$) is introduced as a multiplicative factor on F_S, which proportionally reduces Q. It is assumed that all the radars under consideration have been designed for optimum operation, so that $C_B \approx 1$.

5.2.2 Synthetic-Pulse GPRs

The figure-of-merit conclusions discussed in Section 5.2.1 also apply to synthetic-pulse GPRs. It is necessary only to find and use the appropriate values for the pulse energy and effective prf. A synthetic-pulse radar operates by sequentially transmitting a series of quasi-CW signals (tones), recording a single (complex) number characterizing the entire echo return at each frequency (tone), and transforming the array of numbers into the time domain, as discussed in Section 9.

The n tones separated in frequency by Δf. Each tone is ΔT s long and has power P_n. Then the overall bandwidth and duration of the signal train a single sweep are, respectively,

$$B = a n \Delta f$$

and

$$T = n \Delta T.$$

The factor a accounts for spectral weighting.

Range resolution is determined by the effective pulse length, which is approximately the reciprocal of the overall bandwidth, or

$$\Delta\tau = \frac{1}{B} = \frac{1}{a n \Delta f},$$

and the (maximum) effective prf or sweep rate is

$$f_{prf} = \frac{1}{T} = \frac{1}{n \Delta T}.$$

In a properly designed synthetic-pulse GPR, the signal is reorganized so that the transmitted energy during a sweep, E_T, comes out almost all at once, during the pulse duration interval, τ. Then the effective transmitted power is

$$P_{eff} = E_T B = E_T n \Delta f.$$

E_T is the product of the average power per tone times the total sweep duration,

$$E_T = P_a T = T\frac{1}{n}\sum P_n\,,$$

and E_a is the average energy per tone,

$$E_a = \frac{1}{n}E_T\,.$$

In addition, the incremental noise bandwidth should be arranged to be roughly the reciprocal of the duration of individual tones, or

$$B_n = \frac{1}{\Delta T}\,,$$

so the weighted total effective noise bandwidth will be

$$B_N = anB_n = \frac{an}{\Delta T}\,.$$

Putting these parameters into the expression for the figure of merit, one obtains[10]

$$Q = \frac{\Delta F\ E_a}{F_S k T_0} = 2.5\times 10^{20}\times\frac{\Delta F E_a}{F_S}\,. \tag{5.5}$$

The large advantage, in terms of potential sensitivity, of synthetic-pulse radars over conventional GPRs is associated with the energy per sweep parameter. The associated penalty is cost and more complex and lengthy processing.

5.3 Figures of Merit for Typical Radars

One typical commercially available conventional GPR has a maximum sweep rate of $f_{prf} = 256$ Hz and a radiated pulse energy of 88 pW (Table 5.1). The receiver noise figure has not been stated; however, it can be safely assumed that it is on the order of 15 dB, which is typical for high-dynamic-range, gain-controlled preamplifiers. Then, the calculated Q will be in the 3.2×10^{12} - 1.6×10^{14} s range, or 120 - 140 dB relative to 1 s. These values are consistent with the Q given for another manufacturer's radar---one with greater transmit power (see the inset in Table 5.1).

It is worth noting that the *lowest* frequency system has the best intrinsic sensitivity, and also experiences the least absorption. Theoretically, lower frequencies imply a penalty in spatial resolution, but this is probably not an important issue since the probable detection strategies are to sense subtle changes in (1) the volume scattering coefficient, (2) reflection from interfaces, and (3) bulk refraction. That is, exquisite range resolution is not a requirement for those strategies.

---

[10] Note that the weighting factor, a, divides out in this expression.

Table 5.1. Specifications for a "Typical" Commercially Available GPR

Parameter	Value
Antenna Impedance	240 Ω
Pulse to Antenna	100 V
Radiation Efficiency	35%
Applied Peak Power	41.7 W
Radiated Peak Power	14.6 W
Radiated Average Power	2.63 mW
Center Frequency (CF)	80 MHz
Pulse Duration	6 nS
Radiated Pulse Energy	88 pJ
Bandwidth (BW)	170 MHz
Fractional Bandwidth (BW/CF)	2.1

"Another Radar"
Q = 155 dB
Pulse to Antenna = 400 V

In the course of this work assignment, several GPR manufacturers were contacted. One manufacturer stated that his company has special-order transducers in the "two-kilowatt" range, or about 17 to 20 dB stronger. These would boost the figure of merit to the vicinity of 140 to 160 dB re 1 s. However, the manufacturer seemed reluctant to provide details about this radar, and it is unclear from his information whether such parameters as the prf and noise factor are unaffected; thus, it may not be possible to achieve all of the theoretical improvement implied by the power increase.

Substantial improvement is possible with the transient digitizer approach. The commercial system used as an example in Table 5.1 takes up to 1024 samples per sweep at a maximum prf of 256 kHz, so its effective prf is only about 250 Hz. A hypothetical system that has the same hardware but that uses a transient digitizer could in principle operate at the maximum prf and thus attain a figure of merit in the 150 to 170 dB re 1 s range.

A Q of 190 dB re 1 s may be possible if both higher power and a transient digitizer are used. This may represent the practical limit of short-pulse GPR technology.

Only one synthetic-pulse GPR is known to exist. This system is a prototype developed in the 1970s for the Bureau of Mines [13]. Its characteristics are not well quantified, so it would be necessary to make several assumptions here to estimate its Q value. It is claimed that the power per tone is 5 W and that there can be as many as 1401 tones extending from 20 to 160 MHz (140-MHz raw bandwidth and 80-MHz center frequency). In terms of spectrum it appears to be similar to conventional systems, and it evidently uses standard GPR antennas. For this analysis, it is assumed that the system has a 25% overall radiation efficiency, spectral weighting equivalent to the short-pulse radar system, and a 15-dB system noise factor. Here, Δf (min) is 100 kHz, so there are 1401 tones. It is further assumed that $\Delta T = 10\mu s$, which is the minimum possible (it would take 14 ms to complete a sweep, for $f_{prf} = 70$ Hz). The average energy per tone will be $E_a = 0.25 \times 5 \times 14 \times 10^{-3} = 17.5$ mJ and the potential figure of merit for the prototype synthetic-pulse will be $Q = 1.4 \times 10^{22}$ s, or about 220 dB re 1 s.

This synthetic-pulse GPR, however, dwells far longer on each tone than is theoretically allowed, and evidently does not approach optimum performance. It is likely that the Q for this system is actually on the order of 200 dB. Nevertheless, it is far superior to standard GPRs in terms of Q.

This analysis shows that the performance of the 80-MHz synthetic-pulse GPR is about 60 dB better than the performance of the standard 80-MHz short-pulse GPR, and appears to be roughly equivalent to a hypothetical high-power short-pulse GPR system that uses a transient digitizer. Clearly, synthetic-pulse GPRs offer a tremendous potential advantage over conventional GPRs.

5.4 Processing-Gain Contribution to Figure of Merit

T_{obs}, which is the middle factor in the basic expression for SNR (Eq. (5.2)), embodies all of the processing gain. It is merely the *total* effective time that a GPR "looks" at a target, including all the time spent at locations where contributions to SAR processing are gathered. In principle, due to the intrinsic stationarity of the situation, a GPR can continue recording data in one location and achieve an arbitrarily large SNR. However, a GPR must move across the surface at a useful rate, a factor that limits the dwell time. Suppose that Δl is the along-track resolution requirement and v is the radar velocity. Then the dwell time is $\Delta l / v$ and the number of pulses averaged is

$$m = f_{prf} \frac{\Delta l}{v} .$$

In general, it is difficult to make a specific choice for T_{obs} because of the variability of the environmental situation. A high-Q GPR operating in a low-loss environment can afford a short dwell time. Conversely, a high-loss environment can be at least partly compensated for by moving the GPR very slowly. Then, the cost of doing a remediation survey becomes an issue, and a trade-off assessment appropriate to each site needs to be done. (Such a study was beyond the scope of the present work.) For the purposes of this study and this report, a 1-s observation time has been arbitrarily chosen.

However, an order-of-magnitude estimate of a practical value for T_{obs} can be made. This estimate is based on SAR-processing considerations. Focused-SAR processing can achieve a linear resolution approximately equal to half the dimension of the real aperture of the antenna. Since the aperture size, D, of the small antennas required for GPR work are approximately a half-wavelength ($D \cong \lambda/2$)) at the center frequency, the achievable resolution is about $res \cong \lambda/4$, where λ is the wavelength in the soil. For the nominal center frequency of 100 MHz and soil dielectric constants in the 3 to 10 range, the theoretical resolution ranges from 0.25 to 0.4 m (i.e., about 1 ft). In order to achieve that resolution, however, the length of the synthetic aperture (i.e., the distance the real antenna needs to be moved) must be at least

$$L_{eff} = \frac{\lambda R}{D} \cong \frac{\lambda R}{\lambda/2} = 2R \ ,$$

where R is the range (or depth to the point being reconstructed). For example, measurements need to be made over a 20-m (65-ft) span to maximally reconstruct features at 10-m depth; at 30-m depth, the required span rises to 60 m (200 ft).[11] Furthermore, to avoid grating lobes, the field must be sampled rather densely. Sampling-theory considerations indicate that a new sample needs to be made at quarter-wavelength spacings. Thus the number of samples required is

$$n = \frac{2R}{\lambda/4} = 8\frac{R}{\lambda} \, .$$

GPR SAR sampling needs to be done over a two-dimensional space, however, so the number of samples needed to reconstruct *one subsurface point* is

$$m = n^2 = \left(\frac{8R}{\lambda}\right)^2 .$$

The area is $A = L_{eff}^2 = (2R)^2$, and the time required to cover this area is the coherent observation time:

$$\begin{aligned} T_{obs} &\cong \sqrt{m}\frac{L_{eff}}{v} \\ &= \frac{8R}{\lambda}\frac{2R}{v} \\ &= \frac{16R^2}{\lambda v} \, . \end{aligned}$$

---

[11] Signal loss due to geometrical spreading and, especially, soil attenuation is likely to prevent the achievement of the full aperture width required for maximal reconstruction, particularly at greater depths. Furthermore, note that the formulas presented in this section generally imply that more samples will be required in soils with a high dielectric constant (since λ appears in the denominators). The putative benefit of the cost of collecting and dealing with more samples is higher subsurface resolution. However, soils with high-dielectric constants contain more water and have higher losses in general, and achieving full benefit is unlikely. It may thus be desirable to forgo the processing required to obtain the full theoretical resolution. For example, processing data from an $\varepsilon = 20$ soil at the same resolution as an $\varepsilon = 3$ soil by reducing the span would speed the survey up by a factor of $\sqrt{20/3} = 2.6$.

The observation time can be quite large. For example, at 100 MHz in $\varepsilon = 3$ soil and $R = 10$ m, and a reasonable speed of 0.3 m/s (1 fps), T_{obs} is nominally about 3000 s (50 min). This would produce 35-dB processing gain compared to $T_{obs} = 1$ s.[12]

To sample a subsurface area uniformly (e.g., A), the GPR must be moved over a larger surface area, given by $(\sqrt{A}+2R)^2$. Then the number of samples necessary to reconstruct an area is

$$m = \left(\frac{\sqrt{2A}+8R}{\lambda}\right)^2 \rightarrow \frac{2A}{\lambda^2}.$$

The limiting value applies for large areas. For large areas, the total necessary search time approaches

$$T_{tot} \cong \sqrt{2}\frac{A}{\lambda v}.$$

Suppose, as in the example used above, that reconstruction to a depth of 10 m is desired. Then, the time required to survey a 100x100-m area (about two acres) is about 8 h. This appears to be a reasonable and rather good rate.

5.5 Environmental Contributions to Figure of Merit

The third term in the expression for SNR (Eq. (5.2)) contains the environmental factors. For unity SNR,

$$\frac{\lambda^2 \sigma_{rcs} e^{-2\alpha R}}{(4\pi)^3 R^4} = 1/Q .$$

Thus, the minimum detectable radar cross section is

$$\sigma_{rcs}^{(\min)} = SNR_{\min}\left(\frac{1}{Q}\right)\left(\frac{(4\pi)^3 R^4 e^{2\alpha R}}{\lambda^2}\right). \tag{5.6}$$

For an 80-MHz system with $Q = 220$ dB re 1 s operating in a medium with 1-dB attenuation per meter and a relative dielectric constant of 20,[13] the minimum detectable rcs at 10-m depth for 10 dB SNR is 3×10^{-12} m^2. In comparison, the standard system can detect an rcs of 3×10^{-4} m^2 under the same conditions. A $Q = 190$ dB system (one with high-power pulse plus transient digitization) system could detect an rcs of 3×10^{-9} m^2.

To put this in perspective, consider the detectability of a plane interface between dielectric media. The effective rcs of such an interface is approximately

---

[12] *Every* subsurface point reconstructed would benefit by this amount of gain.

[13] This is a moderately conducting (0.03 S/m) soil with a 50% void fraction fully saturated with water (i.e., a fairly difficult situation).

$$\sigma_{rcs} = |r|^2 \pi R^2 ,$$

where r is the reflection coefficient of a plane interface between dielectric 1 above and dielectric 2 below:

$$|r| = \left| \frac{\sqrt{\varepsilon_1} - \sqrt{\varepsilon_2}}{\sqrt{\varepsilon_1} + \sqrt{\varepsilon_2}} \right| \approx \left| \frac{\Delta\varepsilon}{4\varepsilon} \right| . \tag{5.7}$$

This approximation applies in the case of small differences in dielectric constant. For the $Q = 220$ dB re 1 s system under the above conditions, the minimum detectable reflection coefficient will be about 1×10^{-8}. A reflection coefficient of 1×10^{-8} corresponds to a relative change in dielectric constant, $\Delta\varepsilon/\varepsilon$, of 4×10^{-8}. In principle, the standard system could detect a sharp boundary between layers with a dielectric change of 4×10^{-4}, or 0.01%.

5.6 Section Summary

It was shown above that the performance of a GPR radar system, including the radar hardware and the signal processing, in the environment, can be expressed in terms of a single number, Q, the figure of merit. Q can be used to compare the performance of various hardware items.

If the formula for Q is inverted, the Q required to detect various contaminants in various environmental geometries can be calculated. The concept of Q and the calculation of the required Q for various configurations of environmental geometries are used throughout the remainder of this report.

An important element in this section is the contribution SAR processing can make to the remediation effort. SAR, and particularly three-dimensional SAR processing, can increase a radar's Q by as much as 20 to 40 dB.

Section 6

SOIL CHARACTERISTICS, SOIL MODEL, AND SOIL GEOMETRIES

This section of the report describes the expected electromagnetic properties of the environments that might be found at remediation sites---that is, how various soil materials are distributed around the United States; how these soil types affect the propagation of radar energy through the soil and reflections from the interface between layers; how the propagation and reflection are affected by moisture in the soil; the effects of a water table; and the effects of various contaminant materials in the medium.

6.1 Classification and Distribution of Soil Types

Soil materials can be classified according to the Triangular Classification Chart developed by the U.S. Army Corps of Engineers [14]. This classification scheme, illustrated in Figure 6.1, categorizes soils according to what percentage of three primary components they contain; these components---clay, sand and silt---are categorized according to particle size. As will be shown below, these various mixtures of coarse and fine particles have an effect on the propagation of radar energy into the ground that depends upon the ratio of the mixture. Thus, an engineering assessment of GPR performance must include a description of the soil mixture; a "clay-sand" mixture was used for most of the analysis shown below.

Morey and Harrington [14] include a map that shows the distribution of various soil types throughout the United States. This map, reproduced in Figure 6.2, can be used with the Triangular Classification Chart (and the analysis in Sections 5 and 7) to broadly estimate how the radars described in this report would work in various locations around the U.S. The characteristics of most of the deposits are described as follows.

- *Wind-Blown Deposits*. These include both silt and sand; high concentrations of salts exist in some portions of these deposits.
- *Saprolite*. This generally consists of massive clay. The contact with unweathered bedrock is generally gradational.
- *Coastal Plains Deposits*. These are generally sand, silt, or clay. The water table is high and swamps are numerous, particularly near the coast.
- *Desert Deposits*. These are generally dry sand, silt, or clay. Caliche may be present in some areas.

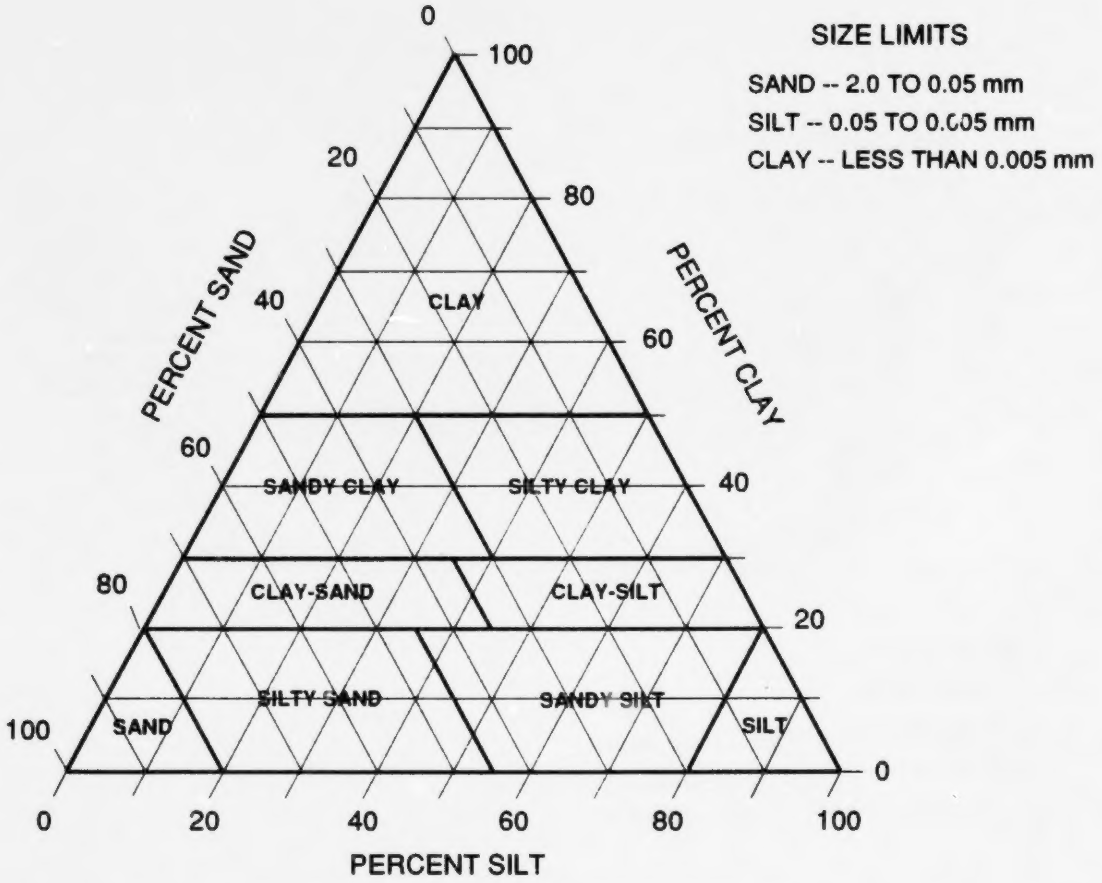

Figure 6.1. Triangular Classification Chart for soil.

- *Basin Deposits*. These are generally dry silt and clay in low areas surrounded by sand and gravel. Deposits and groundwater may be highly mineralized. Caliche is common in some areas.
- *Alluvium*. Materials present are variable. The water table is high in many areas; it may be highly mineralized.
- *Lake Deposits*. These are generally silt and clay. Deposits and groundwater may be highly mineralized.

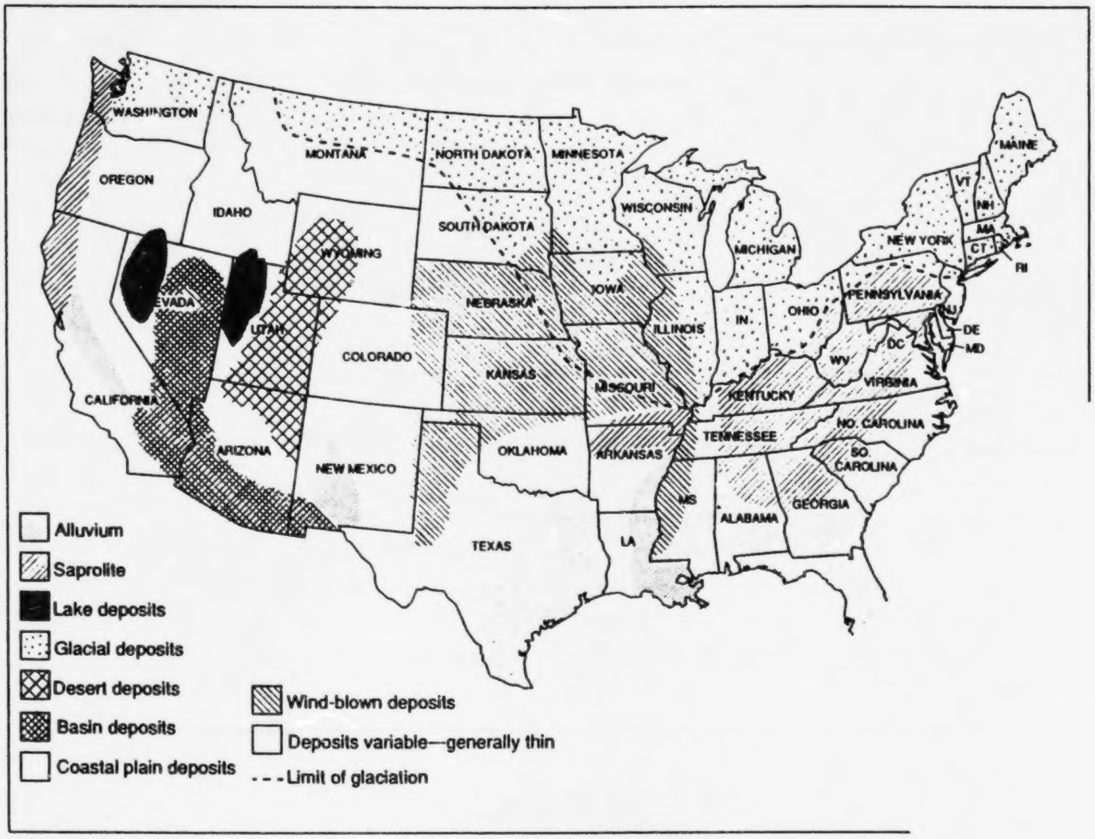
WASHINGTON
OREGON
IDAHO
MONTANA
NORTH DAKOTA
MINNESOTA
MAINE
WISCONSIN
SOUTH DAKOTA
WYOMING
MICHIGAN
VT
NH
NEW YORK
MA
CT
RI
NEVADA
NEBRASKA
IOWA
PENNSYLVANIA
NJ
UTAH
ILLINOIS
IN.
OHIO
DE
MD
COLORADO
DC
WV
KANSAS
MISSOURI
VIRGINIA
CALIFORNIA
KENTUCKY
NO. CAROLINA
TENNESSEE
ARIZONA
NEW MEXICO
OKLAHOMA
ARKANSAS
SO. CAROLINA
MS
ALABAMA
GEORGIA
TEXAS
LA
Alluvium
Saprolite
Lake deposits
Glacial deposits
Desert deposits
Basin deposits
Coastal plain deposits
Wind-blown deposits
Deposits variable—generally thin
- - - Limit of glaciation

Figure 6.2. Distribution of soil deposits.

6.2 Characteristics of Soils and Contaminants

It was noted above that the speed of propagation of electromagnetic energy is determined by the *dielectric constant* of the propagation medium, and that the absorption of the energy is determined by the *attenuation coefficient* of the medium. It was also noted that for a GPR, the effects of the soil can have a strong influence on the propagating energy, depending on the type of soil and its constituents. The values of dielectric constant and attenuation coefficient vary with the type of soil, its moisture content, its conductivity due to ionic materials (i.e., salts in the soil), and the frequency of the electromagnetic energy. Table 6.1 lists typical values for the dielectric constant and conductivity at 100 MHz for a number of common geologic materials. This table also "ranks" the materials in terms of penetration depth at VHF (100-MHz) frequencies.

Soils generally consist of solid grains with relative dielectric constants in the 4.5 to 5.5 range and low conductivity, plus pores filled with variable amounts of air (relative dielectric constant = 1) and water (relative dielectric constant = 80). Due to its large relative dielectric constant, and possibly large conductivity, the amount of water present has a major effect on the properties of the mixture.

Table 6.1. Electromagnetic Characteristics for Common Geologic Materials [11]

Material	Approximate Conductivity σ (mho/m)	Approximate Dielectric Constant	Depth of Penetration
Air	0	1	Max (km)
Limestone (dry)	10^{-9}	7	│
Granite (dry)	10^{-8}	5	│
Sand (dry)	10^{-7} to 10^{-3}	4 to 6	│
Bedded Salt	10^{-5} to 10^{-4}	3 to 6	│
Freshwater Ice	10^{-5} to 10^{-3}	4	│
Permafrost	10^{-4} to 10^{-2}	4 to 8	│
Sand, Saturated	10^{-4} to 10^{-2}	30	│
Freshwater	10^{-4} to 3×10^{-2}	81	│
Silt, Saturated	10^{-3} to 10^{-2}	10	│
Rich Agricultural Land	10^{-2}	15	│
Clay, Saturated	10^{-2} to 1	8 to 12	∇
Seawater	4	81	Min (cm)

Morey and Harrington [14] note that "...[a radar's] operation in materials [in similar soil types] will not differ much [from one location to another] except where different chemical properties result in gross differences in the electrical properties of the soils. For example, silty sand in a non-glaciated region could be expected to have the same characteristics as the silty sand in a glaciated region, but would be quite different if the sample had a high salt content." Thus, while a radar's response to similar environments would be expected to be similar, the actual response is very much related to, and dependent on, the electrical characteristics of the actual site, in addition to the performance of the basic radar as determined by the figure of merit discussed in Section 5. Thus, before the GPR system-and-environment can be estimated, a complete specification of the site is necessary.

Contaminants in the soil also affect the propagation of the electromagnetic energy as a result of their dielectric constants and attenuation coefficients. Table 6.2 lists the dielectric constants for some selected contaminant materials [15]. While there may be exceptions, the electrical conductivity of most of these materials is very low; they are essentially nonconducting. It is noted for Tables 6.1 and 6.2 that the dielectric constants of geologic constituents (solid grains, water, air) and contaminants are generally clearly separated.

Table 6.2. Dielectric Constants of Typical Contaminant Materials

Material	ε
n-Pentane	1.84
n-Hexane	1.89
n-Octane	1.95
n-Decane	1.99
n-Dodecane	2.014
Carbon tetrachloride	2.238
Carbon disulfide	2.641
Methanol	32.63
Trichloroethylene	3.4
Chlorobenzene	5.708
Benzene	2.284
Toluene	2.438
Styrene	2.43
Nitrobenzene	34.82

6.3 Modeled Soil and Contamination Geometries

Models for subsurface conditions are essential for evaluating radar performance. Such models need two parts: (1) a description of the disposition of the contaminant and (2) the effect of a contaminant on radio frequency propagation properties. A review of the literature suggested two fundamental situations, which depend primarily on the groundwater condition. For the purposes of this work, these two basic configurations were termed Model I and Model II, and are illustrated in Figure 6.3.

Model I postulates the presence of a water table, whether it is immediately detectable, as in Model 1A, or not, as in Model 1B. Depending on its source, a contaminant will travel down through drier soil to the water table or flow upwards to it. Because a major interest in this work is petroleum contaminants, which are less dense than and immiscible with water, the main feature of Model I is a layer, possibly thin, of contamination "floating" on the water table. It is reasonable to expect that a sharp boundary will form between the contaminating substance and the water. The radar system question thus becomes: how big an echo contrast is needed in order for the contaminating substance to be detected by a GPR of a given performance (i.e., a given figure of merit)?

Model I is subdivided into two categories, based on the way water and contaminant interact with the soil. In Model IA, the soil is granular so that there is little capillary action, and is either mostly dry or virtually saturated; this results in sharp, detectable discontinuities at the interface between two strata. In this case the water table itself would be seen by the GPR, and the contamination would be revealed as a laterally localized change in reflection at the water table. In Model IB, capillary action leads to gradual transitions from moist to saturated soils, as illustrated by the gradual shading in Figure 6.3b. In this case, the soil's electrical properties also vary slowly with depth, and such changes do not reflect radar pulses well (GPRs are often not able to "see" the water table for this reason). Here, it is postulated that the immiscibility of the contaminant and water will cause a boundary to form between them. There may be no distinct upper surface to the contamination; in this case, contamination would be revealed by the appearance of a laterally localized reflecting boundary. Note that a high-resolution GPR could in principle distinguish between this situation and a local soil stratum, which has finite thickness.

Model I was implemented in a computer code that calculates the reflection coefficients of dielectric boundaries and layers. It uses inputs from the bulk soil properties code described in Section 6.4, written to calculate the electrical properties of various soil/water/contaminant mixtures.

Note that Model I also addresses the situation in which the soil is nowhere saturated (i.e., where there is no water table) but where there is a relatively impermeable layer such as clay below. Then the contaminant will form a layer on the surface of the impermeable medium, which can be detected as described above.

Model II addresses the situation in which there is no water table or impermeable layer to impede the downward spread of contaminant. Here, there is a bottomless "plume" of contamination, which is considered to diffuse laterally as it proceeds from the source. (See Figure 6.3c.) The plume itself does not produce any detectable radar signal, since scattering can only come from sufficiently abrupt discontinuities in the electrical properties. Thus an alternative detection strategy is necessary.

In the scenario depicted in Model II, the presence of the contaminant changes the scattering from subsurface features; it may be possible to take advantage of this change, which is itself a detectable feature. Small changes in soil density or porosity and the presence of discrete scatterers such as rocks and pebbles will produce a "clutter" background. The strength of this background signal depends on the dielectric properties of the medium, which are strongly controlled by the liquid content (be it water or contaminant). Because the dielectric constant of water is about 80, while that of petroleum products is about 2 (see Tables 6.1 and 6.2), the replacement of pore water with contaminant will have a large effect on the electrical properties of the medium and hence on the clutter level. Adding contaminant to dry soil will increase the

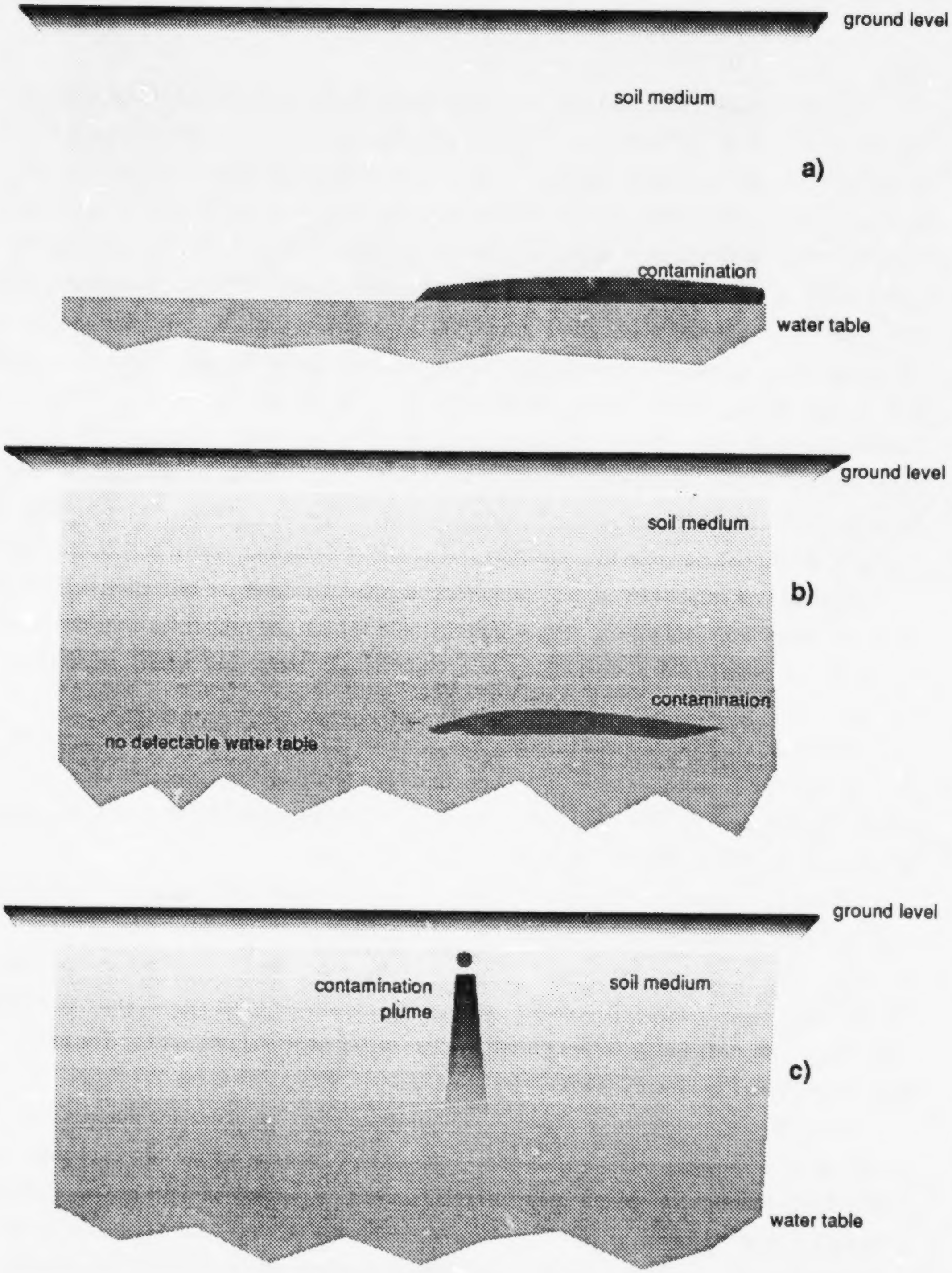
ground level
soil medium
a)
contamination
water table
ground level
soil medium
b)
contamination
no detectable water table
ground level
contamination
plume
soil medium
c)
water table

Figure 6.3. Models of subsurface conditions. In Model IA (a), the contaminant floats on the water table; in Model IB (b) there is a gradual transition from wet to dry, but the immiscibility of the contaminant with water causes a boundary to form at some point; in Model II (c) the contaminant forms a plume that travels downward.

overall dielectric constant and replacing water with contaminant will decrease it. The expected effect of contaminants in this case is to suppress the clutter. Reported occurrences of this scenario have shown a complete washout of the clutter level in the contaminated region.

Model II was implemented as a change in the volume scattering coefficient that depends on contaminant level. As implemented in the model, the "plume" is a simple cone. The goal was to obtain estimates of the amount of contamination that could be detected for a given GPR figure of merit.

A review of the two models shows that, given their parameters, they can be used to represent seven of the ten cases described by Walther et al. [7] as being common at remediation sites.

6.4 Dielectric Properties of Soils and Soil Mixtures

To reliably calculate the strengths of radar echoes returned from subsurface layers, boundaries, and irregularities, there must be a means of calculating changes in the dielectric properties of the soil when contaminated material is present. The soil model chosen for this work was written to implement the Bruggeman-Hanai-Sen (BHS) formula [6], which describes the soil as various interdispersed media (particles, liquid water/contaminant, air). According to the BHS formula, which was extended from the Hanai-Bruggeman-Wagner theory [16], the parameters of a two-phase heterogeneous dielectric soil with complex dielectric constants are related through the expression

$$\phi = \frac{(\varepsilon_m^* - \varepsilon^*)}{(\varepsilon_m^* - \varepsilon_d^*)}\left(\frac{\varepsilon_d^*}{\varepsilon^*}\right)^{1/3} . \tag{6.1}$$

where

ε^* = the complex dielectric constant of the mixture,

ε_m^* = the complex dielectric constant of the "matrix" material (e.g., soil grains),

ε_d^* = the complex dielectric constant of the "disperse" phase (e.g., air or water), and

ϕ = the volume fraction of the dispersed phase (e.g., porosity).

The exponent value of one-third comes from an assumption that the dispersed phase behaves electrostatically in the same way as it does for small spheres.

To obtain ε^*, it is necessary to solve a cubic polynomial equation with complex parameters. A computer program was written to set up the problem with soil parameters (porosity, type of fluid (water or contaminant), and fluid saturation level) and solve the cubic equation. Note that a cubic equation has three roots. Identification of the correct root was sometimes difficult, because occasionally more than one was physically permitted.

Multi-phase mixtures, such as soil particles/water/air, are dealt with by repeated application of this formula. Care must be taken to correctly identify which phase is the "disperse" one and which is the "matrix." The approach chosen here was to first consider particles dispersed in the fluid and then consider air-filled voids dispersed in the moist mixture. Input quantities for the model are the total void fraction, the fraction of the total voids filled with fluid, and the conductivity of the void water. A full range of values for these parameters can be accepted. Either sand particles or clay particles can be specified; these differ in their intrinsic conductivities. Test cases using this code along with reasonable input values produce a range of outputs that agree well with measured soil properties and confirm the expected effects of contaminant. Note that by adjusting the model coefficients for "sand," a wide variety of common geological materials can be modeled, including limestone, shales, silts, granite, and so on.

Examples of calculations of the dielectric constant, conductivity and the attenuation coefficient for various soils and a petroleum contaminant are given in Appendix B. The plots in this appendix show the value of the electromagnetic parameters as a function of radar frequency, from 10 MHz to 200 MHz, for liquid fractions of 0%, 30%, 60%, and 100%.

6.5 Section Summary

Soil types vary widely across the United States. Soil composition (particle type, homogeneity, particle size and distribution of sizes, moisture content, and the presence of ionic materials in the soil) has a dramatic impact on the way a radar wave will propagate in the soil. To address these issues, a bulk soil model was developed that allowed the electromagnetic properties of the soil to be estimated as a function of radar frequency. This model was then used to calculate radar propagation and scattering for two essential geometries.

Section 7

DETECTION STRATEGIES

7.1 Introduction

Section 5 introduced three basic models for the effects of contamination on the soil under different circumstance (e.g., interaction of a contaminant with the water table). It appears that these three models can cover all of the circumstances that appeared to produce changes in subsurface electromagnetic properties amenable to exploitation by a GPR. Here, possible strategies for using a GPR successfully under the different circumstances are explored. For the purpose of this discussion, the GPR is a synthetic-aperture radar, since system SAR/migration processing is essential in this application.

The discussion in this section has been limited primarily to the issue of whether or not there is a detectable signal against noise. This is the *fundamental* starting point, because without the expectation of a measurable signal in the first place there would be no hope of using a GPR even if clutter and subsurface variability were not issues. Although those are critical issues, it is too extensive a subject to attack here and is one which, in any event, cannot be addressed seriously without experimental efforts. Since no two areas are geologically identical, each presents a different problem. SAR processing is an essential step toward reducing clutter due to discrete objects and localizing the energy scattered from a given underground volume.

Here, it is assumed that the "contamination" is a low-loss organic compound or mixture that has a dielectric constant of 2 (see Table 6.2). Petroleum, gasoline, and their constituents, for example, fall in this class. The results could be extended to other classes; however, it would be tedious and would require extensive effort to cover all possible cases and combinations, and the results would not affect the basic conclusions already drawn here.

The effects of contamination on radar scattering can be subtle. High-sensitivity synthetic-aperture GPRs, extensive, high-order data processing, and improved displays will be needed to achieve success. These three elements have been lacking in previous efforts to use GPR for contaminant mitigation, and thus, although GPRs have been touted for decades as tools for remediation, they have not really been used for this purpose. Much of the GPR work in this area seems to have been done as an *ad hoc* aside.

An evidently novel and exciting theoretical finding developed here is that there can often be surprisingly strong contrasts between the volumetric scattering from contaminated and non-contaminated soils. This effect may provide the best method for tracking contamination.

Our mathematical modeling shows that it will usually require a very sensitive GPR to detect this contrast. Although there have been reports of conventional GPRs detecting the contrast, modeling analyses show that such radars cannot, in general, do the job. Another novel prediction developed here is that a thin layer of contaminant (only centimeters thick) will produce a detectable signature. However, it is questionable whether this signature could be exploited successfully, since it is primarily manifested as a time delay and could thus easily be confused with variations in the distance between the GPR and the reflecting layer (i.e., between the surface and the water table).

7.2 Summary of Strategies

Three strategies were developed for detecting contaminants. They are based on the three models that depict underground conditions.[14] The strategies are discussed in detail below, and are summarized in Table 7.1.

Table 7.1. Detection Strategy Summary

Model Identifier	Is There a Water Table Influence?	Is There a Significant Water Table Echo?	Expected Phenomenon (Produced by an Immiscible Contaminant)	Detection Strategy	Method
I-A	Yes	Yes	Changes Interface Reflection Signature	Look for Specific Lateral Changes in the Plane-Layer Reflection Coefficient	Map the Plane-Layer Reflection Signature
I-B	Yes	No	Forms a Reflecting Layer or Interface	Look for the Appearance of Plane-Interface Reflections	Map Plane Interface Reflections
II	No	No	(1) Changes the Volume Reflection Coefficient	Look for Contiguous Changes in Background Echo Contrast	Measure and Map the Spatially Averaged Volume rcs
			(2) Changes the Bulk Refractive Index	Look for Changes in Propagation Velocity	Map the (Adaptive) SAR Migration Parameter

Clearly, Models IA and IB focus on a light contaminant floating on water. As noted in Section 6, the situation in Model IA is very similar to that of a contaminant resting on a relatively impermeable layer, such as rock or clay, and thus also applies to such a situation.

---

[14] It was previously noted that these three models were distilled from a larger set, and in fact cover most "common cases" (7 of 10) at remediation sites [7].

There are two basic issues. First, is there sufficient radar sensitivity to detect the echo contrasts? Second, will the variations in underground geology mask the echo contrasts due to contaminants? Presumably, the first question can easily be answered. The second issue, however, is so site-specific that only an estimate of the lower bound of detectability can be made here.

A subsidiary matter related to the second issue involves SAR processing. Perhaps the most important aspect of SAR is to localize energy scattered from large discrete objects. However, SAR does not do this perfectly, and sidelobes are generated. Thus there may be a varying apparent clutter level due to the sidelobes of migrated echoes from discrete buried objects. Results from the numerical analytic studies described in Section 9 show that post-migration sidelobe levels for a point scatterer are 30 to 40 dB below the peak. Another effect that needs to be considered is the possibility of scattering from above-ground objects.

7.3 Model IB Strategy: Reflection from a Contaminant/Water Interface in Soil

This situation, in which strong reflections will invariably be created, will be considered first because it is probably the easiest to deal with. Because they are immiscible, it is postulated that contaminant will displace pore water and induce a discontinuity between soil saturated with contaminant and the same soil saturated with water. A distinct boundary will be produced only in the region of the contaminant pool. The only significant variable is the void fraction.

A special approach needs to be taken to calculate the effective rcs of a plane layer or interface. Normally, the rcs is defined for finite objects with plane-wave illumination (i.e., for an infinitely distant transmitter), but in this case it is necessary to deal with large, nearby scatterers. It can be shown that the effective rcs of an infinite plane interface is approximately

$$\sigma_p = |r|^2 \pi R^2 ,$$

where r is the plane-wave reflection coefficient and R is the distance to the interface. Normally, the range to an object is irrelevant to its rcs. Here, the increase in rcs with range is interpreted as the result of expansion of the effective scattering area with range. The scattering region is roughly defined by the first Fresnel zone radius, which also defines the approximate lateral extent over which the interface needs to appear "plane." The radius of the Fresnel zone for backscatter is

$$F = \sqrt{\lambda R/2} .$$

The rf wavelength, λ, is measured in the soil, and is thus shorter than its free-space value by the factor $1/\sqrt{\varepsilon_r}$. For wavelengths on the order of 1 to 2 m and ranges between 3 and 30 m, F is in the 1- to 6-m interval. If it is larger than this, a plane interface will appear to be "infinite." What this says is that points on the surface that are quite distant from the geometrical point of reflection do not contribute much to the total signal. On the other hand, a radar pulse reflected from a "facet" smaller than the Fresnel zone will be weaker than it might otherwise be. Thus, the diameter of the contaminant pool must be as least as big as about $2F$ to achieve the full rcs value.

This approximation for the rcs involves using the plane-wave reflection coefficient for dielectric interfaces at normal incidence instead of the true boundary condition, which depends on the off-axis angle of incidence. This approximation is justified by the relatively weak dependence on the incidence angle, the relatively small variation of the angle of incidence over the span of the Fresnel zone, and the large uncertainties in the actual subsurface environments, which do not justify highly precise predictions. The plane-wave reflection coefficient at normal incidence for a plane interface between media 1 and 2 is

$$r = \frac{Z_1 - Z_2}{Z_1 + Z_2},$$

where the Zs are the (complex) wave impedances in the two media. For low-loss dielectric media, this reduces to the formula used in Section 5.5,

$$r = \frac{\sqrt{\varepsilon_2} - \sqrt{\varepsilon_1}}{\sqrt{\varepsilon_2} + \sqrt{\varepsilon_1}}.$$

Table 7.2 lists values for the reflection coefficient for a plane boundary between soils of various void fractions saturated with contaminant ($\varepsilon = 2$) and saturated with water of various conductivities. These values were actually calculated as a special case (i.e., zero-thickness) of the method described above.

It is assumed here that all facets are sufficiently flat over distances that are large compared to the Fresnel zone, so that the interfaces can be considered to be effectively infinite. The only remaining factor, then, is the reflection coefficient. It was noted in Section 5.5 that the minimum detectable reflection coefficient (at 10 dB SNR) was $|r| = 1 \times 10^{-8}$ for a $Q = 220$ dB re 1 s synthetic-pulse GPR operating against a soil with 1 dB/m attenuation. For a standard GPR system with $Q = 140$ dB re 1 s, the magnitude of the minimum detectable reflection coefficient was 1×10^{-4}. Here, the goal is to determine what this means in terms of the layer parameters, the most important of which is its thickness, d.

The reflection coefficients are also weak functions of frequency. Their magnitudes tend to decrease slightly with increasing frequency and their phases approach 180° more closely. Even in the most extreme case (50% porosity, 0.3 S/m conductivity), the magnitude of the reflection coefficient varies only 13% between 10 and 500 MHz and its phase changes by only 4.3°. In the 50- to 150-MHz band most likely to be employed by GPRs in this application, the magnitude and phase change only 7% and 1.3°, respectively.

Table 7.2. Plane-Interface Complex Reflection Coefficient at 100 MHz

Porosity	Water Conductivity - s/m			
	0.01	0.03	0.1	0.3
30%	$0.303\angle 179.8^{\circ}$	$0.305\angle 179.5^{\circ}$	$0.305\angle 178.4^{\circ}$	$0.314\angle 176.3^{\circ}$
40%	$0.402\angle 179.8^{\circ}$	$0.403\angle 179.4^{\circ}$	$0.405\angle 178.3^{\circ}$	$0.417\angle 176.0^{\circ}$
50%	$0.495\angle 179.8^{\circ}$	$0.496\angle 179.4^{\circ}$	$0.498\angle 178.8^{\circ}$	$0.514\angle 175.8^{\circ}$

It is apparent that the porosity controls the magnitude of the reflection coefficient but has little effect on its phase angle. On the other hand, conductivity changes slightly alter both the phase angle and the magnitude, although the effect is weak. The complex reflection coefficient of an interface between lossless dielectrics is purely real. Loss in the lower (water-saturated) medium introduces a finite imaginary component. However, the magnitude of the imaginary part of the complex reflection coefficient is mores than 20 dB lower than that of the real component. It would be virtually impossible to detect it.

The main point here is that an interface formed between contaminant- and water-saturated regions will produce very strong reflections. Virtually any GPR should be able to detect it under reasonable conditions.

A less-dense contaminant will displace water downwards. Consequently, the region above the contaminant should be relatively dry and thus have low attenuation. This condition would enhance the visibility of such regions.

7.4 Model IA Strategy: Reflection from a Thin Layer of Contaminant Sandwiched between Layers of "Dry" and Wet Soil

In this case the presence of a distinct water table is postulated. "Distinct" means that the transition from "dry" to saturated appears abrupt to a radar pulse. Generally in order for this transition to be detectable, it must occur within a distance that is short compared to the rf wavelength, say 10%. Such situations evidently occur in coarse-grained soils where capillarity is not a strong factor. A light contaminant would be expected to pool and form a thin layer floating on the water table [17]. The solid lines in Figures 7.1a and 7.1b illustrate how, in the case of a distinct water table, the depth profile of the dielectric constant might change between clean and contaminated regions.

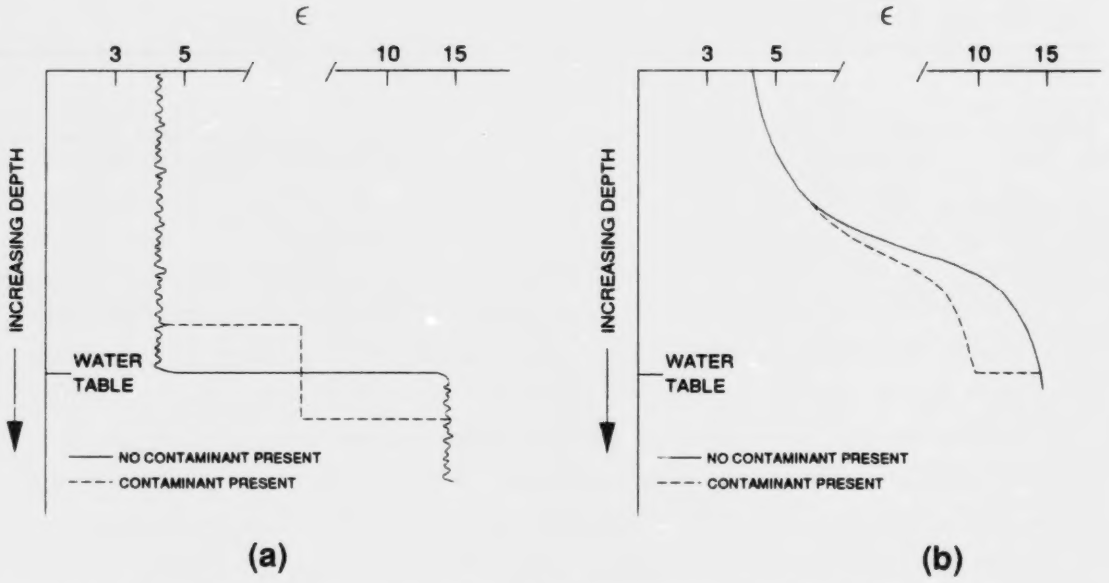

Figure 7.1. Profiles of dielectric constant vs. depth: (a) distinct water table, and (b) indistinct water table.

A similar situation arises when a high-density contaminant falls toward a relatively impervious stratum that produces a radar echo. The strategy in either case is to detect the signatures of changes between the reflection properties of the interface where there is no contaminant and where contaminant has pooled.

The concern (and the thrust of this analysis) is with detecting thin layers. Detecting thick layers appears to present no challenge because the echoes from each of the two interfaces will be time-resolved and strong, so that multiple reflections will be seen as a decaying train of reverberating echoes.

Plane-wave reflection at normal incidence is assumed. The reflection coefficient of a layer sandwiched between dissimilar media can then be easily computed from transmission-line impedance theory. This approach accounts for all the multiple reflection between the two interfaces, which leads to reverberation phenomena that would be noticeable, in the case of a thick layer of contaminant, as a series of discrete repetitive echoes. Consider the situation depicted in Figure 7.2, where a plane layer of thickness *d* and relative dielectric constant ε_2 is between infinite media with ε_1 and ε_3. All three media may have complex dielectric constants. The reflection coefficient may also be a complex number. It is referenced to the top surface of the first interface. The effect of the intermediate layer and lower medium can be lumped into an equivalent "input impedance," Z_i. Then, the reflection coefficient is

$$r = \frac{Z_i - \eta_1}{Z_i + \eta_1},$$

where η_1 is the (complex) wave impedance of the upper medium.[15] Z_i, in turn, is

$$Z_i = \eta_2 \frac{1 + r' \exp(-2\gamma_2 d)}{1 - r' \exp(-2\gamma_2 d)},$$

where η_2 and γ_2 are respectively the impedance and propagation constant in the layer.[16] Finally, r' is the reflection coefficient between media 2 and 3 considered alone, or

$$r' = \frac{\eta_3 - \eta_2}{\eta_3 + \eta_2}.$$

As this set of formulas is rather complicated, a computer program was written to the calculate numerical values for $|r|$ under various conditions. It calls subroutines derived from the earlier programs developed to provide values for the soil dielectric constants.

For a thin layer, where $2\gamma d \ll 1$, and where the soil dielectric constants have negligible imaginary components (i.e., have low losses), a simple analytic form is possible:

$$r \cong \left(\frac{\eta_3 - \eta_1}{\eta_3 + \eta_1} \right) \left(1 - j2k_2 d \, \frac{\eta_1}{\eta_2} \frac{\eta_2^2 - \eta_3^2}{\eta_3^2 - \eta_1^2} \right).$$

This formula has the general form

$$r = r_r (1 + j\, f/f_c),$$

where r_r is the reflection coefficient if there is no intermediate layer and f_c is a "cutoff" frequency.

Figures 7.3 through 7.6 present some typical results. This example is for a 30%-porosity soil and an operating frequency of 100 MHz, which is approximately in the middle of what seems to be the optimum band for this GPR application.[17] Consistent with Model IA precepts, this example involves a layer saturated with $\varepsilon_r = 2$ contamination sandwiched between dry soil and water-saturated soil. In this example the water has a moderate conductivity of 0.03 S/m.

---

[15] The wave impedance is given by

$$\eta = \frac{Z_0}{\sqrt{\varepsilon_r}},$$

where Z_0 is the impedance of free space (377 ohms).

[16] The propagation constant is

$$\gamma = i k_0 \sqrt{\varepsilon_r},$$

where $k_0 = 2\pi/\lambda$ is the free space wavenumber and $i = \sqrt{-1}$.

[17] The 50- to 150-MHz band appears to provide the best balance between penetration, which favors low frequencies, and resolution, which improves at shorter wavelengths. For this application, high resolution does not seem to be necessary, and may actually be disadvantageous.

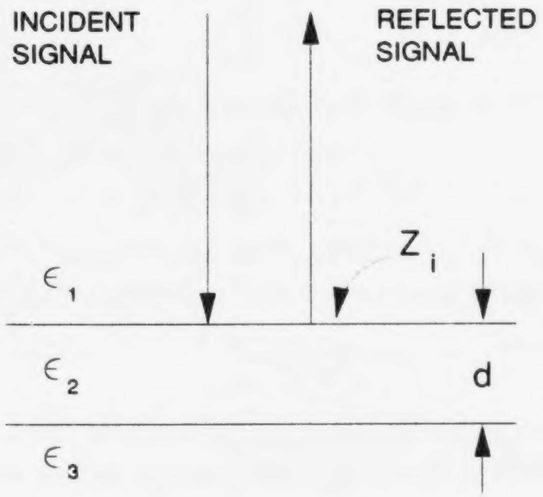

Figure 7.2. Incident vs. reflected signal.

The main effect for layer thicknesses in the 1- to 10-cm interval is a large increase in the imaginary part of the reflection coefficient. The real part of *r* and its magnitude stay relatively constant. For thin layers, then, the appropriate detection strategy here is to process and inspect data associated with reflections from the water table so as to look for an imaginary component to *r*. It appears that contaminant layers only a few centimeters thick might be detectable.

Note that because the magnitude of the reflection coefficient is much larger than the minimum detectable level and is only slightly affected by the contaminant, the layer will produce strong echoes (for wideband GPRs) that should be easily detectable under most circumstances and to relatively great depths. A prerequisite of Model IA is that there be relatively dry soil above the contaminant layer, because of the presence of a distinct water table and the tendency of low-density contamination to displace water and dry the soil. Thus, low rf propagation loss is expected above the layer.

Neither changes in soil porosity nor conductivity affect this low rf propagation loss significantly. Increased porosity enhances the overall magnitude of the reflection coefficient but has little effect on the ratio of the imaginary part of *r* to its magnitude. This ratio tends to remain relatively constant for a given layer thickness. The reason is that porosity has a small effect on the dielectric constant of the layer because the dielectric constant of the contaminant is relatively close to that of the soil particles. The increased magnitude of *r* with porosity is due to the increased differences of ε_r between layers. Conductivity effects are minor because it only affects the reflection at the $\varepsilon_2/\varepsilon_3$ interface. Not only is the effect of conductivity small there (as can be seen in the results presented in Table 7.2), but the intervening layer tends to shield changes. Almost by definition, the layer itself has very low conductivity (and hence loss) because it is saturated with contaminant and contains a negligible amount of water.

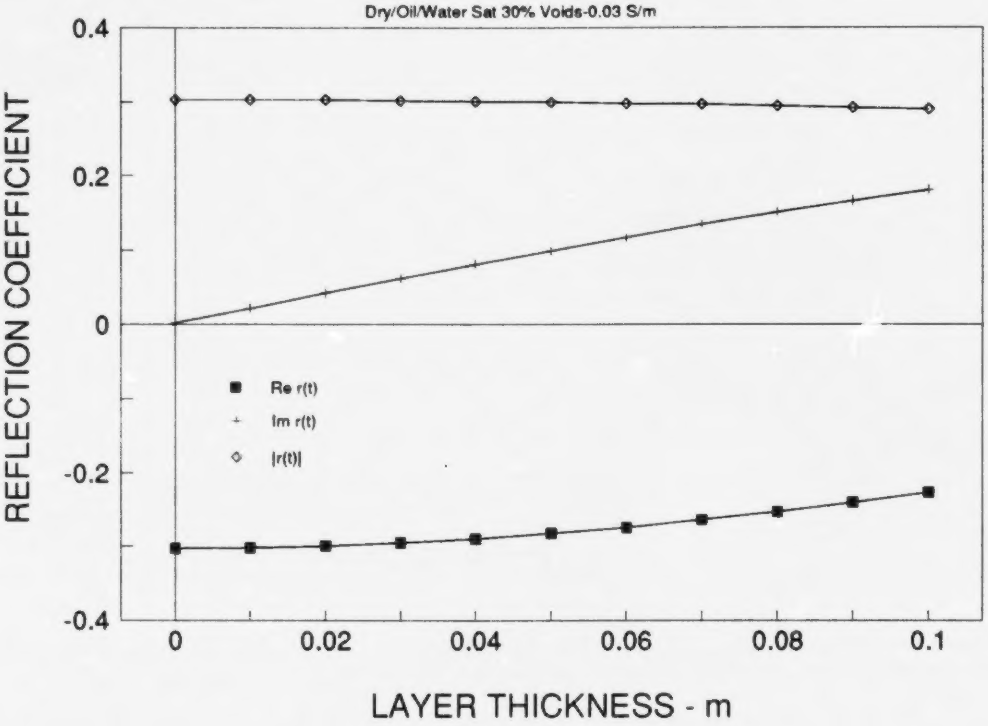

Figure 7.3. Real part, imaginary part, and magnitude of the reflection coefficient vs. layer thickness of a contaminant-saturated layer sandwiched between dry and water-saturated soils (30% porosity and 0.03 S/m water conductivity.

As might be expected, changing the operating frequency in the case of thin layers has a nearly proportional effect on the relative strength of the imaginary component of r. Figure 7.5 illustrates this. The imaginary part of r arises from multiple reflections and interference between the two interfaces, which become larger relative to the period of an rf cycle as the frequency increases. Eventually, as the frequency increases or the layer gets thicker, cyclical interference phenomena appear. Note that the behavior in Figure 7.6 fairly closely follows the $r = r_c(1 + jf/f_c)$ behavior predicted for thin layers.

The emphasis here has been on the detectability of thin layers, since they are apparently both more likely to occur and harder to detect. Thick layers will produce strong, reverberating echoes that would be relatively easy to detect.

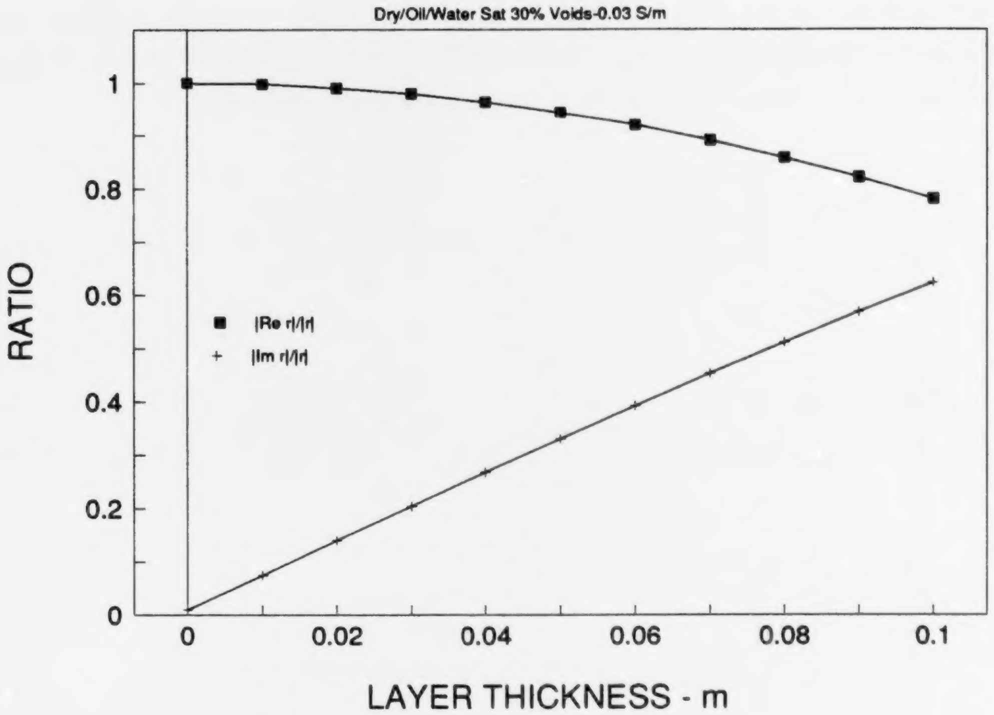

Figure 7.4. $|\Re r(t)|/|r(t)|$ and $|\Im r(t)|/|r(t)|$ vs. layer thickness for a contaminant-saturated layer sandwiched between dry and water-saturated soils (30% porosity and 0.03 S/m water conductivity).

The final consideration is how to detect the presence of a significant imaginary component of r. Information on r is contained in the GPR output signal. Although this signal is real, it is convenient to treat it as being the real part of a complex, "analytic" signal. The imaginary part of the signal, or echo from the layer, can be obtained directly if the GPR employs a quadrature detection system (the only GPR known to do this directly is the existing synthetic-pulse GPR). For the more common type of GPR, which directly digitizes the entire real signal, the alternative is to compute the imaginary part using a Hilbert transform (Appendix A). It would not be necessary to compute the Hilbert transform of the entire GPR sweep; only the part of the echo from the water table interface needs to be analyzed because it is the signature of that feature which is needed.

In the time domain, a GPR output signal is actually the convolution of the transmitted radar pulse with a function that describes the scattering medium. For reflection from a plane interface in non-dispersive media, this simplifies to convolution with a delta function, so that the received signal is a delayed, reduced-in-magnitude replica of the transmitted signal. In the frequency domain, this convolution corresponds to multiplication by a function

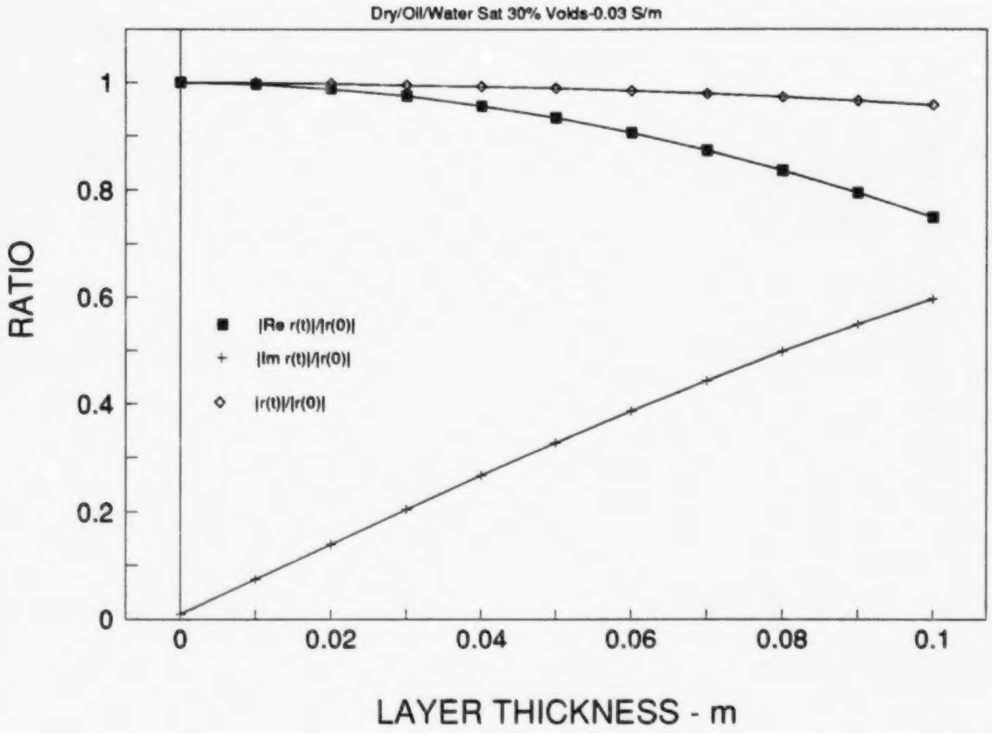

Figure 7.5. $|\Re r(t)|/|r(0)|$, $|\Im r(t)|/|r(0)|$, and $|r(t)|/|r(0)|$ vs. layer thickness for a contaminant-saturated layer sandwiched between dry and water-saturated soils (30% porosity and 0.03 S/m water conductivity).

$$H(f) = r_0 = r_r \exp\{-j2\pi f(\tau_0 + \Delta\tau)\} .$$

Here, τ_0 is the macroscopic delay due to propagation to the layer and back and $\Delta\tau$ is a perturbation, which could be caused by a small change in range or delay. For small perturbations, $2\pi f \Delta\tau \ll 1$, so

$$r_0 \cong r_r e^{-j2\pi f \tau_0}(1 - j2\pi f \Delta\tau) ,$$

which is the same form as reflection from a sandwiched layer. Indeed, for a thin, relatively low-loss layer,

$$\Delta\tau = 2k_2 d \frac{\eta_2^2 - \eta_3^2}{\eta_1^2 - \eta_3^2} \Delta\tau_0 = \frac{\varepsilon_3 - \varepsilon_2}{\varepsilon_3 - \varepsilon_1} \Delta\tau_0 ,$$

where $\Delta\tau_0$ is the additional time delay if the range to the water table is increased by a distance equal to the thickness of the layer. Thus, the effect of a localized, thin layer is qualitatively the same as a local increase of depth of the water table. It would be difficult to distinguish between the presence of a layer and a local drop in the level of the water table.

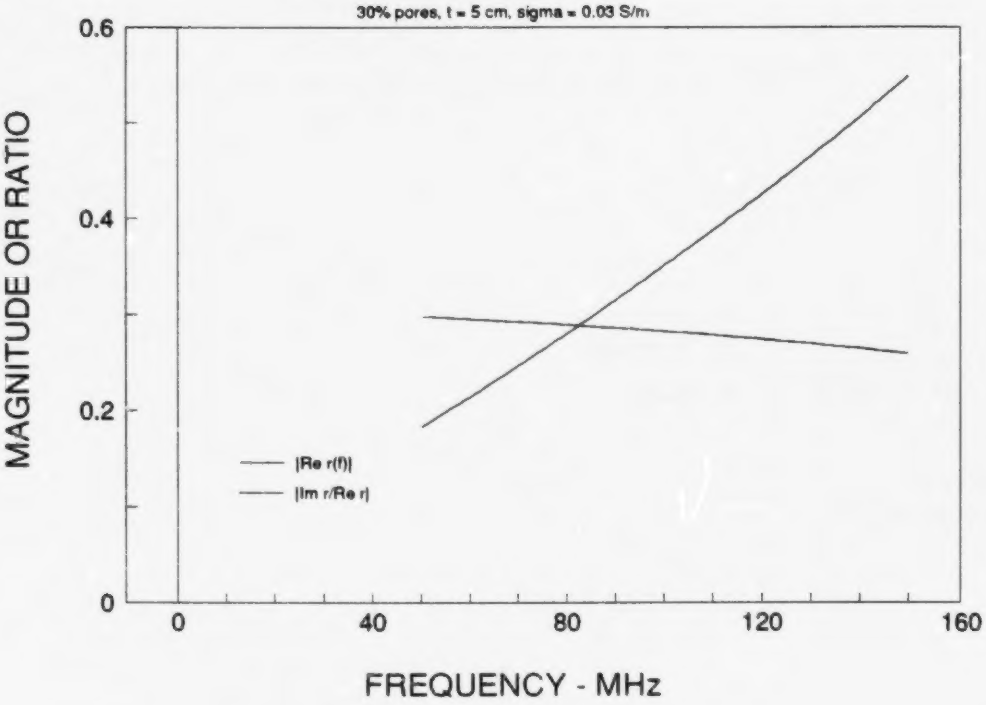

Figure 7.6. Magnitude of the real part of *r* and the ratio of the imaginary to real parts vs. frequency (30% porosity, 5-cm thickness, and 0.03 S/m water conductivity).

However, from a remediation standpoint, one would naturally look for low places in the water table because that is where contamination would be expected to collect. This analysis shows that any contamination filling low spots on the water table will at least not suppress the effect. The key to detecting thin layers of contamination floating on the water table may be SAR processing, because it acts to automatically remove macroscopic phase shifts due to propagation as well as concentrating the signal from the specular reflection point.

7.5 Model II Strategy: Volume Scattering from Soils

The idea here is that small density variations in the soil due to pebbles, rocks, different grain sizes, and even the pores between and inside the grains will produce some level of volume scattering. It is well established that a medium with a spatially varying dielectric constant (or refractive index) will scatter rf energy. It is postulated that contaminant will displace air or water in the pores and thus alter the strength of the dielectric constant variations.

To start with, we need a model for the scattering from a spatially randomly varying medium. Perhaps the simplest of these leads to the Booker-Gordon formula for the backscatter per unit volume due to statistically homogeneous and isotropic refractive-index (or dielectric constant) fluctuations:[18]

$$\rho = \frac{k^4 l^3 < (\varepsilon_r - 1)^2 >}{2\pi(1 + 4k^2 l^2)} .$$

Here, $k = 2\pi/\lambda$ is the rf wavenumber in (average background) medium, and l is the correlation distance of dielectric constant fluctuations in the medium. This medium is assumed to have an exponential correlation function; for example,

$$B_{\varepsilon_r - 1}(r_d) = < (\varepsilon_r - 1)^2 > \exp(-r_d/l) .$$

It will be seen that the magnitude of l is about the same as the average grain size. There are some other assumptions. First, the correlation distance l is to be much smaller than the size of the scattering volume. Second,

$$(\varepsilon_r - 1)kl \ll 1 .$$

This expression essentially says that the rf field inside a grain is to be the same as the one outside; it thus puts a restriction on the product of grain size and relative dielectric change. In addition, there is a much more severe assumption that $\Delta\varepsilon_r = (\varepsilon_r - 1)$ itself should be small compared to unity. Although it turns out that this last assumption (i.e., that $< \Delta\varepsilon_r^2 >$ can be small) is often reasonably well justified for dry and contaminated soils in a statistical sense, it is not true for soils with significant amounts of water. Furthermore, the approximation is not generally satisfied at a more fundamental level of the electromagnetic problem. In addition, weak-scattering theory is being applied to a situation where strong scattering may occur. Thus it must be recognized that the numerical results presented are approximate and in some cases may be correct only to an order of magnitude. These approximations are justified by the intrinsically great uncertainties in soil properties, the immediate need to obtain even order-of-magnitude estimates, and the fact that such estimates are adequate for comparing different GPRs.

However, it appears that a simple extension of the Booker-Gordon theory will produce a better approximation than the formula presented above over a wider range of dielectric constant

---

[18] If the mean value of the fluctuations relative to the surrounding medium is unity, and the fluctuations are weak, so that $\Delta\varepsilon \cong 4\Delta n$, where n is the refractive index, this expression takes on its more familiar form:

$$\rho = \frac{2}{\pi} \frac{k^4 l^3 < \Delta n^2 >}{1 + k^2 l^2} .$$

fluctuations. The modified Booker-Gordon scattering formula is presented in Appendix C. The new expression for the backscatter per unit volume is:

$$\rho = \frac{k^4 l^3 < \xi^2 >}{2\pi(1+4k^2 l^2)},$$

where

$$\xi = \frac{3(\varepsilon_r - 1)}{(\varepsilon_r + 2)}.$$

For small $< \Delta\varepsilon_r^2 >$, this provides the same predictions as the standard Booker-Gordon formula. It is more conservative for large values of $\Delta\varepsilon_r$.

The next step is to relate the correlation function to soil properties. A simple, two-constituent soil model with different dielectric properties will be used. As one proceeds along an imaginary line through the soil, the local dielectric constant will jump back and forth at random points between the two dielectric values. One example is solid rocks and pebbles imbedded in smaller-grained material. At the other extreme one can imagine an essentially homogeneous soil of fine particles with some void fraction. The primary difference between the two is in the correlation distance.

This model is an example of one of the classic "random telegraph" waveforms, where the signal jumps randomly between values y_1 and y_2 at an average rate ζ. The number of jumps in an interval are assumed to follow the Poisson probability law. It is a straightforward matter to show that the corresponding correlation function is in fact exponential (Appendix D):

$$B_\xi(r_d) = < \xi^2 > \exp(-2\zeta r_d).$$

Now, the relationship between soil conditions and the model parameters must be determined. One required parameter is the correlation distance, l. To estimate this, suppose that there are m particles of interest per unit volume and that the average particle size is $\bar{d}$. Then the volume fraction occupied by the particles will be

$$\phi \cong m\bar{d}^3,$$

the number of shifts per unit length will be

$$\zeta \cong 2m^{1/3} \cong \frac{2\phi^{1/3}}{\bar{d}},$$

and the correlation distance will be

$$l = \frac{1}{2\zeta} \cong \frac{\bar{d}}{4\phi^{1/3}}.$$

The correlation distance can also be expressed in terms of the average distance between particles, $\bar{s}$. The number of particles per unit volume is approximately

$$m = \left(\frac{1}{\bar{s}^3}\right).$$

Consequently,

$$\phi \cong m\bar{d}^3 \cong \left(\frac{\bar{d}}{\bar{s}}\right)^3,$$

and

$$l \cong \frac{\bar{s}}{4}.$$

These expressions are thought to be reasonably accurate so long as ϕ is not too large ($\phi \leq 0.5$).

The other required parameter is the variance of fluctuations. Suppose that a fraction ϕ of the soil has an effective refractive index ε_{r1} and the rest has ε_{r2}. Then, approximately,

$$p(y = \varepsilon_{r1}) = \phi^{1/3},$$

$$p(y = \varepsilon_{r2}) = 1 - \phi^{1/3},$$

$$< \varepsilon_r^2 > = \phi^{1/3}\varepsilon_{r1}^2 + (1 - \phi^{1/3})\varepsilon_{r2}^2,$$

$$< \Delta\varepsilon_r^2 > = \phi^{1/3}(1 - \phi^{1/3})(\varepsilon_{r1} - \varepsilon_{r2})^2,$$

and

$$< \xi^2 > = \phi^{1/3}\xi_1^2 + (1 - \phi^{1/3})\xi_2^2.$$

For the case of a soil consisting of small grains with ε_1 and voids with ε_2, the soil porosity is given by $(1 - \phi)$. Table 7.3 lists some representative values for $< (\varepsilon_r - 1)^2 >$ and $< \xi^2 >$ for three mixtures of soil and void material (i.e., air, water, and contaminant) at three porosities. Also included in Table 7.3 are the corresponding values of the dielectric constant of the medium, ε_{ave}, which are obtained independently from the soil mix dielectric properties calculation. These examples are intended to illustrate the range of magnitudes of these quantities. Intermediate levels of saturation will produce intermediate values of these parameters. As anticipated, using the modified Booker-Gordon formula produces similar values for $< (\varepsilon_r - 1)^2 >$ and $< \xi^2 >$, and hence the predicted scattering strength, except when the dielectric changes are large, as when water is added, where the modified form predicts a significantly lower backscatter level. Note that there is a rather strong sensitivity to the presence of contaminant.

Similar values of $< \xi^2 >$ can be expected for other mixes, such as rocks and pebbles imbedded in soils. For example, consider a mixture consisting of $\phi = 5\%$ rocks ($\varepsilon = 4.5$)

Table 7.3. ε_{ave}, $<(\varepsilon_r - 1)^2>$, and $<\xi^2>$ vs. Porosity and Mixture Type

ε_{ave}	$<(\varepsilon_r - 1)^2>$	$<\xi^2>$	**Porosity - $(1-\phi)$**							
		30%			**40%**			**50%**		
Mixture	Soil Grains (ε=4.5) -Air (ε=1)	3.0	0.27	0.25	2.6	0.51	0.39	2.2	0.94	0.57
	Soil Grains (ε=4.5) -Water (ε=81)	10.4	5.5	0.92	14.2	3.9	1.2	19.5	2.5	1.3
	Soil Grains (ε=4.5) -Contaminant (ε=2)	3.7	0.067	0.070	3.4	0.11	0.11	3.2	0.16	0.14

imbedded in dry soil that itself has 30% porosity, which has a dielectric constant $\varepsilon_{soilmix} = 3.0$. Here, $<\xi^2> \cong 0.068$. Table 7.4 summarizes the changes if the soil becomes saturated with water or contaminant. These changes should produce a detectable contrast between dry, wet, and contaminated mixtures. As expected, the presence of contaminants is revealed by a reduction in scattering, which would appear as a blank region in a picture of the underground environment.

Table 7.4. ε_2 and $<\xi^2>$ for a Mixture of Rocks and 30% Porosity Soil

Mixture	ε_2	$<\xi^2>$
5% Rocks/95% Dry Soil	3.0	0.068
5% Rocks/95% Water-Saturated Soil	10.4	0.18
5% Rocks/95% Contaminant-Saturated Soil	3.7	0.013

It is expected that the rf wavelength will usually be significantly larger than the correlation distance. In that case, the radar cross section per unit volume becomes

$$\rho \cong \frac{k^4 l^3 < \xi^2 >}{2\pi}.$$

The strong dependence on *l* mirrors our expectation that a soil consisting of rocks and pebbles imbedded in dirt will be a much stronger scatterer than small grains and voids. After inserting the values for *l* and $<\xi^2>$, one obtains

$$\rho = \frac{k^4 \overline{d}^3}{128\pi}\left(\frac{\phi^{1/3}\xi_1^2 + (1-\phi^{1/3})\xi_2^2)}{\phi}\right).$$

Finally, one needs to consider the scattering volume in order to calculate the rcs; in this application the post-migration volume is the appropriate quantity. An estimate of the smallest volume can be obtained from SAR concepts. For a focused synthetic-aperture GPR, which typically uses an antenna size of approximately one-half wavelength, the lateral resolution is of the order of one-quarter wavelength. The range resolution is determined by the pulse length, and is typically about three-quarters of the center-frequency wavelength for the wideband GPRs. Thus the minimum scattering volume is on the order of

$$V_{\min} \cong 0.15\lambda^3 \cong (\lambda/2)^3$$

(here, λ is the wavelength *in* the ground). The rcs is thus

$$\begin{aligned}\sigma_{\min} &= \rho V_{\min} \\ &= \frac{(\pi \bar{d})^3 \varepsilon_{ave}^{1/2}}{64\lambda_o}\left(\frac{\phi^{1/3}\xi_1^2 + (1-\phi^{1/3})\xi_2^2)}{\phi}\right) \\ &= \frac{(\pi \bar{d})^3 \varepsilon_{ave}^{1/2}}{64\lambda_o}\left(\frac{<\xi^2>}{\phi}\right),\end{aligned}$$

where λ_o is the free-space center-frequency wavelength.[19]

These considerations show that contamination could produce detectable changes in volume scattering. But first it must be determined whether there is sufficient scattering to produce a detectable echo at all. The lower limit is scattering from the intrinsic graininess of the soil. Soils containing a distribution of pebbles, gravel, stones, etc., will presumably yield larger volumetric scattering.[20]

The next task is to ascertain the radar sensitivity required to detect volume backscatter from the intrinsic graininess of the soil. Table 7.5 lists values at 100 MHz for the rcs and minimum value of Q needed to detect volume scattering at 10-m depth in low-loss (dry) soil with a 1-s observing time duration vs. the mean particle diameter. The soil is assumed to be homogeneous with 30% porosity, and has an average dielectric constant of 3.0. Table 7.5 shows that it would not be possible to detect the intrinsic scattering due to soil graininess with a conventional GPR (e.g., with Q = 140 dB re 1s) unless the soil were very coarse (i.e., made up of stones bigger than 10 cm) or the observing time was much greater than 1 s. The implication is that an advanced synthetic-pulse GPR would be needed in order for this detection strategy to be considered a possibility.

---

[19] Note that this formula does not apply for small values of ϕ, which is the case for mixtures with widely spaced scatterers. The requirement that the correlation distance be small compared to both the scattering volume and rf wavelength imposes the condition

$$\phi^{1/3} \gg \frac{\bar{d}}{2\lambda}.$$

[20] Note that a distinction is being made between a more or less homogeneous distribution of scatterers that occupy a multiplicity of resolution volumes and widely spaced, isolated scatterers. The former produce a relatively smooth picture, whereas the latter, after SAR migration, are distinctly resolved. With this detection strategy, one looks for relatively slow changes in background level that are due to contaminants. Individual scatterers are a nuisance (a major aspect of the SAR processing is to localize their influence).

Table 7.5. Minimum Q vs. $\bar{d}$

$\bar{d}$ **(mm)**	σ **(m²)**	Q_{min} **(dB re 1 s)**	Q_{min} **(dB) (τ_{obs} = 3000 s)**
0.01	1×10^{-16}	260	225
0.1	1×10^{-13}	230	195
1	1×10^{-10}	200	165
10	1×10^{-7}	170	135
100	1×10^{-4}	140	105

Adding water or contaminant to the soil changes the picture. As seen in Table 7.3, when the 30%-porosity soil used in this example is saturated with water, $<\xi^2>$ increases by about a factor of 4; furthermore, ε_{ave} rises from 3.0 to 10.4, so the rcs, which is proportional to

$$\varepsilon_{ave}^{1/2} < \xi^2 > ,$$

increases by 8 dB. However, according to the soil dielectric properties calculation, if the added water has moderately high conductivity ($\sigma = 0.03$ s/m), the attenuation becomes 0.4 dB/m at 100 MHz, or 8 dB for 10-m depth. Thus, this increased attenuation nearly counteracts all of the rcs increase due to the water. Higher values of water conductivity or soil porosity will greatly increase the losses and reduce detectability.

Contaminants will generally reduce the rcs. For example, saturating the soil in this example with contaminant will cause the rcs to drop by 4 to 5 dB. This contrast should be big enough to provide a good opportunity to detect contaminant-soaked soils. Another important point discovered here is that scattering from fairly small-scale graininess is in principle detectable with an advanced (synthetic-pulse/SAR), high-Q GPR.

Imbedded pebbles, rocks, etc., lead to soil conditions that usually produce much greater radar signal than the intrinsic graininess. For example, consider a mixture consisting of $\bar{d}$ = 2.5-cm stones, whose average spacing is $\bar{s}$ = 10 cm, imbedded in the 30%-porosity soil. Here,

$$\varepsilon_1 = 4.5 ,$$

$$\varepsilon_{ave} \equiv \varepsilon_2 = 3.0 ,$$

$$l \equiv \bar{d} = 2.5 \text{ cm},$$

$$\phi = \left(\tfrac{1}{4} \right)^3 = 0.0156 ,$$

and

$$< \xi^2 > = 0.046 .$$

For this mixture, the calculated rcs at 100 MHz is about $\sigma = 1.3 \times 10^{-5}$ m². Thus, adding 5% rock will raise the scattering level by more than 110 dB above the intrinsic scattering from silty soil with ($\bar{d}$ = 10 μm) grains. A standard GPR with a Q = 140 dB re 1 s would just be on the verge of seeing this enhanced scatter under the conditions used in the example (i.e., dry, low-loss soil). Increased losses, of course, will reduce the visibility.

Table 7.6 shows what happens in this example when the soil part of the mixture contains water or contaminant instead of being dry. Listed there is the average dielectric constant of the background medium plus the value of the quantity

$$\varepsilon_{ave}^{1/2} < \xi^2 > ,$$

which is proportional to the rcs. For a water-saturated 30%-porosity soil, the predicted rcs rises to 3×10^{-5} m^2; with contaminant saturation, it drops to 2×10^{-6} m^2. There will be about a 6- to 7-dB contrast between dry and contaminant-saturated soil in this example, somewhat larger than the 4- to 5-dB contrast produced in scattering from the fine-scale graininess. Clearly, the presence of larger particles can dominate the volumetric scattering and enhance the volume scattering contrast produced by contaminants. However, volumetric scattering contrasts are generally subtle, which implies that careful and extensive spatial averaging would be needed to bring out the desired features.

Table 7.6. ε_{ave} and $\varepsilon_{ave}^{1/2} < \xi^2 >$ for $\bar{d}$ = 2.5 cm, $\bar{s}$ = 10 cm Stones in Various Soils

Soil Condition	Porosity of Soil Component			
	30%		50%	
Dry	3.00	0.080	2.22	0.22
10% Water	3.38	0.041	2.75	0.11
30% Water	4.35	0.00061	4.25	0.0017
60% Water	6.35	0.066	8.24	0.21
100% Water	10.4	0.39	19.5	1.18
10% Contamination	3.12	0.066	2.34	0.19
30% Contamination	3.25	0.052	2.52	0.15
60% Contamination	3.45	0.035	2.79	0.11
100% Contamination	3.71	0.019	3.16	0.060

Table 7.6 also illustrates another phenomenon. Under partial water saturation the dielectric constant of the soil-plus-water component can match that of the rocks, which makes the rocks invisible to the GPR. However, no amount of contaminant can produce this effect. Thus, regions where contaminant displaces soil moisture will become visible to a GPR.

Table 7.7 lists various quantities, including the minimum required Q to just detect (SNR=1) this scattering at 10-m depth in dry, low-loss soil and a 1-s total observation time. Operation in other soils can be readily scaled from these numbers. In no case would a standard GPR be able to detect the scattering.

Table 7.7. Backscatter Quantities for Solid Particles Imbedded in Dry, Low-Loss, 30%-Porosity Soil at 10-m Depth (T_{obs} = 3000 s)

ϕ	$<\xi^2>$	$\bar{s}$ (mm)							
σ-m^2	Q_{min}-dB	3		10		30		100	
	1	0.037	0.061	0.001	0.018	3.7×10^{-5}	0.0061	1×10^{-6}	0.0018
		5×10^{-10}	160	5×10^{-9}	150	5×10^{-8}	140	5×10^{-7}	130
	3	0.5	0.025	0.027	0.055	0.001	0.018	2.7×10^{-5}	0.0055
$\bar{d}$		2×10^{-9}	155	1.5×10^{-8}	145	1.4×10^{-7}	140	1.5×10^{-6}	125
(mm)	10	$\phi > 1$	-	0.5	0.15	0.037	0.061	0.001	0.018
		-	-	9×10^{-8}	140	5×10^{-7}	130	5×10^{-6}	120
	30	$\phi > 1$	-	$\phi > 1$	-	0.5	0.15	0.027	0.055
		-	-		-	2×10^{-6}	125	1.5×10^{-3}	115

The approach taken here was to model soil irregularities such as the fine-scale graininess and imbedded macro-scatterers (pebbles, stones, etc.) as statistical fluctuations in the local dielectric constant. The theoretical development and results are valid for relatively closely spaced scatterers that are small compared to the rf wavelength. An alternative approach, which is valid for widely spaced individual scatterers, is to sum the contributions from the individual scatterers (various degrees of multiple scattering and interaction could be introduced to account for closer spacing). This approach, however, does not seem particularly useful because it does not bring out the effect of adding contaminant. In other words, one would never be sure whether the radar is detecting a small rock in a contaminant-free zone or a larger rock in a contaminated region.

Real soils cannot be expected to be homogeneous. Variations in porosity over the scattering volume will also produce scattering. Reports indicate that the porosity varies from point to point with a standard deviation of 5 to 20% of the mean, but do not provide any information concerning the distance scale (i.e., the correlation length) [18]. This information would be needed to calculate the volume scattering coefficient due to porosity variations. Larger-scale variations of porosity will produce a texture that could add to or compete with the volume scattering. However, the effects of contaminants would be expected to be the same as for homogeneous soils. That is, changes in the scattering from porosity variations should also track the contaminant.

Note that the lateral dimension of the minimum scattering volume is on the order of 50 to 100 cm, depending on the average soil dielectric constant and operating frequency. Since this is probably much smaller than the plume dimension, it is possible to obtain processing gain by spatially averaging the migrated echoes. Essentially, it is desirable to process the data three-dimensionally through filters matched to expected plume characteristics. Another useful strategy might be to increase the effective scattering volume by reducing the radar bandwidth (i.e., increasing the pulse width) and restricting the SAR aperture. These trade-offs should also be looked at.

Also note that the radar cross sections per unit volume are generally very small in these examples. This means that additional propagation loss due to scattering will be negligible and multiple scattering will not be important.

In conclusion, it appears that contaminants can produce detectable changes in volume scattering if a high-Q radar is used. The remaining question is whether these changes are masked by natural variations in volume scattering that are *on the same scale* as those found in the plume.

7.6 Model II Strategy: Deducing Changes in the Local Average Refractive Index

SAR processing requires the dielectric constant of the soil as an input. As this parameter is unknown, it is necessary to estimate it somehow. One way is to use the radar data themselves. One vendor, for example, has an analysis program that permits the operator to manually superimpose a computer-generated hyperbola on a data display and adjust it to match observed features due to discrete scatterers. The computer-generated hyperbola incorporates the dielectric constant. It is then used to migrate the data over the field. This is successful to the extent that the dielectric constant remains uniform over the field. Otherwise, the hyperbolas change shape and/or deviate from hyperbolic form altogether.

This suggests that localized changes of the dielectric constant could be detected by (1) adaptively changing the migration parameter over the field or (2) quantifying the mismatch between the "average" hyperbolas and the local curves. Of course, to do this in a "traditional" way would require a sprinkling of strong discrete scatterers throughout the field both above and below the suspected contamination region. However, as shown above, the volumetric scattering even from uniform soils is detectable with high-Q radars. It may be possible to devise a test of migration quality of volumetric scattering or find out how much perturbation of the local dielectric constant is required to achieve a sharp migration "focus" of small-scale variations of the volumetric scatter level.

7.7 Section Summary

The impact of these strategies on the required radar performance can now be assessed. Several new and interesting findings have come out of the work described in this section. These relate to the strategies associated with Models IA and II.

First, it appears that when the contaminant has a low dielectric constant there are fairly large contrasts (up to 7 dB) in volumetric scattering between contaminated and uncontaminated regions. Most contaminants possess this electrical characteristic. Of course, the contaminant has to be present in sufficient concentration to appreciably alter the electrical properties of the soil. The intrinsic volumetric scattering from the soil itself can be detected if a sufficiently sensitive GPR is used. (This is true of nearly all soils.) A GPR with significantly greater sensitivity than provided by the standard commercial units is needed, unless the soil happens to have a lot of large rocks in it. This finding evidently provides an explanation as to why GPRs have not been generally employed for remediation and contaminant mapping, although there is some reported experimental evidence that a contaminant having a low dielectric constant does suppress volumetric scattering [17]. This analysis may be the first attempt to quantify both the effect of the shifts in dielectric constant and the consequent requirements of the GPR.

Second, while the results for fine particles (silts and clays) would at first suggest that unachievably high values of Q are necessary to detect Model II contamination, such high Q may not really be required. This is because it is likely that fine materials have larger particles (sand, pebbles, etc.) interspersed in the volume. The larger particles may thus contribute to detectable levels of volume scattering contrasts.

Third, it was determined that a thin layer of contaminant "floating" on the water table will produce a measurable signature if it is more than a few centimeters thick. The echo from the water table will be modified in a distinctive fashion. Since the reflection coefficient of the water table interface is generally very large, a GPR may not need a very high Q in order to detect this change. Since the effect appears as a local increase in the depth of the water table, it may be difficult to distinguish an apparent depth increase due to a thin contaminant layer from an actual increase. However, from a remediation standpoint, depressions in the water table would be the most likely places to look for contaminants.

Thick layers of contamination would be easier to distinguish because the changes produced in the signature are on the same order as the echoes themselves. The only sensitivity issue is, then, the desired depth of penetration, which is so soil-dependent and variable that it is impossible to make a general statement about it except to say that more sensitivity is better.[21]

---

[21] This advice is given with the caveat that if the GPR is too sensitive, clutter (especially from above-ground reflections) can mask the desired signal.

Lastly, we note that there are no particularly strong GPR requirements associated with the Model IB strategy. A large reflection coefficient and resultant strong echo will be produced by the formation of a contaminant/water interface. As with Model IA, more sensitivity is generally better, since it permits a greater depth of penetration.

Section 8

RADAR SYSTEM DESIGN

Radar system design begins with a specification of the externally determined operating requirements, such as range coverage, resolution, search rate, and minimum detectable target size. These specifications must be tempered by practical limits imposed by technology and cost. Invariably, there are compromises made to arrive at an optimum design. Here, there are only two basic specifications, sensitivity and resolution. These determine the GPR configuration (e.g., short pulse vs. synthetic pulse), center frequency, and bandwidth.

It is desirable to maximize resolution to the extent possible, which implies a system with a fractional bandwidth near unity. Then only the center frequency remains to be specified. Due to the extreme variability of the environment, a single "best" center frequency is difficult to specify. Because of the large fractional bandwidth, the analysis approach is to consider frequency bands spaced by half-decades. These trade-off analyses for a variety of conditions showed that a center frequency near 100 MHz affords a reasonable and generally applicable compromise between penetration depth and resolution. The 30-MHz band has lower attenuation, and thus permits greater penetration, but has a SAR-processed resolution on the order of 2 to 3 m (6 to 10 ft), which is probably inadequate. The 300-MHz band has good resolution (20 to 30 cm, or about 1 ft), but suffers high attenuation except under unusual circumstances. A further consideration regarding resolution involves the blanking of the receiver during pulse transmission, which limits the minimum range depth coverage.[22] In the 30-MHz band, the pulse width will be about 33 ns, so echoes from at least the first several meters (6 to 10 ft) into the ground will be lost. The choice of operating frequency also affects sensitivity. There is somewhat more GPR power generally available at lower frequencies, and this improves sensitivity. However, the volumetric scattering rcs is proportional to the cube of the frequency, a fact that appears to favor higher frequencies. However, since attenuation enters as an exponential factor that increases rapidly with frequency, it will sooner or later dominate the advantage provided by improved rcs at higher frequencies.

---

[22] For short-pulse GPRs, there is also a time delay while the receiver recovers from overloading due to the powerful transmitted pulse. This does not affect a synthetic-pulse GPR, which must be designed to operate in the continuous presence of the transmitted tone.

GPR sensitivity is determined primarily by the product of its figure of merit and the observation time, $Q \times T_{obs}$. The observation time is determined by the desired search rate, and involves the cost of surveying a remediation site. That is, it will require a relatively long time to survey a site with high losses and low intrinsic volumetric rcs compared to one where losses are low and where there are many underground scatterers. This is because, for a site with high losses, the GPR must move slowly in order to achieve a sufficient dwell time at each of its locations. Once the rcs and range requirements are specified for a given soil condition and a minimum search rate is stated, the minimum value for Q can be established.

As described above, a GPR design intended for remediation work is site-dependent, but in general it must have the largest practically attainable value of Q. Table 8.1 bounds the problem and list values of Q_{min} for several scenarios; this table is intended to suggest the range of values for Q_{min} that would be required. The entries in this table show the value(s) of Q_{min} needed to detect the radar scattering (with an SNR of 10dB) from four different "targets," in three different soil environments, for targets located at four different depths. The targets in the table are: (1) a long, 2-inch-diameter, conducting object such as a pipe,[23] (2) a layer of contaminant above a well-defined water table (Model I contamination), (3) a Model II contamination geometry with 0.1% by volume of imbedded 3 mm grains (which may be more representative of a "real" soil than a pure, intrinsic soil [8, 9], and (4) an intrinsic Model II geometry. The descriptions of the "soils" in this table (sandy silt, silty sand, and clay) are based upon particle size, as shown in the table; for all of the soils here, a 30% saturation is assumed. For each combination of soil, target, and target depth, two values of Q_{min} are given. The first value is the Q_{min} needed to detect that scenario with a T_{obs} of 1 s; this was the T_{obs} used for most of the analysis described above. The second value is the Q_{min} needed to detect that scenario with a 3000-second T_{obs}; this T_{obs} is a likely value for surveying an area at a site and using three-dimensional coherent processing, as discussed in Section 5.4. These values are approximate, and it should be noted that these values represent the underlying detectability of structures that produce scattering; the strategies for locating contamination depend on detecting changes in the echoes from these targets. Depending on the "target" and soil, detectability ranges from "very easy" to "impossible." In general, high attenuation severely limits GPR performance. High-Q (i.e., Q >> 140 dB re 1s) GPRs can access a significantly greater span of possible soil conditions.

---

[23] Perpendicular polarization of the electric field was assumed; while this was not discussed in the report, perpendicular polarization will result in a weaker echo signal strength for the pipe than parallel polarization; thus the polarization used here represents a "worst case" geometry.

Table 8.1. Values of Q_{min} Necessary to Detect Various Targets in Various Environments with SNR of 10 dB

	Depth - meters			
Soil/Target	**5**	**10**	**15**	**20**
Sandy/silty soil, 30% saturation (particle size = 0.5 mm)				
2-in.-diameter pipe-like object	95/60	105/70	110/75	115/80
Model I contamination	60/25	70/35	75/40	80/45
Model II contamination				
-with 0.1% imbedded 3-mm grains	150/115	160/125	170/135	175/140
-with 0% imbedded 3-mm grains	180/145	195/160	200/165	205/170
Silty/sandy oil, 30% saturation (particle size = 0.05mm)				
2-in.-diameter pipe-like object	100/65	115/80	125/90	135/100
Model I contamination	65/30	80/45	90/55	100/65
Model II contamination				
-with 0.1% imbedded 3-mm grains	155/120	170/135	180/145	190/155
-with 0% imbedded 3-mm grains	215/180	235/200	245/210	255/220
Clay soil, 30% saturation (particle size = 0.005 mm)				
2-in.-diameter pipe-like object	240/215	>300	>300	>300
Model I contamination	205/170	>300	>300	>300
Model II contamination				
-with 0.1% imbedded 3-mm grains	270/235	>300	>300	>300
-with 0% imbedded 3-mm grains	>300	>300	>300	>300

One conclusion drawn from the GPR industry survey accomplished during the course of this work is that the basic short-pulse GPR technology has essentially matured. There appears to be little potential for significant further rf hardware development; that is tens of dBs improvement in terms of antenna, pulse, receiver, and so on, are unlikely. Some incremental improvement in power-bandwidth product may result from high-power optically triggered pulser technology currently being developed.[24] However, a 30-dB improvement in *Q* can be obtained by replacing the "sampling-oscilloscope" method of recording the data with a transient digitizer method. It was noted in Section 5.2.1 that a *Q* of perhaps 190 dB re 1 s could be achieved using a high-power pulser and transient digitization. Such a radar could be assembled at the subsystem level (i.e., by connecting a commercially available rf head and controller to an available digitizer/recording system). For the application considered here, however, it is not considered cost-effective to develop or build short-pulse GPR hardware at the subsystem level and below.

---

[24] Optical triggering also provides a benefit by eliminating stray radiation from cabling, since non-conducting optical fibers can be used to connect the GPR head to the control and recording unit. For the same reason, optical fibers are also used to carry the received signals. Note that in the Bureau of Mines synthetic-pulse GPR the original coaxial cables have been replaced by optical fibers.

The status of synthetic-pulse GPR technology is somewhat different. There is only one known prototype unit. As that unit employs older technology, there appears to be considerable opportunity for improvement. According to its specified characteristics, it has a potential Q of about 220 dB re 1 s. It is not well characterized, however, but it is believed that it actually has a Q about two orders of magnitude less than its potential, or about 200 dB re 1 s. This unit nevertheless appears to outperform short-pulse GPRs, and would be adequate for proof-of-principle testing in appropriate soils. Further development of synthetic-pulse GPR technology at both the subsystem and system level is indicated if a more generally useful system is to be developed.

As noted above, the environment is a key factor in selecting a Q for the radar design. A 1988 EPA study described the types of soils found at various Superfund sites around the U.S. [9,19]. This work found that, based upon a total of 151 samples (119 in the Eastern U.S., 32 in the Western U.S.), 40% provided, no information on soil type, 30% were described at "sandy clay," and 20% were described as "sandy." Only 10% of the samples were described as "primarily clay." Thus, based upon this work, one could expect that most soils in areas where radar might be used as a remediation tool would be "sandy clay" or "sandy." Thus, a design choice Q of 220 dB re 1 s would be expected to meet the requirements as much as 90% of the time.

Section 9

Numerical Analytic Model

9.1 Introduction

In Section 7 detection strategies were presented for each of the contamination models described in Section 6. As noted in Section 7, detection depends on radar sensitivity and the environment in which the contaminated soil or water is imbedded. The sensitivity issue is easily resolved within the context of the quality factor for and integration time for the particular radar and the scattering characteristics of the contaminated region as dictated by the models developed in Section 6. The primary purpose of the numerical analytic model is to demonstrate the viability of the detection strategies under conditions more representative of real environments.

Only two generic types of scattering interactions are considered, namely, discrete scattering and reflection. The simplest discrete scatter is an isotropic point source. The simplest reflection occurs at a dielectric interface between two homogeneous media. With appropriate distributions of the location and strength of these elemental scatterers, a wide variety of contamination models can be simulated. A predictive geophysical model must accommodate considerably more detail both in its constituent parts and their mutual scattering interactions; nonetheless, the imbedded non-interacting scatterer (INS) model captures the essential elements of a real scattering environment, and is therefore adequate for optimizing a GPR design and evaluating its capabilities. The INS model, moreover, provides a tractable means of demonstrating the improvements in detection that can be achieved by advanced signal processing.

The numerical analytic model assumes that in the absence of scattering, the ground is a lossy dielectric. Signal attenuation due to ohmic losses is the most severe problem that must be overcome in designing an effective GPR for detection of soil contamination. Thus, the ability of a radar to concentrate energy at depth is the primary figure of merit of the system. The radar parameters that affect this figure of merit have been collected in a single parameter, as described in Section 6; however, signals from a large number of radar locations can be processed coherently to enhance the detectability of a localized scattering region. Matched-filter processing of the combined GPR returns should provide a nearly optimum detection scheme for weak localized scattering regions.

Section 9.2 reviews the draws on the material in Sections 5 and 6 to describe the INS model, which is specified in terms of a minimal set of radar, soil, and cross-section parameters. The model is effectively calibrated so that for a given quality factor and integration time, the output intensity has units of signal-plus-noise power normalized to the average noise power. Thus, unity or zero dB corresponds to the average receiver noise level. By simulating the echo-strength-vs.-depth profiles for a large number of adjacent receiver locations, one can synthesize the "wiggle" display that is commonly used for GPR data presentation. It is more convenient to present the data as contours of constant normalized signal-plus-noise power plotted against ground distance and true depth. In this unprocessed display format, the detected GPR echoes from discrete targets are smeared over hyperbolic arcs.

Section 9.3 describes a matched-filter processing procedure, which is effectively a near optimum time-migration scheme that minimizes the deleterious effects of weak signal contributions to the reconstruction at any subsurface point. One should think of the reconstruction process as a point-by-point interrogation of each subsurface point for scattered energy. The effective size of the interrogation point depends on the bandwidth of the radar and the maximum separation of the receivers. The unambiguous region that can be interrogated depends on the frequency separation or pulse repetition rate and the receiver spacing. Unambiguous angle resolution requires a receiver separation of one half the minimum wavelength in the medium. Similarly, the unambiguous depth is determined by the propagation velocity times twice the reciprocal of the minimum frequency separation. The enhanced detectability of processed radar returns is two-fold. The coherent integration reduces noise and the resultant localization reduces clutter from adjacent targets.

Section 9.4 presents a number of examples that demonstrate these effects for representative systems. The intent here is not to present an exhaustive case study but rather a few examples that clearly illustrate the processing gain that can be used to advantage for remediation of petroleum or chemical spills.

9.2 The INS Model

For a single scatterer at a distance r_{mn} from receiver element n, the GPR signal generator computes the return signal contribution as

$$\hat{v}_n(f) = \hat{p}(f) C_m \exp\{4\pi i f r_{nm}/c(f)\} \frac{\exp\{-2\gamma_r r_{nm}\}}{r_{nm}^2} + \xi_n, \tag{9.1}$$

where ξ_n is a gaussian random variable with variance σ_N^2 and $p(f)$ is a spectral weighting factor, which will be described shortly. For reference,

$$\gamma = -(i\omega\sqrt{\mu\varepsilon})^* = -\left(i \frac{2\pi f}{c_0} \sqrt{\varepsilon/\varepsilon_0}\right)^* \tag{9.2}$$

as defined by the soil model described in Section 6.4. Thus, γ_r is the one-way loss factor, and $\gamma_i = 2\pi f/c(f)$ is the propagation factor.

The depth-dependent return signal is the Fourier transform of Eq. (9.1), which is implemented with an FFT algorithm as

$$v_n(k\Delta r) = \sum_j \hat{v}_n(f_j)\exp\{2\pi ijk/N\}. \tag{9.3}$$

The output is converted to distance units by using $\delta_r = c_0/(2B)$ with c_0 the velocity of light at the center frequency, and B the bandwidth. The pulse spectrum is scaled so that

$$\sum_j \hat{v}_n(f_j) = 1. \tag{9.4}$$

For a pulse with a real nonnegative frequency envelope, this ensures that the maximum value of $p(t)$, the inverse Fourier transform of $\hat{p}(f)$, is unity. The frequency envelope implicitly absorbs any weighting imposed to control range sidelobes.

To display the GPR model output in its simplest form, one plots

$$P_n(k\Delta r) = |\, v_n(k\Delta r)\,|^2 . \tag{9.5}$$

In the absence of frequency dispersion, it follows from Eq. (9.1) and Eq. (9.3) that

$$< P_n(k\Delta r) > = |\, p(2(k\Delta r - r_{nm})/c_0)C_m\,|^2 \frac{\exp\{-4\gamma_r r_{nm}\}}{r_{nm}^4} + \sigma_N^2 . \tag{9.6}$$

The angle brackets denote averaging, and the principal energy content of P_n lies within an interval τ. Eq. (9.6) summarizes the GPR output in arbitrary units. The strength factor C_m implicitly contains all the system parameters as well as the strength of the scatterer. To calibrate the model in real units, note that average power should have the form

$$< P_n(r) > = m4\pi P_T G^2 \lambda_c^2 \sigma_{rcs} \frac{\exp\{-4\gamma_r r_{nm}\}}{(4\pi r_{nm})^4} + F_s k T_0 B_N \tag{9.7}$$

at the peak of the peak of the transmitted pulse, which has been forced to be unity by Eq. (9.4). The m factor implies a coherent integration of m independent returns to form the estimate. The remaining terms are standard elements in the radar equation. To isolate the system factors from environmental and operational factors, a GPR figure of merit has been defined:

$$Q = \frac{f_{prf} P_T G^2}{F_s k T_0 B_N}, \tag{9.8}$$

where f_{prf} is the pulse repetition frequency. Thus, $m = f_{prf}T$ where T is the dwell time. Here B_N is the noise bandwidth, which need not be equal to B, the frequency extent of the incident waveform. The quality factor is a ratio of average received power to the total noise power at the receiver output. In terms of the quality factor,

$$P_n(r) = \left[4\pi Q T \lambda_c^2 \sigma_{rcs} \frac{\exp\{-4\gamma_r r_{nm}\}}{(4\pi r_{nm})^4} + 1 \right] F_s k T_0 B_N \,, \tag{9.9}$$

where T represents the dwell time for the measurement. It is obviously more convenient to express the total received power to total noise power ratio, namely

$$\frac{P_n(r)}{P_N} = Q T \lambda_c^2 \sigma_{rcs} \frac{\exp\{-4\gamma_r r_{nm}\}}{(4\pi)^3 r_{nm}^4} + 1. \tag{9.10}$$

Thus, let

$$C_m = \sqrt{\frac{Q T \lambda_c^2}{N(4\pi)^3} \sigma_{rcs}^m} \,, \tag{9.11}$$

and

$$\sigma_N = 1/\sqrt{N} \,. \tag{9.12}$$

With C_m in Eq. (9.1) defined by Eq. (9.11), the detected intensity as defined by Eq. (9.5) is the ratio of total received power to total noise power. With this definition, the predetection integration or dwell time is accommodated effectively by scaling the receiver noise level. The model parameters that need to be specified are summarized in Table 9.1.

Table 9.1. Model Parameters

Parameter	Definition
Q	Figure of Merit (seconds^{-1})
T_{obs}	Dwell Time (seconds)
σ_{rcs}^m	Radar cross section for mth scatterer (meters^2)
f_c	Center frequency
Δf	Frequency step
N	Number of frequencies (even) distributed about f_c
$f_j = f_c + (j - N/2 - 1)\Delta f$	jth frequency
$\lambda_c = f_c/c(f_c)$	*In situ* wavelength at center

There is considerable interest in a pulsed radar because it provides a comparatively inexpensive way to get a lot of power into a short pulse. In the frequency domain, the pulse is adequately represented by the gaussian form

$$\hat{p}(f + f_c) = \Delta f \sqrt{\pi\tau^2} \exp\{-(\pi\tau f)^2\}. \tag{9.13}$$

With this definition of $\hat{p}(f)$, the pulse envelope has the gaussian form

$$p(t) = \exp\{-(t/\tau)^2\}, \tag{9.14}$$

which satisfies the normalization condition automatically. A typical system might run from 67 to 133 MHz with a center frequency of 100 MHz with $\tau = 2/(\pi B)$.

Modeling propagation and scattering in a dense, highly inhomogeneous medium is currently one of the most challenging problems in electromagnetics and acoustics. Nonetheless, it is possible to construct a simple model that captures the essential elements of the signal environment in which a practical GPR must operate. The model is based on simplified physical descriptions of contamination structures that preserve the dominant signal characteristics although not their complete manifestation in a real radar environment. The resulting radar model is adequate for GPR performance analysis, consistent with design efforts in this phase of the work, but it is not intended for geophysical interpretation of the radar data.

In a homogeneous region of space, Eq. (9.1) effectively describes the backscattered radiation from an isolated point source. Consider an aggregate model consisting of non-interacting scatterers (NIS). It is recognized that the real propagation environment is much more complicated than can be accommodated by the NIS model; however, the model can be expanded in a straightforward manner to accommodate the ground contamination models described above. For example, Model II can be simulated by a wedge- or cone-shaped region of contamination that manifests itself by a randomly distributed collection of point scatterers. Similarly, to model contaminant floating on a water table interface (Model I), a localized reflecting layer can be introduced. In the GPR model, only the receivers very nearly overhead see the reflection. To complete the model, white noise is added to the GPR signal.

9.3 Signal Processing

Coherent, synthetic aperture processing (also referred to as "time-migration" processing in the case of a static target environment) is intuitively motivated by the hyperbolic spread of a single point target return when observed from multiple GPR radar positions. It is clear, however, that integrating the signal returns over hyperbolic signal space sectors is neither optimum nor efficient. A more general procedure uses matched-filter principles; an estimate is made of the contribution of the return signal from position r′ that minimizes the effects of receiver noise. This is achieved by matching the signal with a weighting function that emphasizes the strongest returns. Thus,

$$\bar{\sigma}(\mathbf{r}') = \sum_{j} \sum_{n} \hat{v}_{n}(f_{j}) \exp\left\{ \frac{-4\pi i f_{j} \mathbf{r}'_{n}}{c_{j}} \right\} \left[\frac{\exp\{-2\alpha_{j} r_{n}\}}{\mathbf{r}'_{n}} \right], \tag{9.15}$$

where r'_n represents the distance from the *nth* receiver to the point r′. The reconstruction assumes knowledge of the frequency-dependent attenuation and phase velocity in the medium, which must be estimated. It should also be noted that the reconstruction is performed in the temporal frequency domain. Thus, for a pulsed system, the return from each pulse is discrete-Fourier-transformed to generate the frequency samples at *fj*. For a swept-frequency system, the reconstruction proceeds directly.

The matched-filter operation implied by Eq. (9.5) is applied for each subsurface point within a region below the antenna array. For display purposes, a subsurface image can be formed by computing

$$I_p(\mathbf{r}') = |\,\bar{\sigma}(\mathbf{r}')\exp\{2\gamma_r f_c r_{ns}\} r_{ns}^2\,|^2 . \tag{9.16}$$

The renormalization compensates the weighting that was introduced to minimize noise contamination in the reconstruction. Thus, a point source is reconstructed at the level it would be observed by an overhead receiver. If one further compensates for the signal spreading loss and the attenuation due to absorption, the noise level will increase with depth. For detection purposes, it may be best to accept the same average signal variation that is inherent in the unprocessed displays. Once the processing algorithms have been tested on real data, techniques can be developed to reproduce a fully compensated image to the limits of detection for the particular system.

9.4 Representative Examples

To illustrate the detection capability implied by various systems that could be exploited for GPR leak detection applications, we use a 100-MHz system with a 66-MHz bandwidth. In the simulations this is implemented with 66 discrete frequencies separated by 1 MHz; however, as noted Section 6, this is mathematically equivalent to a 15-ns pulsed system with a free-space unambiguous range of 150 m. That is, the bandwidth primarily establishes the ability of the system to resolve targets in range. The effectiveness of the particular system for GPR is dictated mainly by the quality factor, which is also the primary driver in the cost of the system.

To provide a demanding but realistic propagation environment, the soil model used 100% saturation, 30% void fraction, and 0.003 mhos conductivity, which is representative of saturated silt soil. To address the detection issue in its simplest form, two isolated point targets, one above the other, were inserted at depths of 5 and 30 m. Both scatterers have an equivalent rcs of -70 dB relative to one square meter. This scattering level is representative of the equivalent cross section of typical leak scenarios as discussed in Section 7. The simulations used 80 receiver locations separated by 0.2 m, which provides unambiguous angle resolution at the center frequency of the pulse. The detected radar data are displayed as contours of constant signal-plus-noise intensity, as described above. Matched filter processing is then applied over a 40-by-40 point grid covering a 15-m swath below the receivers to a depth of 35 m. To accommodate the large dynamic range of these processed data, a perspective plot of the reconstructed intensity is used.

Figure 9.1 shows the signals that exceed the average noise level for a Q=140 dB system of the type that is routinely used to detect shallowly buried pipes. No evidence of the targets can be seen. The matched-filtered data are shown in Figure 9.2. The origin of the coordinate system is at -35-m depth and 0-m horizontal displacement. Thus, the left-hand edge of the plot represents the signal at the surface. The vertical axis extends from -50 to 20 dB. The processed data do not recover either of the targets at Q=140 dB. Figure 9.3 shows the same plot as Figure 9.1 for a Q=160 dB system. Here one begins to see the hyperbolic band that is associated with a point scatterer. The processed data shown in Figure 9.4 clearly resolve the upper scatterer. In the unprocessed data the target returns are less than 10 dB above the noise level, whereas the processed data provide about 20 dB of signal-to-noise improvement. Even so, the lower target cannot be detected. It should also be noted that the noise fields for the simulations are identical. This is convenient in that Figures 9.1 and 9.2 can be used to identify purely noise-induced features or false alarms.

As shown in Figure 9.5, increasing the quality factor to 180 dB does not reveal the lower target; however, when the processed data shown in Figure 9.6 to Figure 9.2 are compared, the lower target begins to emerge above the noise level. Figure 9.7 shows the detected returns from a Q=190 dB system, which is just beginning to "see" targets at a depth of 35 m. The processed data shown in Figure 9.8 clearly reveal the lower target. Figures 9.9 and 9.10 show the corresponding simulations for a Q=220 dB system. Here both targets are easily detected in the raw data. The processed data, moreover, are beginning to show the azimuthal sidelobe structure of the matched filter. Because of the complexity of the propagation environment, the sidelobe structure and, to a lesser extent, azimuthal resolution vary with depth. Even so, matched-filter processing will resolve scatterers with 30 to 40 dB of suppression of the returns from adjacent scatterers. This is illustrated in Figures 9.11 and 9.12, which show the effect of moving the lower scatterer to within 5 m of the upper scatterer.

The resolving capability of matched-filter processing is crucial because a real ground environment will contain a variety of imbedded discrete scatterers; moreover, as discussed in Section 7, random variations in the properties of the soil itself are a potential source of backscatter. To simulate this type of environment within the context of the soil contamination models that have been developed for this study, the researchers generated a wedge-shaped region containing a large number of randomly located scatterers with -30-dB cross sections. At the apex of the cone, a single scatterer with a -20-dB cross section was included for reference. Figure 9.13 shows the detected signal plot. One sees a broadened hyperbolic region, which suggests a collection of local scatterers, but the details of the configuration cannot be inferred directly. The processed data shown with a slightly different perspective from the previous plots in Figure 9.14 clearly reveal both the scatterer at the apex and the wedge-shaped extent of the scatterers.

All the reconstructions presented here used perfect knowledge of the average propagation characteristics, whereas this would have to be estimated as part of the reconstruction for real data. Thus, considerable work needs to be done to develop a viable but efficient processor for real data. If the radar has appropriate sensitivity, however, the method holds considerable promise for GPR remediation of underground leak and soil contamination detection.

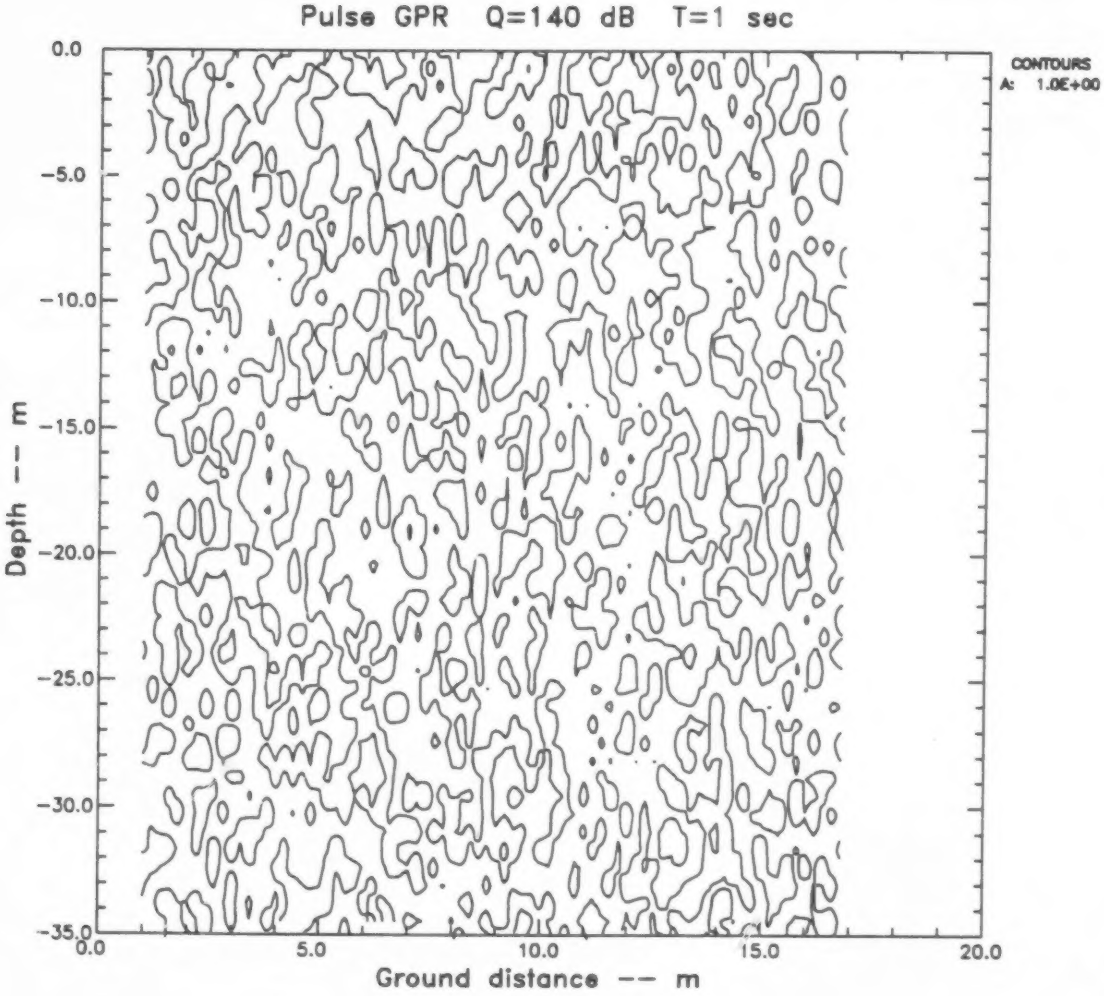

Figure 9.1. Unprocessed simulated returns for Q=140-dB GPR. Point targets are located at 10-m and 30-m depths.

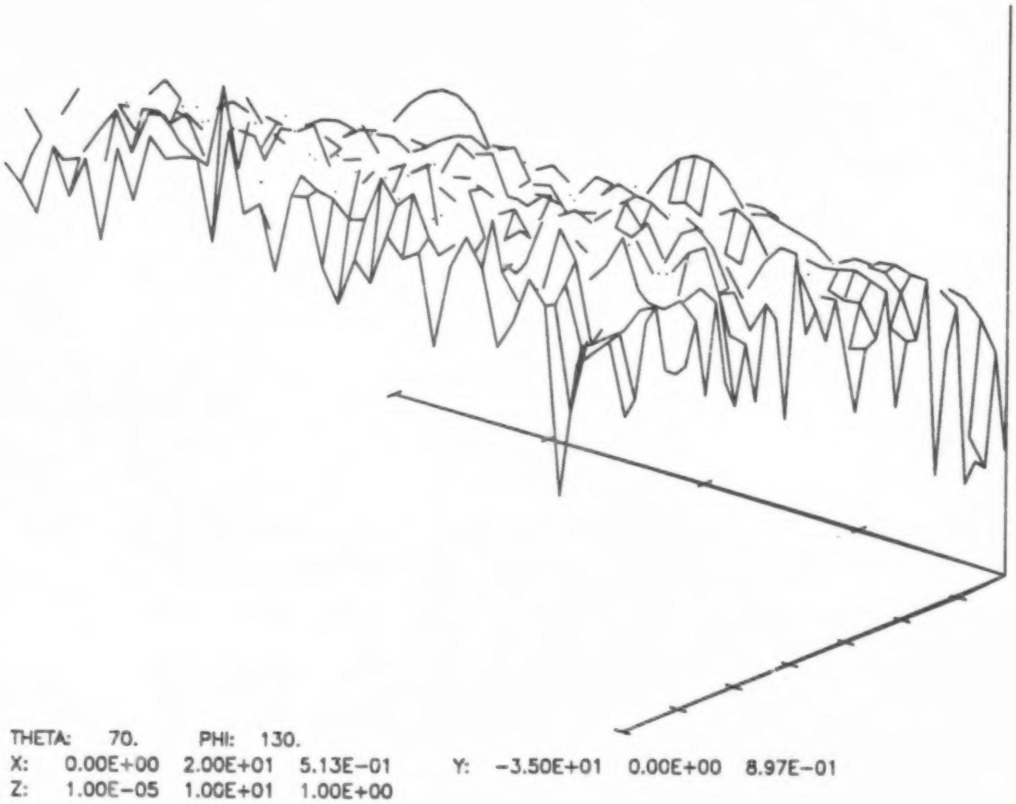

Figure 9.2. Processed returns for Q=140-dB GPR in perspective with 60-dB logarithmic display.

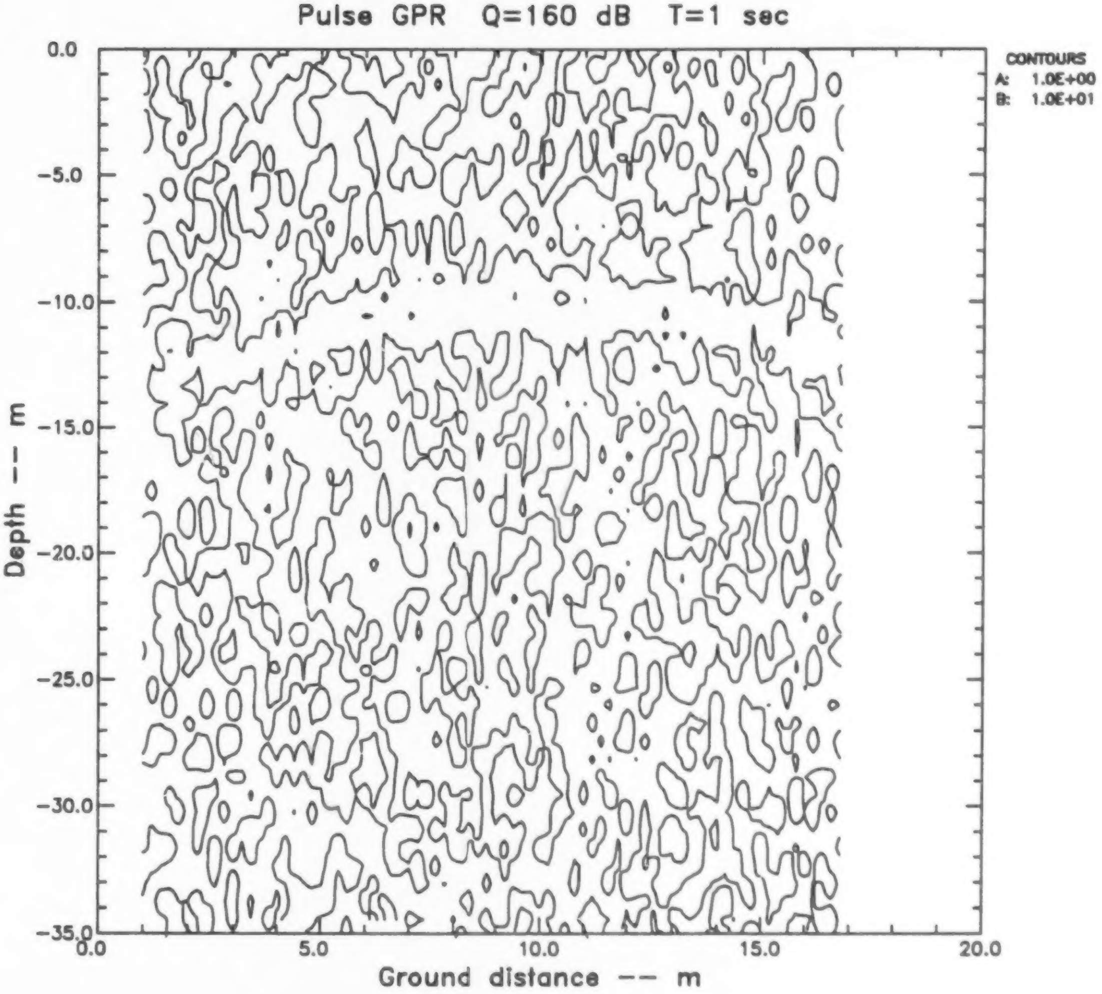

Figure 9.3. Unprocessed simulated returns for Q=160-dB GPR. Point targets are located at 10-m and 30-m depths.

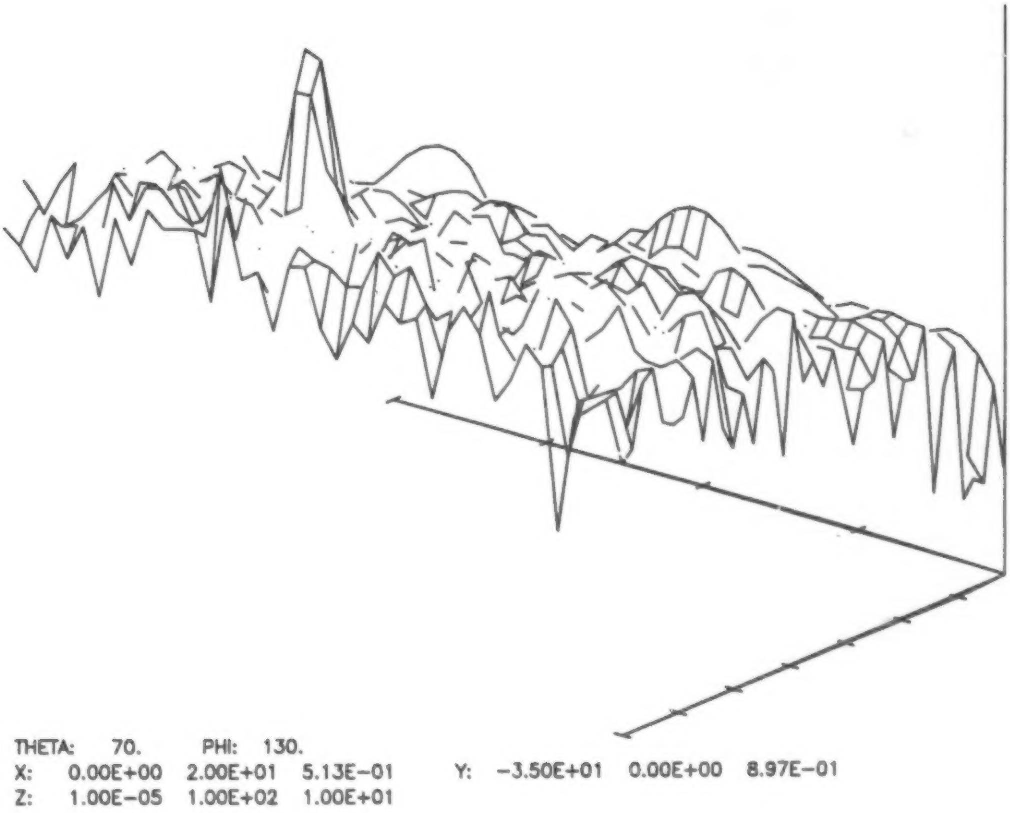

Figure 9.4. Processed returns for Q=180-dB GPR. Upper target is visible.

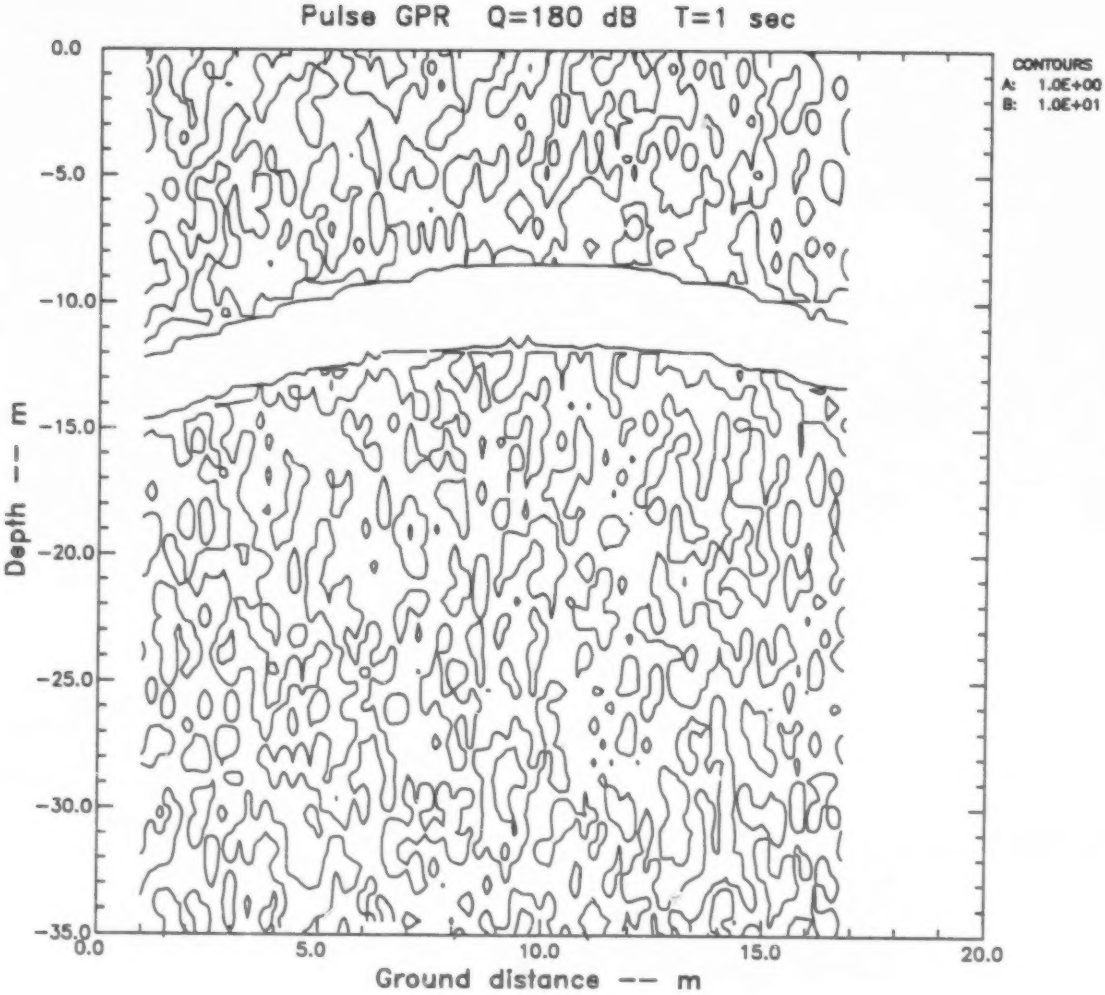

Figure 9.5. Unprocessed returns for Q=180-dB GPR. Point targets are located at 10-m and 30-m depths.

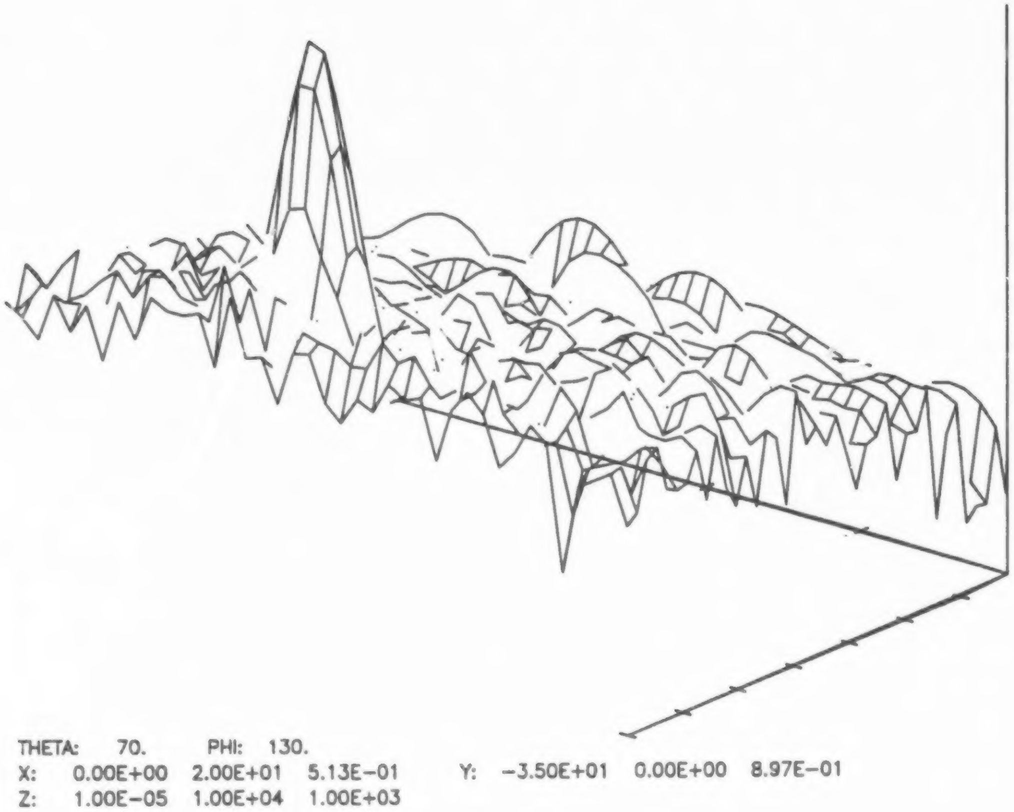

Figure 9.6. Processed returns for Q=180-dB GPR. Both targets are visible.

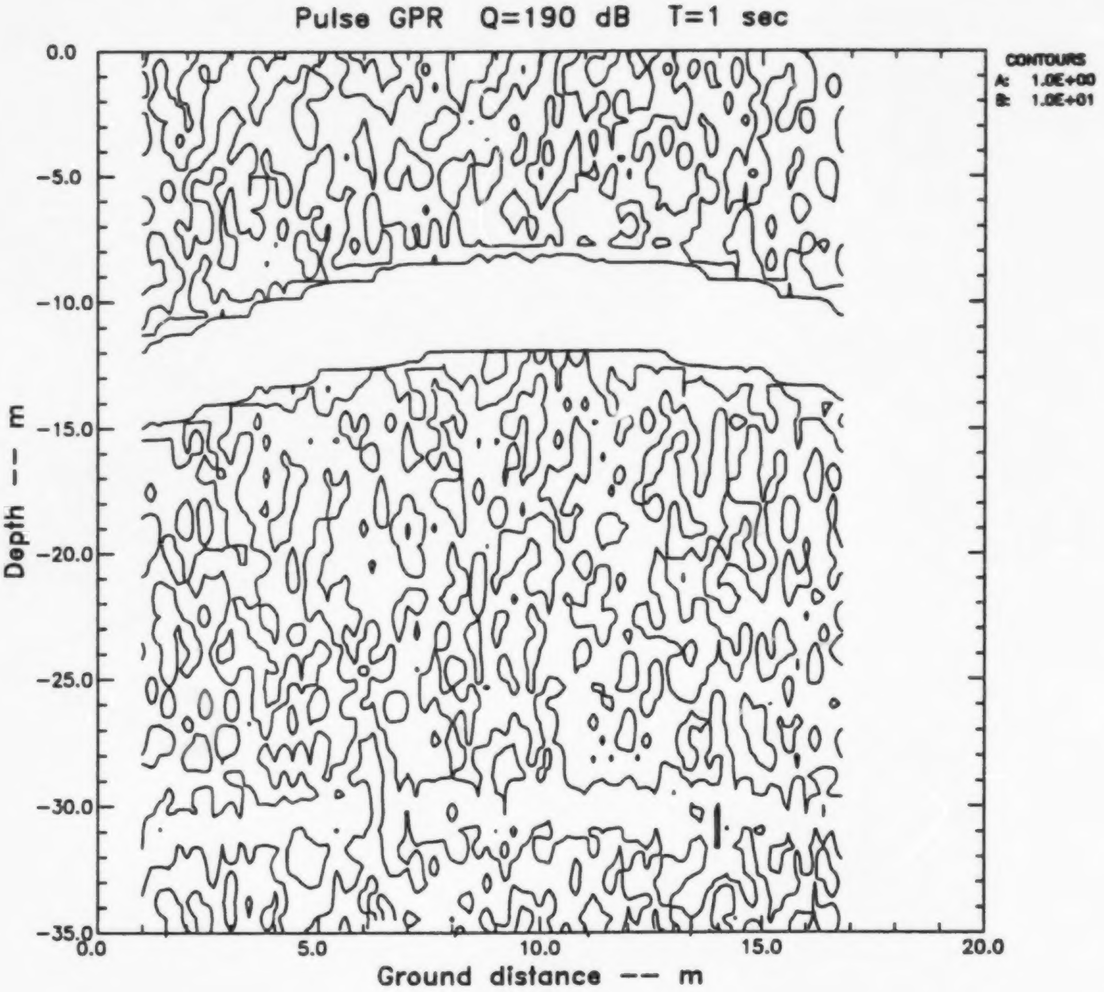

Figure 9.7. Unprocessed returns for Q=190-dB GPR.

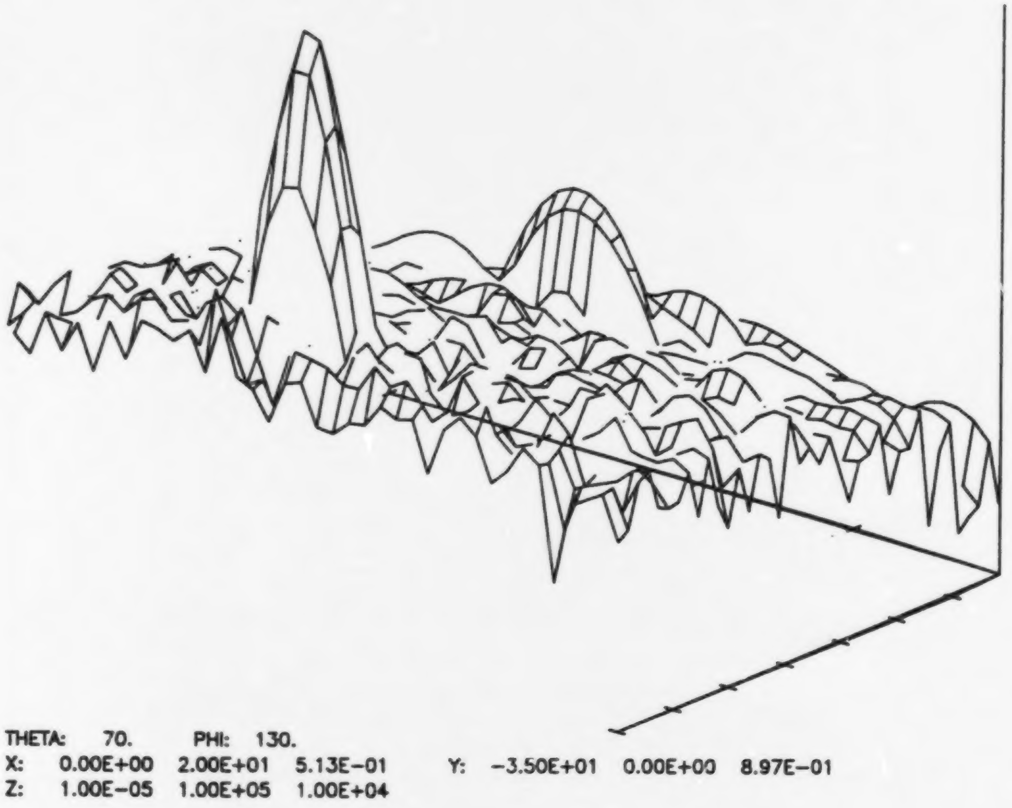

Figure 9.8. Processed returns for Q=190-dB GPR.

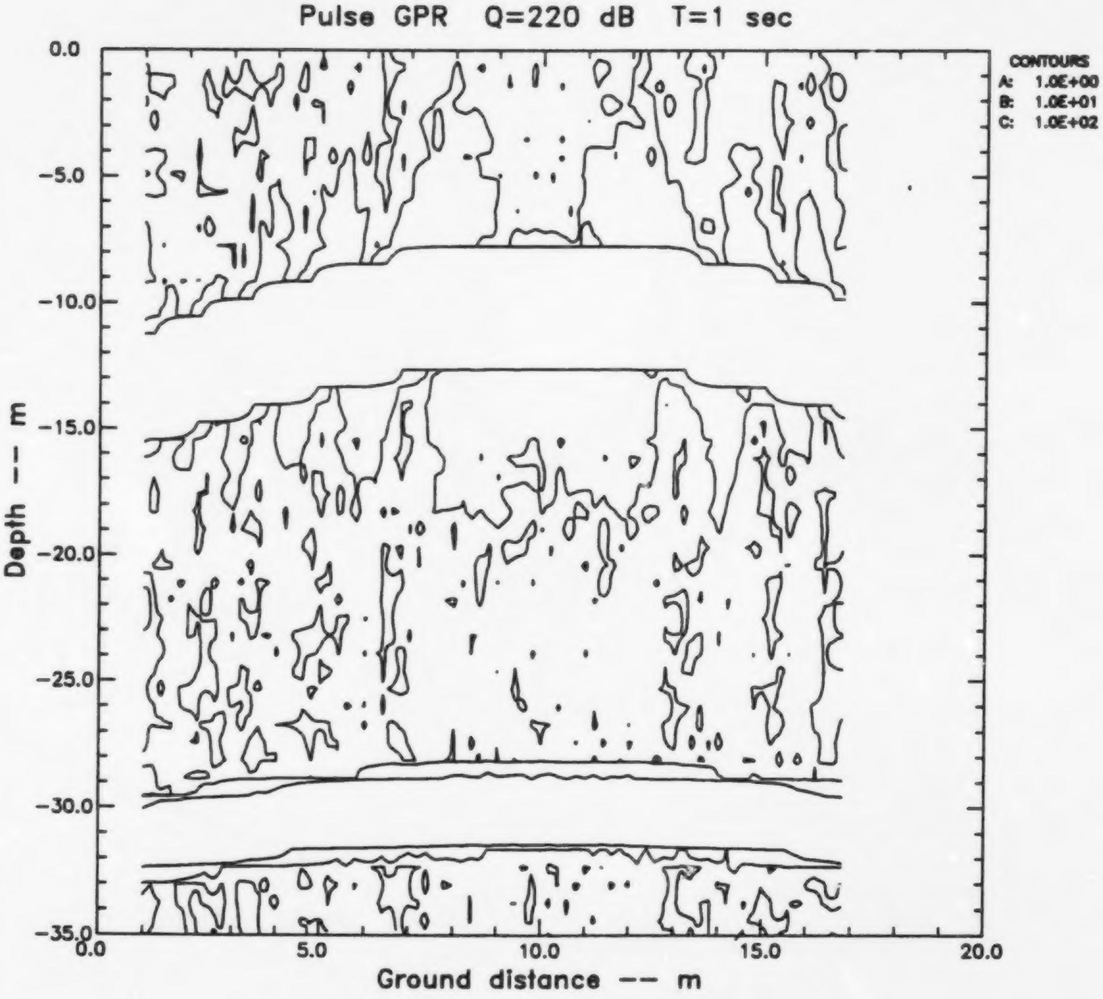

Figure 9.9. Unprocessed returns for Q=220-dB GPR.

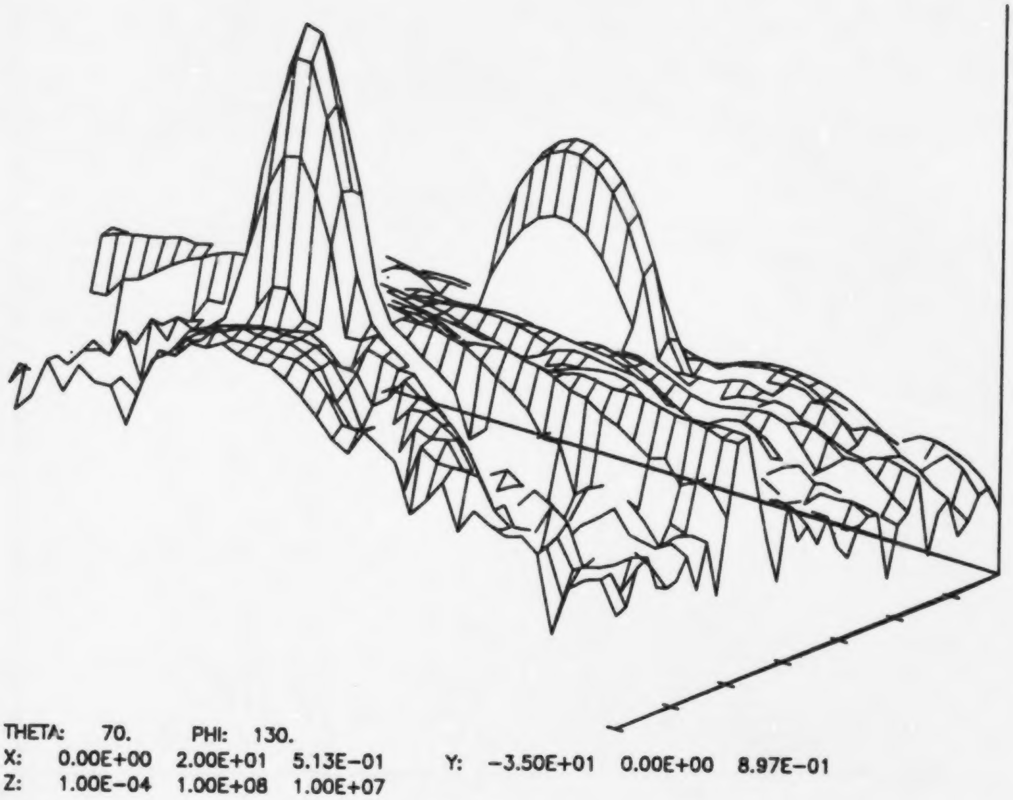

Figure 9.10. Processed returns for Q=220-dB GPR. Processing sidelobes are visible for target at 10 m.

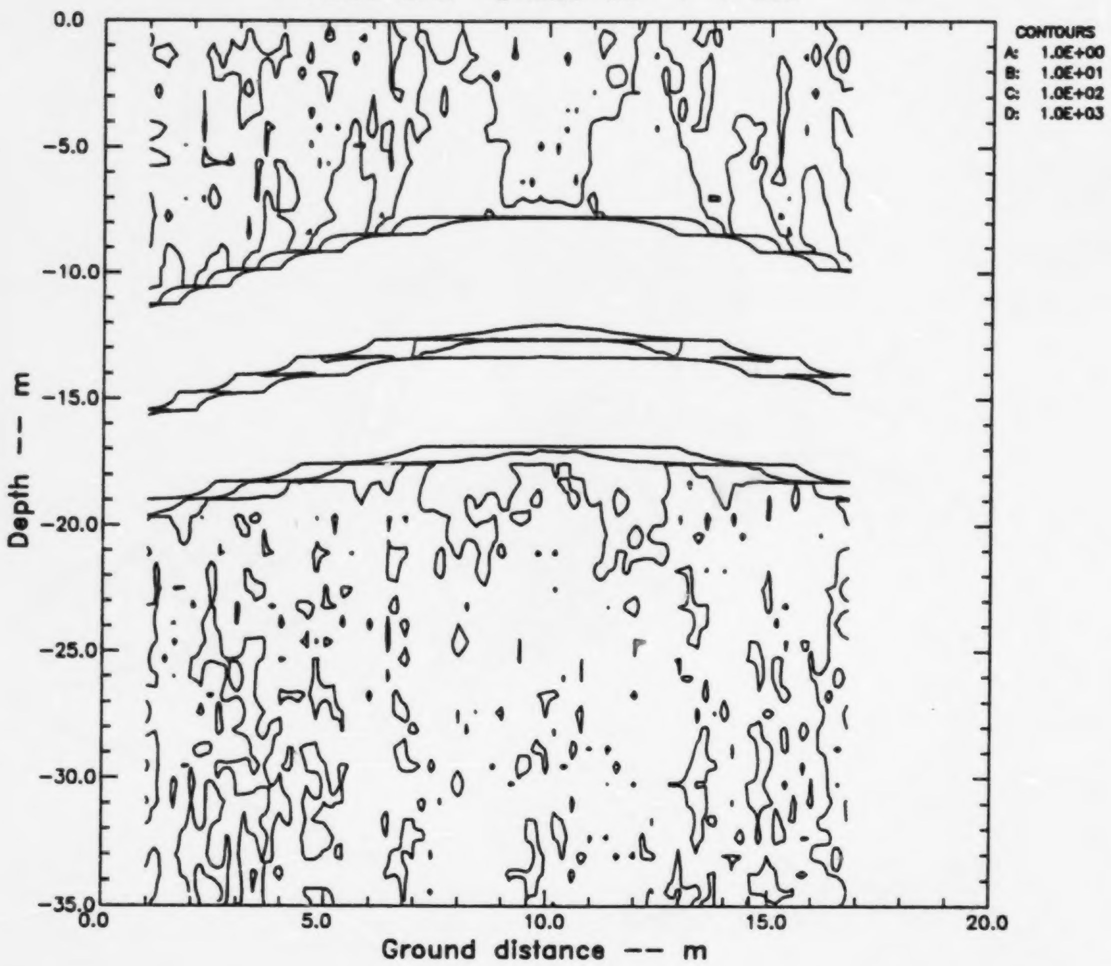

Figure 9.11. Unprocessed returns for Q=220-dB GPR with two closely spaced targets at 10-m and 15-m depths.

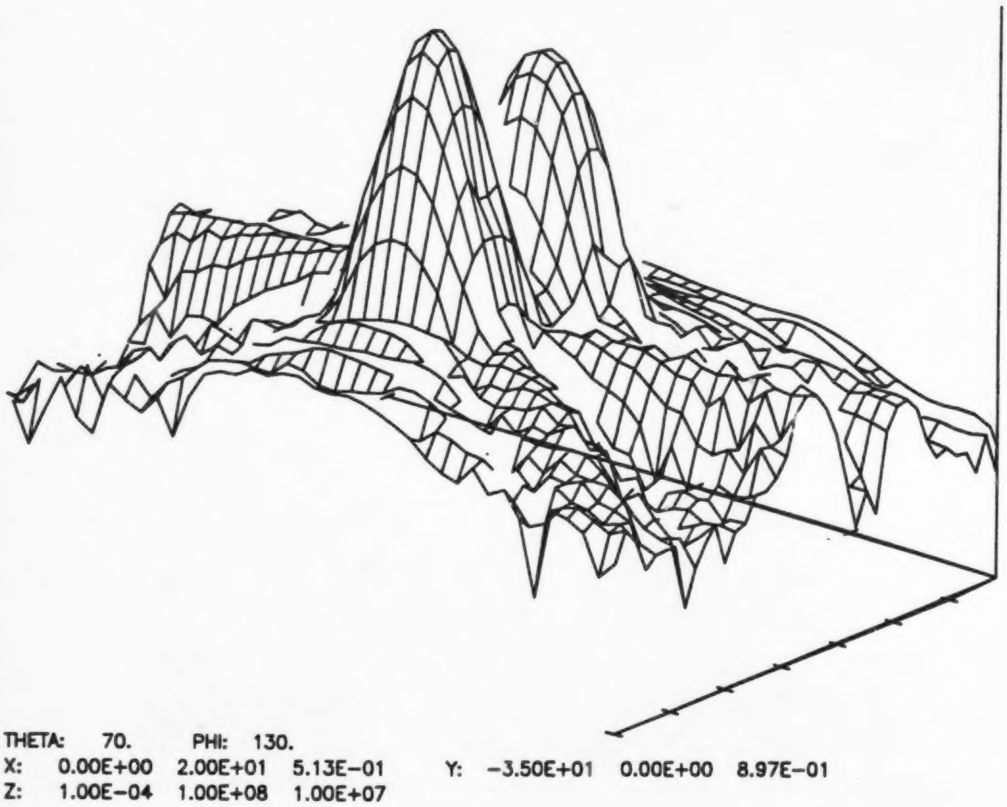

Figure 9.12. Processed returns for Q=220-dB GPR with closely spaced targets.

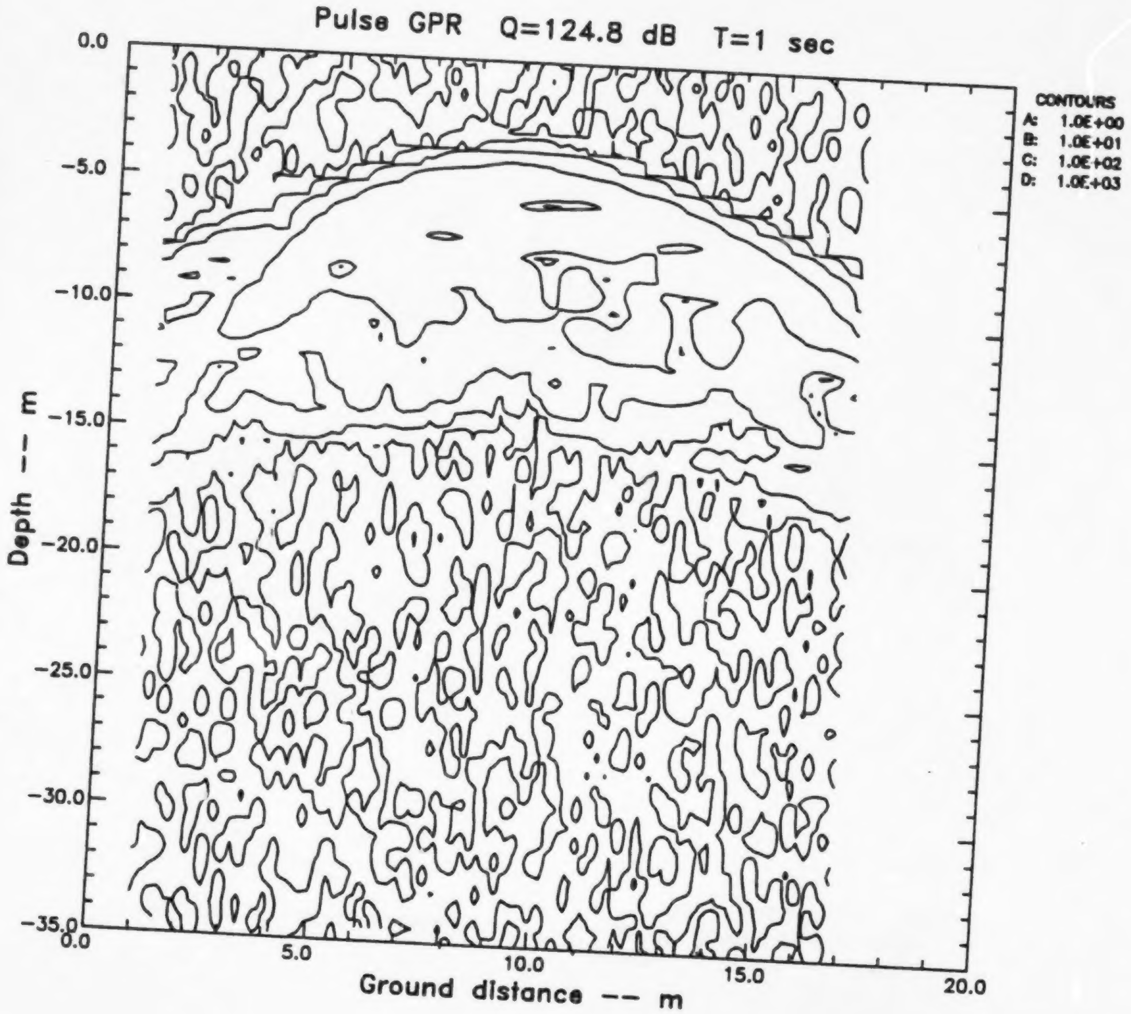

Figure 9.13. Unprocessed returns for Q=220-dB GPR illuminating a wedge of randomly located scatterers.

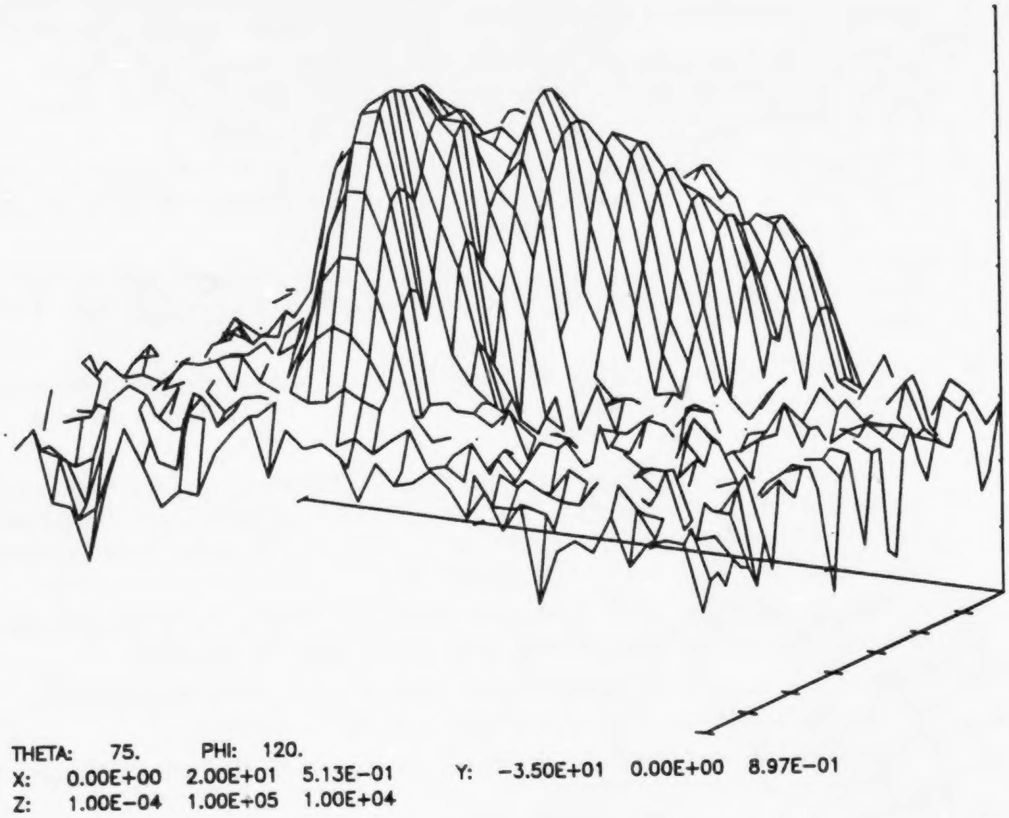

Figure 9.14. Processed returns from Q=220-dB GPR illuminating wedge.

REFERENCES

1. R. M. Koerner and A. E. Lord, Jr., "Spill Alert Device for Earth Dam Failure Warning," Project Summary, EPA-600/S2-84-007, U.S. EPA Municipal Environmental Research Laboratory, Cincinnati, Ohio (February 1984).
2. A. E. Lord, Jr., and R. M. Koerner, "Nondestructive Testing (NDT) Techniques to Detect Contained Subsurface Hazardous Waste," EPA-600/S2-87-078, U.S. EPA Hazardous Waste Engineering Research Laboratory, Cincinnati, Ohio (February 1988).
3. R. M. Koerner and A. E. Lord, Jr., "Microwave System for Locating Faults in Hazardous Materials Dikes," EPA/600/S2-85-014, U.S. EPA Hazardous Waste Engineering Research Laboratory, Cincinnati, Ohio (July 1986).
4. G. R. Olhoeft, "Tutorial: High Frequency Electrical Properties," *Proceedings of the 3rd International Conference on Ground Penetrating Radar*, Open-File Report 90-414, U.S. Geological Survey, Lakewood, Colorado (May 1990).
5. Peter Ulriksen, *Application of Impulse Radar to Civil Engineering*, Doctoral Thesis, LUTVDG/(TVTG-1001)/1-175/1982, Lund University of Technology, Lund, Sweden (1982).
6. S. K. Duke, "Calibration of Ground Penetrating Radar and Calculation of Attenuation and Dielectric Permittivity Versus Depth," Report No. T-3920, Master's Thesis, Colorado School of Mines, Golden, Colorado (13 June 1990).
7. E. G. Walther, A. M. Pitchford and G. R. Olhoeft, "A Strategy for Detecting Subsurface Organic Contaminants," *Proceedings of the NWWA/API Conference on Petroleum Hydrocarbons and Organic Chemicals in Ground Water*, Houston, Texas, National Water Well Association (12-14 November 1986).
8. M. E. Tabak, W. Glynn and R. P. Traver, "Evaluation of EPA Soil Washing Technology for Remediation at UST Sites," Camp Dresser & McKee, Inc. (no date).
9. Synthetic Soil Matrix (SSM-SARM) User's Manual, U.S. EPA Risk Reduction Engineering Laboratory, Edison, New Jersey (December 1988).
10. M. I. Skolnik, ed., *Radar Handbook*, 2nd ed., McGraw-Hill Publishing Company, New York, New York (1990).
11. D. V. Smith, "Propagation of Ground Penetrating Radar Signals in Soils," *2nd International Symposium on Geotechnical Applications of Ground-Penetrating Radar*, University of Florida, Gainesville, Florida (10 March 1988).
12. W. M. Brown and L. J. Porcello, "An Introduction to Synthetic Aperture Radar," *IEEE Spectrum* (September 1969).
13. R. C. Kemerait and J. N. Griffin, "Synthetic Pulse Radar," *Proceeding of the 3rd Technical Symposium on Tunnel Detection*, Colorado School of Mines, Golden, Colorado (12-15 January 1988).
14. R. M. Morey and W. S. Harrington, Jr., "Feasibility Study of Electromagnetic Subsurface Profiling," Report No. EPA-R2-72-082, Office of Research and Monitoring, U. S. Environmental Protection Agency, Washington, D.C. (October 1972).

15. R. C. Weast, ed., *CRC Handbook of Chemistry and Physics*, 52nd ed., The Chemical Rubber Co., Cleveland, Ohio (1972).

16. Darold Wobschall, "A Theory of the Complex Dielectric Permittivity of Soil Containing Water: The Semidisperse Model," *IEEE Trans. on Geosci. Elec.*, Vol. GE-15, No. 1 (January 1977).

17. G. R. Olhoeft, "Direct Detection of Hydrocarbon and Organic Chemicals with Ground-Penetrating Radar and Complex Resistivity," *Proceedings of the National Water Well Association Conference on Petroleum Hydrocarbons and Organic Chemicals in Ground Water*, Houston, Texas (November 12-14, 1986).

18. CDM Report under Work Assignment 3-30 on the Variability of Soils at Superfund Sites, Memo from Michael Borst, U.S. EPA, Soil and Material Engineering Section, RCB Superfund Technology Demonstration Division, to Carolyn K. Offutt, U.S. EPA, Special Projects Support Staff, Hazardous Site Control Division (28 February 1991).

19. P. Esposito, "Characterization of RCRA/CERCLA Sites with Contaminated Soil," Bruch, Hartman & Esposito, Inc., Cincinnati, Ohio, prepared for the EPA on Extractive Treatment of Excavated Soil, Edison, New Jersey (1-2 December 1988).

Appendix A

REAL SIGNALS, ANALYTIC SIGNALS, AND COMPLEX ENVELOPES

The Hilbert transform relates a real signal, $x(t)$, to a complex "analytic" signal,

$$s_H(t) = x(t) + i\,y_H(t)\,,$$

where

$$y_H(t) = \frac{1}{\pi}\mathcal{P}\int_{-\infty}^{\infty}\frac{x(\xi)}{t-\xi}\,d\xi$$

is the Hilbert transform of $x(t)$ ($\mathcal{P}$ denotes the Cauchy principal value of the integral). The Hilbert transform is most easily implemented by means of a Fourier transform,

$$y_H(t) = \mathcal{F}^{-1}\{X_H(f)\}\,,$$

where $X_H(f)$ is the positive-frequency side of the spectrum of $x(t)$, or

$$X_H(f) = \left\{\begin{matrix} 2X(f) & f > 0 \\ X(f) & f = 0 \\ 0 & f < 0 \end{matrix}\right\},$$

and

$$X(f) = \mathcal{F}\{x(t)\}\,.$$

The analytic signal is also related to the quadrature and complex-envelope representations of the real signal. In the former case, the real signal is written in terms of amplitude and phase modulations:

$$\begin{aligned} x(t) &= a(t)\cos[2\pi f_0 t + \Psi(t)] \\ &= p(t)\cos 2\pi f_0 t - q(t)\sin 2\pi f_0 t\,. \end{aligned}$$

$a(t)$ is the real amplitude-modulation envelope of the signal. The quadrature components are

$$p(t) = a(t)\cos\Psi(t)$$

and

$$q(t) = a(t)\sin\Psi(t)\,.$$

Next, the complex signal representation of the real signal is $s(t)$, where

$$x(t) = \Re\, s(t)\,,$$

where $\Re$ denotes the real part and

$$\begin{aligned} s(t) &= x(t) + i\,y(t) \\ &= a(t)\exp(i(2\pi f_0 t + \Psi(t))) \\ &= u(t)\exp(i2\pi f_0 t)\,. \end{aligned}$$

$u(t)$ is the complex envelope, which in turn is related to the quadrature components according to:

$$\begin{aligned} u(t) &= a(t)\exp(i\Psi(t)) \\ &= p(t) + iq(t)\,. \end{aligned}$$

The analytic signal can also be written in the "modulation/carrier" form:

$$s_H(t) = u_H(t)\exp(i2\pi f_0 t)\,.$$

For "narrow-band" signals,

$$u_H(t) \rightarrow u(t)\,.$$

Appendix B

CALCULATIONS OF DIELECTRIC CONSTANT, CONDUCTIVITY, AND ATTENUATION COEFFICIENT FOR VARIOUS SOILS AND A PETROLEUM CONTAMINANT

soil, void fraction = 0.5; water conductivity = 0.03

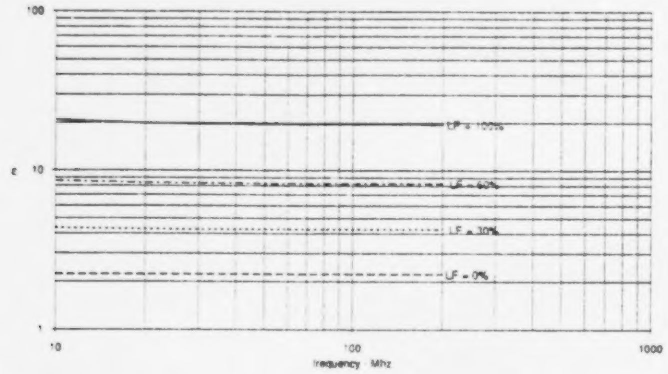

soil, void fraction = 0.5; water conductivity = 0.03

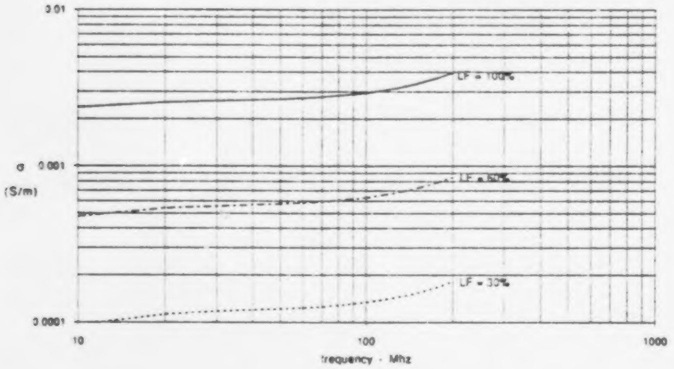

soil, void fraction = 0.5; water conductivity = 0.03

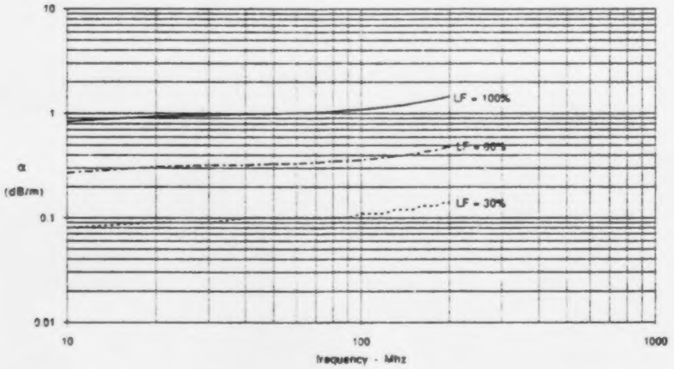

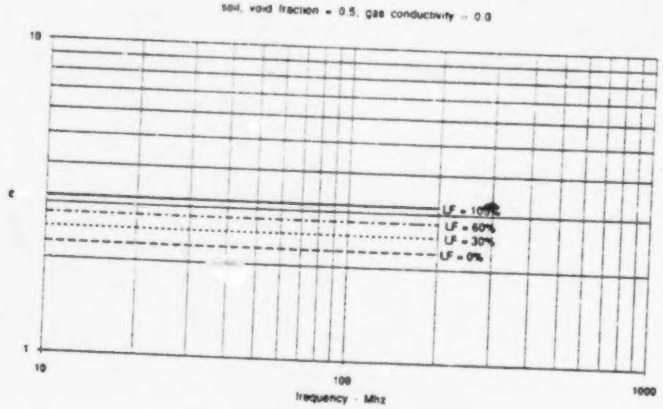
soil, void fraction = 0.5; gas conductivity = 0.0
10
ε
1
LF = 100%
LF = 60%
LF = 30%
LF = 0%
10
100
1000
frequency - Mhz

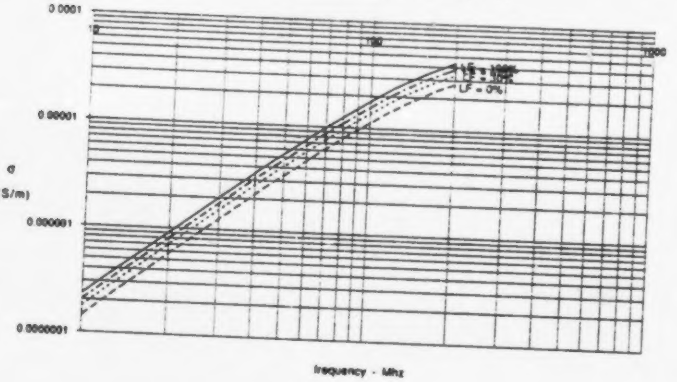
soil, void fraction = 0.5; gas conductivity = 0.0
0.0001
0.00001
σ
(S/m)
0.000001
0.0000001
10
100
1000
LF = 0%
frequency - Mhz

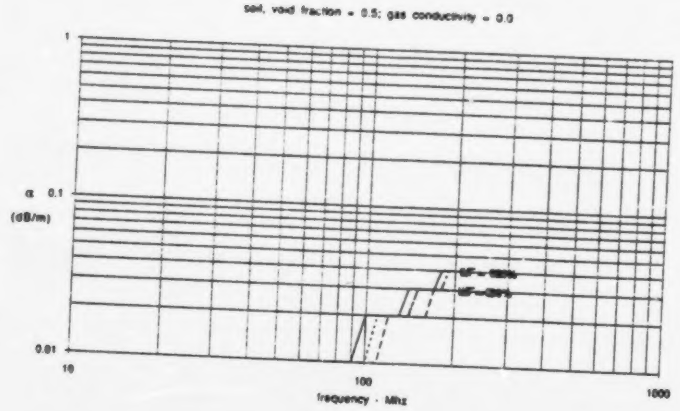
soil, void fraction = 0.5; gas conductivity = 0.0
1
α 0.1
(dB/m)
0.01
10
100
1000
frequency - Mhz

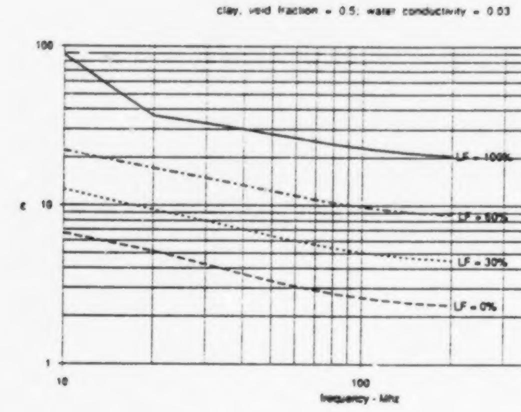
clay, void fraction = 0.5; water conductivity = 0.03
100
10
1
ε
10
100
1000
frequency - Mhz
LF = 100%
LF = 60%
LF = 30%
LF = 0%

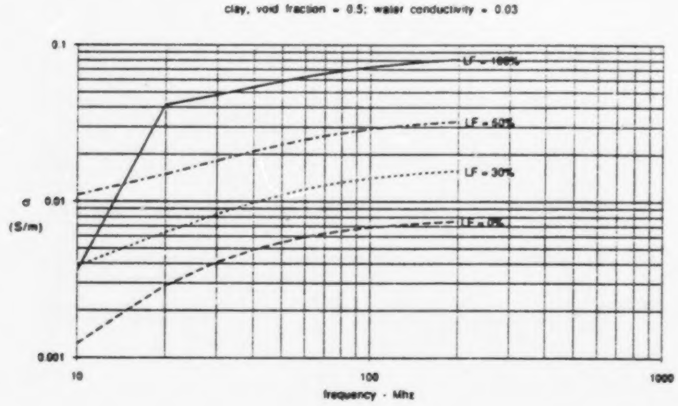
clay, void fraction = 0.5; water conductivity = 0.03
0.1
0.01
0.001
σ
(S/m)
10
100
1000
frequency - Mhz
LF = 100%
LF = 60%
LF = 30%
LF = 0%

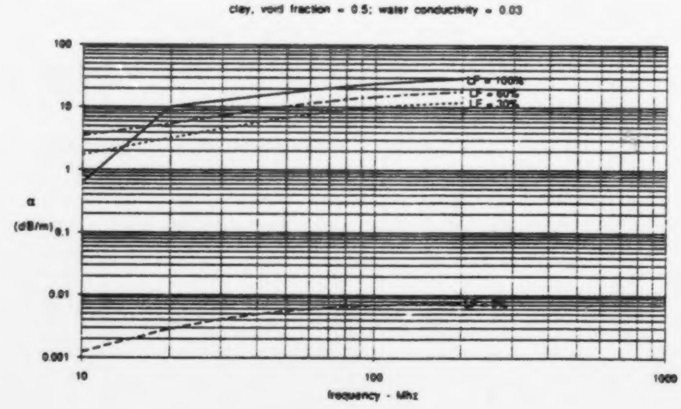
clay, void fraction = 0.5; water conductivity = 0.03
100
10
1
0.1
0.01
0.001
α
(dB/m)
10
100
1000
frequency - Mhz
LF = 100%
LF = 60%
LF = 30%
LF = 0%

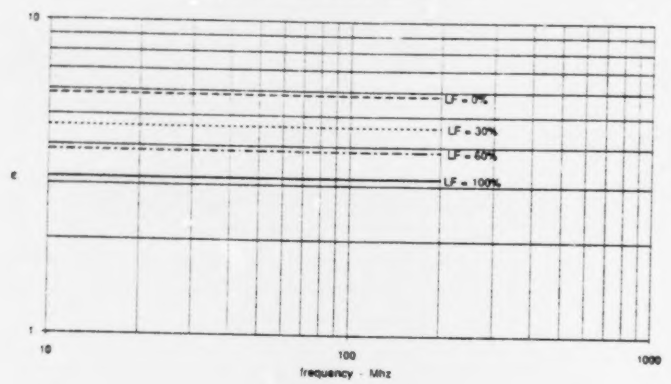
clay, void fraction = 0.5; gas conductivity = 0.0

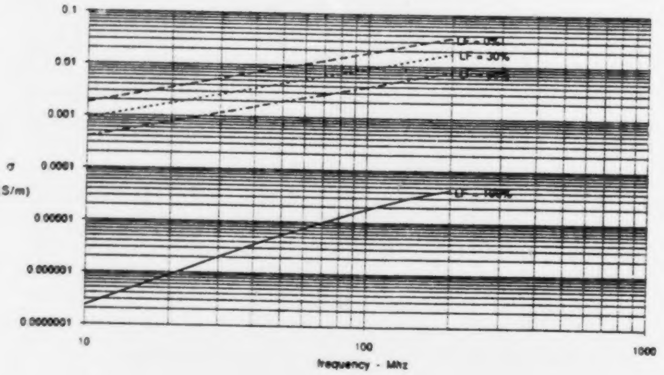
clay, void fraction = 0.5; gas conductivity = 0.0

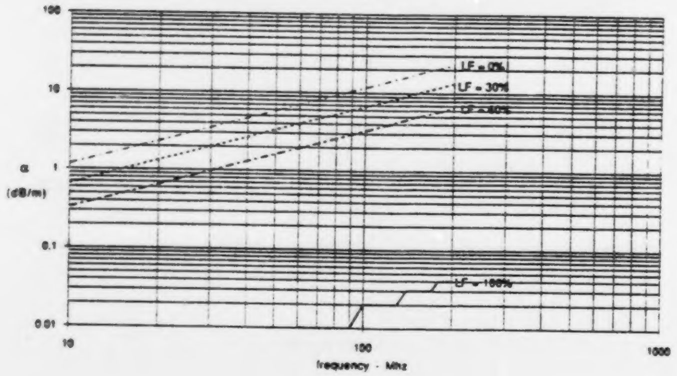
clay, void fraction = 0.5; gas conductivity = 0.0

Appendix C

MODIFIED BOOKER-GORDON SCATTERING FORMULA

The Booker-Gordon formula is based on the Born approximation, whereby the total electric field in the medium is replaced by the incident field. In general, the backscatter cross section is given by

$$\sigma_b = 4\pi |f(\hat{o}, -\hat{o})|^2 ,$$

where

$$f(\hat{o}, -\hat{o}) = \frac{k^2}{4}\pi \int_V \{-\hat{o} \times (\hat{o} \times \vec{E}(\vec{r}\,'))\} \{\varepsilon_r(\vec{r}\,') - 1\} \exp(-ik\vec{r}\,' \cdot \hat{o}) dV' ,$$

$\hat{o}$ is a unit vector to the receiving (and transmitting) point, k is the wave vector in the medium, and $\vec{E}(\vec{r}\,')$ is the total electric field in the medium. Under the Born approximation, the total field is replaced by the (unit strength) incident field,

$$\vec{E}(\vec{r}) \cong \vec{E}_i(\vec{r}) = \hat{e}_i \exp(ik\vec{r} \cdot \hat{\imath}) ,$$

where $\hat{\imath} = -\hat{o}$ is a unit vector in the incident propagation direction for backscatter. This leads to the expression where the rcs is proportional to

$$< (\varepsilon_r - 1)^2 > = < \Delta\varepsilon_r^2 > .$$

Now, because the characteristic dimensions (correlation length, grain size, etc.) of the soil medium are taken to be small compared to the wavelength and isotropy is assumed, this suggests using the Rayleigh approximation in place of the Born approximation. The Rayleigh approximation is based on electrostatics, where the field inside a homogeneous sphere is known to be uniform and given by

$$\vec{E} = \frac{3}{\varepsilon_r + 2}\vec{E}_i .$$

If this is used in place of the Born approximation, the factor $< \Delta\varepsilon_r^2 >$ is replaced by

$$< \left(\frac{3(\varepsilon_r - 1)}{\varepsilon_r + 2} \right)^2 > = < \left(\frac{3\Delta\varepsilon_r}{3 + \Delta\varepsilon_r} \right)^2 > .$$

For small values of $\Delta\varepsilon_r$, this reduces to the Born approximation. Note that this formulation applies equally well for *complex* ε_r (i.e., lossy objects).

Appendix D

CORRELATION FUNCTION FOR SOIL VARIABILITY MODEL

Let y be a random variable which can have two values, y_1 and y_2, as described in the text. The autocorrelation of a function $f(y)$ is

$$B_f(r_d) = \int\int_{-\infty}^{\infty} f(y_1)f(y_2)p(y_1)p(y_2|\, y_1;r_d)d\,y_1 d\,y_2 .$$

According to the Poisson probability law, the probability of having n shifts in a distance r_d is

$$P_{r_d}(n) = e^{-\zeta r_d}\frac{(\zeta r_d)^n}{n!} .$$

Because y must shift between its two values, the conditional probability is

$$\begin{aligned} p(y_2|\, y_1;\tau) &= P_{r_d}(0)\delta(y_2 - y_1) + P_{r_d}(1)\delta(y_2 + y_1) + P_{r_d}(2)\delta(y_2 - y_1) + \ldots \\ &= \delta(y_2 - y_1)\sum_{n\,even} P_{r_d}(n) + \delta(y_2 + y_1)\sum_{n\,odd} P_{r_d}(n) . \end{aligned}$$

Thus

$$\begin{aligned} B_f(r_d) &= \int_{-\infty}^{\infty} f^2(y)p(y)\sum_{n\,even} P_{r_d}(n)dy - \int_{-\infty}^{\infty} f^2(y)p(y)\sum_{n\,odd} P_{r_d}(n)dy \\ &= < f^2(y) > e^{-\zeta r_d}\left\{1 + \frac{(\zeta r_d)^2}{2!} + \frac{(\zeta r_d)^4}{4!} + \ldots - \frac{(\zeta r_d)^3}{3!} - \frac{(\zeta r_d)^5}{5!} - \ldots\right\} \\ &= < f^2(y) > e^{-2\zeta r_d} \end{aligned}$$

In particular, if $f(y) = y - < y >$,

$$B_y = < \Delta y^2 > e^{-2\zeta r_d} .$$

TECHNICAL REPORT DATA

(Please read Instructions on the reverse before compl

1. REPORT NO. EPA/600/R-92/089	2.	PB92-169382
4. TITLE AND SUBTITLE A Study to Determine the Feasibility of Using a Ground-Penetrating Radar for More Effective Remediation of Subsurface Contamination		5. REPORT DATE May 1992 6. PERFORMING ORGANIZATION CODE
7. AUTHOR(S) D.C. Douglas, A.A. Burns, C.L. Rino, J.W. Maresca, Jr. Vista Research, Mountain View, CA 94042		8. PERFORMING ORGANIZATION REPORT NO.
9. PERFORMING ORGANIZATION NAME AND ADDRESS Foster Wheeler Enviresponse, Inc. Building 209, Bay F Woodbridge Avenue Edsion, New Jersey 08837		10. PROGRAM ELEMENT NO. FRSV1A 11. CONTRACT/GRANT NO. 68-C9-0033
12. SPONSORING AGENCY NAME AND ADDRESS Risk Reduction Engineering Laboratory Office of Research and Development U.S. Environmental Protection Agency Cincinnati, Ohio 45268		13. TYPE OF REPORT AND PERIOD COVERED Project Report/Project Summary 14. SPONSORING AGENCY CODE EPA/600/14

15. SUPPLEMENTARY NOTES

Project Officer: James J. Yezzi, Jr. Comm: (908) 321-6703

16. ABSTRACT

Remediation of hazardous material spills is often costly and entails cumbersome procedures. The traditional method is to drill core samples in the area where the contaminant is thought to be present and then analyze these samples in a laboratory. The denser the sampling grid, the more effective it is; unfortunately, it is also more expensive to implement and more damaging to the environment. A nonintrusive method for detecting subsurface contamination, therefore, would be highly desirable. Toward this end, the capability of ground-penetrating radar (GPR) to identify natural subsurface features, detect man-made objects buried in the soil, and both detect and define the extent of contaminated soil or groundwater was assessed.

The study concluded that the technology for the envisioned GPR already exists. In terms of hardware, it was found that a synthetic-pulse radar has the potential to operate effectively in the three types of subsurface environments modeled in this study, environments representative of seven out of ten "common cases" found at remediation sites. In terms of signal processing, it was found that synthetic-aperture-radar (SAR) processing is preferable because better horizontal resolution can be achieved; the system can operate at lower frequencies and thus can achieve deeper penetration; and most importantly, ambient noise is reduced. The study found that a high-performance radar, when combined with SAR processing, match-filtering, and one of several detection strategies, can detect even a thin layer of contaminant floating on the water table, and can distinguish the acoustic returns from contaminant-saturated soil as opposed to those from water-saturated soil. Simple proof-of-principle experiments were recommended to validate the models developed in this study.

17. KEY WORDS AND DOCUMENT ANALYSIS

a. DESCRIPTORS	b. IDENTIFIERS/OPEN ENDED TERMS	c. COSATI Field/Group
synthetic aperture radar subsurface investigation method ground penetrating radar mapping subsurface contamination non-intrusive subsurface investigation detecting subsurface contamination electromagnetic subsufrace investigation		

18. DISTRIBUTION STATEMENT Release to Public	19. SECURITY CLASS *(This Report)* Unclassified	21. NO. OF PAGES 115
	20. SECURITY CLASS *(This page)* Unclassified	22. PRICE

EPA Form 2220-1 (9-73)

*U.S. GOVERNMENT PRINTING OFFICE: 1992-648-003/41841